THESIS REPORT

Ph.D.

Study of Human Laryngeal Motion through Mathematical Modeling

by L. Zhang
Advisor: W.S. Levine

Ph.D. 94-14

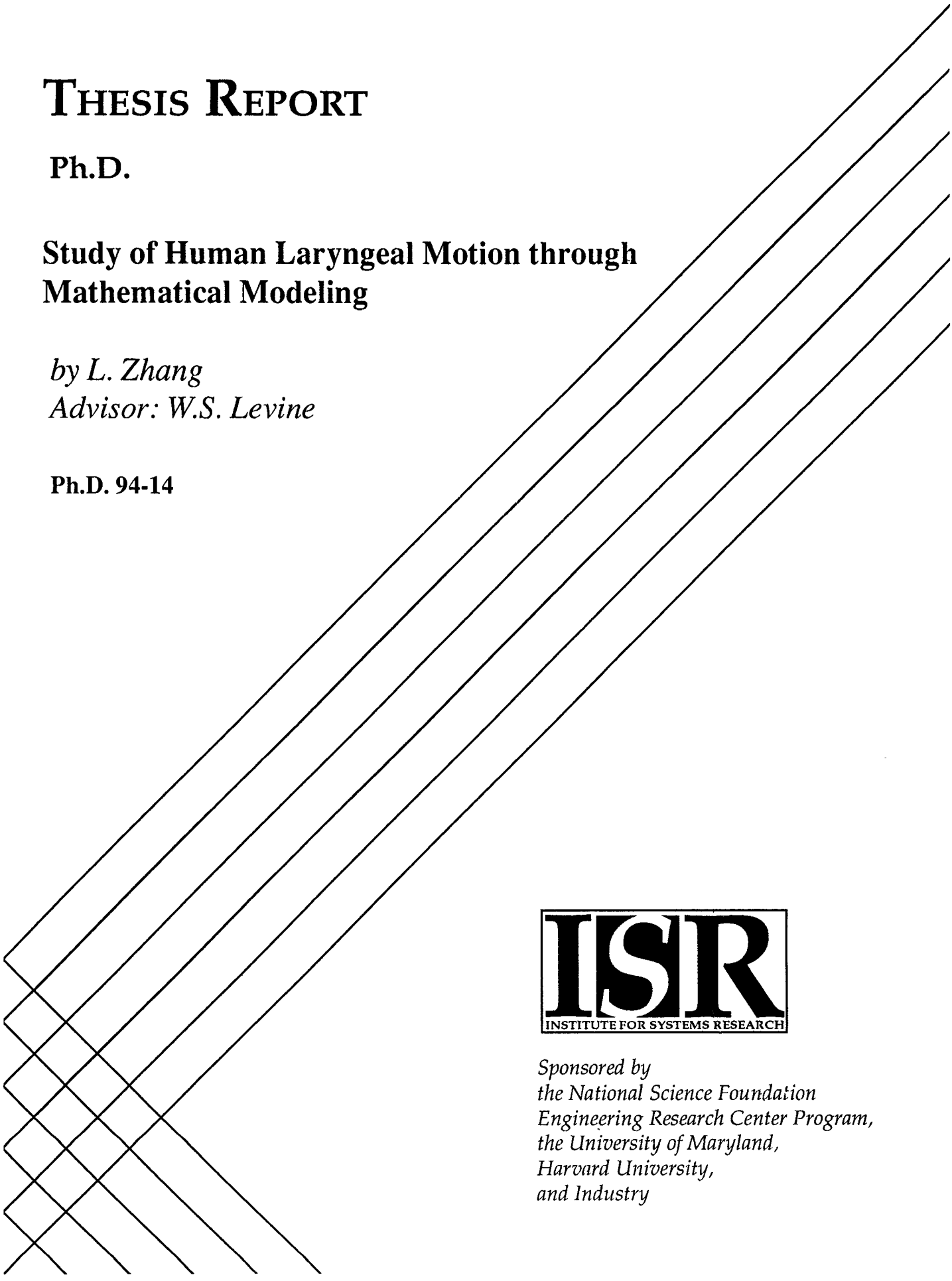

Sponsored by
the National Science Foundation
Engineering Research Center Program,
the University of Maryland,
Harvard University,
and Industry

STUDY OF HUMAN LARYNGEAL MOTION THROUGH MATHEMATICAL MODELING

by

Lei Zhang

Dissertation submitted to the Faculty of the Graduate School
of The University of Maryland in partial fulfillment
of the requirements for the degree of
Doctor of Philosophy
1994

Advisory Committee:

Professor William S. Levine, Chairman/Advisor
Professor Robert Newcomb
Professor Wijesuriya P. Dayawansa
Professor Avis H. Cohen
Dr. Christy L. Ludlow
Dr. Scott Selbie

Abstract

Title of Dissertation: STUDY OF HUMAN LARYNGEAL
MOTION THROUGH
MATHEMATICAL MODELING

Lei Zhang, Doctor of Philosophy, 1994

Dissertation directed by: Professor William S. Levine
Department of Electrical Engineering

The research presented in this dissertation concentrates on the motion of the arytenoid cartilages of the human larynx. Quantitative measurement and analysis was performed on the anatomy and motion of the cricoarytenoid joint. A dynamic neuro-musculo-skeletal model which describes such motion was developed.

To quantify the joint geometry, a 3D digitization method was proposed and implemented using a milling machine. This method was then applied to the digitization of the cricoarytenoid joint surfaces. Using the joint surface data, an optimization problem was formulated to locate the best feasible rotation axis for the joint. Rotating around this axis results in a motion that is often referred to as the "rocking" motion of the arytenoid. The 2D movement trajectory of the vocal process of the arytenoid cartilage produced by rotating around this optimal axis is consistent with the experimental data. A locally optimal vertical axis of rotation was also found. However,

this axis was offset from the cartilage, did not have as low a value of the performance measure and a rotation around it did not match the experimental data.

A dynamic neuro-musculo-skeletal model of the human larynx was established that includes the neural control input to the muscle (EMGs), the musculotendon actuators, and the skeletal (cartilage) dynamics. This model concentrates on the movements of the arytenoids. The motion at the cricothyroid joint is ignored and the cricoarytenoid joint is treated as an ideal pin joint. The location of the joint axis used in the model was determined by the optimization procedure mentioned above. Four intrinsic laryngeal muscles (TA, PCA, LCA, IA) are included in the model. A lowpass digital forward-backward Butterworth filter was designed to filter the rectified muscle EMG to obtain a smoothed envelope which was used as the neural input to the muscle model. The muscle and skeletal system parameters used in the model were measured where possible or estimated based on experimental data on the human larynx found in the literature. Computer simulation results have shown that the model produces laryngeal motions consistent with recordings of similar gestures reported in other studies.

STUDY OF HUMAN LARYNGEAL MOTION THROUGH MATHEMATICAL MODELING

by

Lei Zhang

Dissertation submitted to the Faculty of the Graduate School
of The University of Maryland in partial fulfillment
of the requirements for the degree of
Doctor of Philosophy
1994

Advisory Committee:

Professor William S. Levine, Chairman/Advisor
Professor Robert Newcomb
Professor Wijesuriya P. Dayawansa
Professor Avis H. Cohen
Dr. Christy L. Ludlow
Dr. Scott Selbie

Dedication

To the memory of my father

Acknowledgements

First, I would like to thank my advisor, Dr. William S. Levine, for his guidance and support over the years. It has truly been a privilege to be his student. His intuition and deep insight, his persistence in pursuing scientific research, his careful attention to detail, and his commitment to his students and science will continue to influence me for the rest of my life. Without his encouragement, patience and understanding, this dissertation would not have been possible.

I would especially like to thank all the members of the Voice and Speech Section at the National Institute on Deafness and Other Communication Disorders (NIDCD) - Dr. Christy Ludlow, Dr. Scott Selbie, Dr. Karen Rhew and many other individuals. Without their help this research would not have been possible. They provided clinical motivation and experimental data, answered questions, and gave feedback along every step of the way. Their support, patience and understanding were the keys to the success of our collaboration.

A special thanks goes to Dr. Wijesuriya P. Dayawansa for being helpful and supportive over the years; to Dr Robert Newcomb and Dr. Avis Cohen for their generous effort and time spent in reading the manuscript, and for their valuable advice and suggestions concerning my work.

I am grateful to Dr. Baoming Ma for his generous help to my study and work over the years, and for spending numerous hours in the machine shop to help me with the digitization experiment.

To all my friends at Maryland – past and present – who I have had the pleasure of working with, Baoming Ma, Xiaolin Chen, Xua Wang, Chujen Lin, Gil Yudilevitch,

Benjamin Bachrach, John Reilly, Dimitrios Tsakiris, Bruce Douglas, Qifeng Wei, Wei Zhang, Jian Zhou, Peter Yan, Jiqin Pan, Xiaoguang Chen, I want to thank you all for your caring, help, and the fun we had over the years. You have made my experience here truly enjoyable and memorable.

I am deeply thankful to my parents and grandparents for their unconditional love, encouragement, support and high expectations. My father had devoted all his life to higher education but could not share the happiness with me. Dad, I didn't let you down, I finally made it! To my brother and sister, thank you for your constant support, love, and many sacrifices you have made over the years.

Finally, a special thanks goes to my family. To my husband, Xuewei Tang, for his immeasurable love, friendship, support and extreme patience over the past ten years, I could not have gone this far without him. To my daughter, Rachel, who was born during this long process, for behaving so well during the nine month of pregnancy as well as in the early months of her life after birth to allow me to continue my work. To my mother-in-law, Yifang Pan, for taking such good care of my daughter and helping with the household chores so that I could concentrate on my work.

This research was financially supported by NIH Contract #N01-DC-1-2116.

Table of Contents

List of Tables

List of Figures

Chapter 1

Introduction

1.1 Motivation

Since the time of Ferrein (1741), who was the first to perform experiments with excised human and animal larynges, our knowledge of the human larynx has been much improved by information obtained along this line[110]. Considerable attention has been given to studying and modeling the biomechanics of the phonatory function of the human larynx, which is the vibration of the vocal folds. Little attention has been paid to dynamic aspects of laryngeal movement and muscle actions during other laryngeal gestures which require the active opening and closing of the vocal folds, such as: effort closure, swallowing, phonation onset and offset, etc. Over the past several years, researchers at the Voice and Speech Section of the National Institute on Deafness and Other Communication Disorders (NIDCD) have conducted numerous studies on laryngeal muscle activation patterns in patients with vocal fold movement disorders (vocal fold paralysis, adductor spasmodic dysphonia, abductor spasmodic dysphonia and vocal fold tremor) as well as in normal controls[55,56,57,58]. Their results have

raised the need to model the dynamic inter-relationships between muscle forces and laryngeal gestures. A dynamic model would allow researchers to predict the contribution of each individual muscle action to a laryngeal gesture, and estimate the limits on muscle forces necessary for normal phonation, respiration and swallowing. As a result, a better understanding of laryngeal motor control can be reached, followed by new methods for treating patients with laryngeal motor control disorders.

Another motivation comes from the success of biomechanical studies of movement. The mathematical models developed by researchers have played important roles in gaining better understanding of how the central nervous system coordinates limb movement in humans and animals[10,20,33,34,52,53,61,82,98,124]. In general, a biomechanical model consists of three components: (1) a neural input representing the stimulus, (2) a muscle model which converts the stimulus into force, and (3) a model of the skeletal system to which the muscle forces are applied to produce movement. Many different mathematical models have been proposed for mammalian muscle. There are extremely simple models. Such models have generally been constructed to study very specific biomechanical questions. An example of such a study is McMahon's use of simple springs to model human leg muscles in order to determine the ideal compliance for a running track[67]. There are also extremely complex models which are intended to incorporate all that is known about mammalian muscle and replicate its microscopic behavior. Such models are generally intended for use in studying muscle itself. An example is Wood's model[119]. The class of model most practical for researchers studying locomotion is of middling complexity[116]. The idea is to capture all that is physiologically important about the macroscopic behavior of mammalian muscle in a

model that is computationally tractable. Tractability means that computer simulation of movements involving several such muscles can be completed within reasonable time. Most of these models are of Hill's type[36]. A survey of muscle models of this type can be found in [122]. Similar modeling and analysis approaches can be adapted to the study of human laryngeal movement.

1.2 Objectives, Basic Approach and Contributions

A review of the literature shows the lack of research on the biomechanical aspects of the the protective and respiratory functions of the human larynx. These functions depend highly on the movements of the arytenoid cartilages. Therefore, understanding the motion at the cricoarytenoid joints is a key. The lack of quantitative information about the human larynx, especially in the areas of muscles, joints, and laryngeal ligaments, is the primary reason that the biomechanics of the cricoarytenoid joint is still uncertain. Although there were a couple of hypotheses on the motion of the arytenoids, they have not been verified against experimental data. The objective of the current research is to create a mathematical/computer model of the human larynx, concentrating on the motion at the cricoarytenoid joints (non-phonatory functions), based, where possible, on the reported data (of the joints, muscles, ligaments, etc.). Due to the fact that the number of muscles and rigid components (cartilages) of the larynx is relatively small, it is feasible to develop a mathematical model of the larynx, mathematically determine the motion of the model under precisely stated hypotheses about the joints, the muscles, the ligaments, and any other structures believed relevant, and display an animated picture of the motion on a computer terminal. This animated

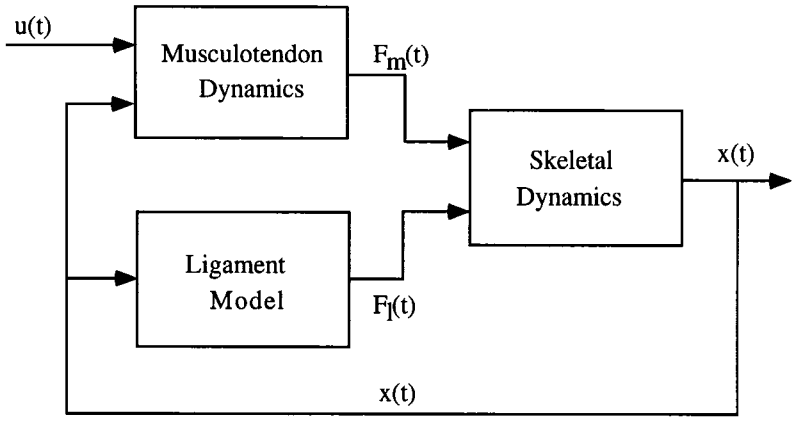

Figure 1.1: The structure diagram of the proposed model.

display will allow investigators to view the laryngeal motion in 3D from any viewpoint, thus offering a great deal of intuitive and qualitative insight. Using the animated display, the resulting motions of the mathematical models corresponding to different hypotheses can be easily compared.

The system structure diagram of the proposed model is shown in Figure 1.1. It consists of three parts: (1) skeletal model; (2) muscle model; and (3) ligament model. In order to complete such model, the following work needs to be done:

- Create a joint model for the cricoarytenoid joint.
- Choose a muscle model and estimate muscle parameters.
- Model the ligaments and other connective tissues.
- Determine what to use as the control signal to drive the model.
- Model simulation.

Our research work was concentrated on building such a model. The following

work has been done to achieve the goals:

1. Three dimensional digitizations were made of the cricoarytenoid joint surfaces.

2. Based on the joint surface data, the best motion axis was determined using an optimization algorithm, assuming that the major motion at the cricoarytenoid joint was a rotation motion.

3. The cricoarytenoid joint was modeled as an ideal pin joint having the optimal rotation axis determined by the above optimization process.

4. A dynamical skeletal-musculotendon model of the larynx was developed which includes the dynamics of the cartilages/joints and the dynamics of the musculotendon actuators.

5. The parameters of the model were estimated based on experimental data found in the literature or our own experiments.

6. The input signals that drive the model were taken to be the processed muscle EMGs. Digital filters were designed to process the rectified EMG signals to obtain the smoothed envelopes required by the muscle model.

7. Movement trajectories of the arytenoid produced by the model were projected to the viewing plane of the observation and compared with the experimental trajectories (collected by Selbie et al [93].).

8. 3D computer graphics software was developed on the IRIS to display the laryngeal cartilages (Selbie et al.[sel94.]), joint surfaces and animate the motion of the arytenoids.

The contributions of this dissertation can be summarized as follows:

- A dynamical model of the human larynx was developed, which includes:
  - Dynamics of the cartilages and joints;
  - Dynamics of the musculotendon actuators;
  - Passive elements such as ligaments;
- A 3D digitization technique was proposed and implemented using a milling machine. This method is suited for small, irregularly shaped objects with wet surfaces (like the cartilage) for which many advanced techniques may fail.
- 3D digitization was performed on the entire joint surface of the cricoarytenoid joint to obtain quantitative information about the joint anatomy.
- Using the joint surface data, the location of the best rotation axis for the joint was determined by formulating and solving an optimization problem. The minimum variation in distance between the two joint surfaces was used as the performance objective.
- Digital forward-backward Butterworth filters were designed to process the rectified muscle EMG signals to obtain the smoothed envelopes required by the muscle model.

1.3 Organization

This dissertation is organized into six chapters. Chapter 2 contains the anatomical and physiological information about the human larynx and a comprehensive survey of

previous research on human laryngeal movement.

Chapter 3, 4 and 5 contains the major work performed on building the model shown in Figure 1.1. In Chapter 3, a 3D digitization technique used to obtain joint surface measurements is described. Based on the measurement data, an optimization problem was formulated to determine the optimal rotation axis for the cricoarytenoid joint, assuming that the major motion at the joint is a rotation. The movement trajectories of the arytenoid cartilage predicted by the optimization algorithm were compared with experimental data (collected by Selbie et al [93].).

The muscle EMG signal processing techniques are investigated in Chapter 4. Based on the processing requirements, forward-backward Butterworth digital filters were designed and used to filter the rectified laryngeal muscle EMGs (collected by Ludlow et al.) to obtain the smoothed envelope signals required by the muscle model.

In Chapter 5, a dynamical neuro-musculo-skeletal model of the human larynx is developed. Parameters of the model were estimated based on previously published experimental data on the human larynx and on the results of our own research. A generic muscle model which was used previously in the study of human locomotion was adapted in our study to model the laryngeal muscles. The cricoarytenoid joint was modeled as an ideal one degree of freedom pin joint with the location of the joint axis determined by the optimization procedure described in Chapter 3. The rectified and smoothed muscle EMG signals obtained in Chapter 4 were used as the input neuro-stimulus signals to the muscle model.

Finally, in Chapter 6, conclusions are given, and topics for future research are discussed.

Chapter 2

Background

2.1 Introduction

The human larynx is the organ of voice and plays an important role in respiration and swallowing. It is located at the upper part of the air-passage, between the trachea and the base of the tongue. The skeletal structures of the human larynx consist of four major cartilages: the thyroid, the cricoid and the paired arytenoids as shown in Figure 2.1. The four cartilages articulate through two pairs of joints: the cricothyroid joints and the cricoarytenoid joints. There are nine intrinsic laryngeal muscles attached to the four cartilages. These muscles control the movement of the larynx. They are the cricothyroid (CT), the thyroarytenoid (TA), the posterior cricoarytenoid (PCA), the lateral cricoarytenoid (LCA) and the interarytenoid (IA). As shown in Figure 2.2, the interarytenoid is the only unpaired muscle in the larynx. Besides the muscles, there are some ligaments and membranes attached to the cartilages as well. The most important ligaments are the vocal ligaments (folds) which are attached to the vocal processes of the arytenoid cartilages and extend anteriorly to the deep surface of the

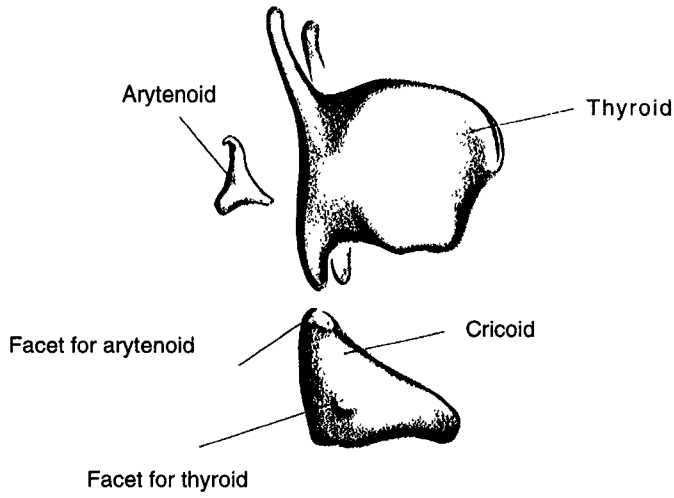

Figure 2.1: Laryngeal cartilages of the human larynx (from Fink[16])

thyroid angle. The movement of the arytenoids controls the opening and closing of the vocal folds so that various laryngeal functions can be achieved.

The larynx serves three basic functions in humans. They are protection, respiration, and phonation[87]. The development of each of the functions is the result of responses to evolutionary needs. Among the basic functions, the protective and respiratory functions are sometimes considered to be the biological functions of the larynx. Sound production is regarded as the nonbiological function of the larynx[126]. As a protective device of the lower respiratory tract, the larynx acts as a valve, it (1) prevents air from escaping the lungs, (2) prevents foreign substances from entering the lower respiratory tract, and (3) forcefully expels foreign substances which threaten to enter either the larynx or trachea. The larynx performs the phonatory function only when it is not fulfilling the vital biological functions mentioned above. During phonation, the larynx is a mechanical variable resistance to the flow of air in and out

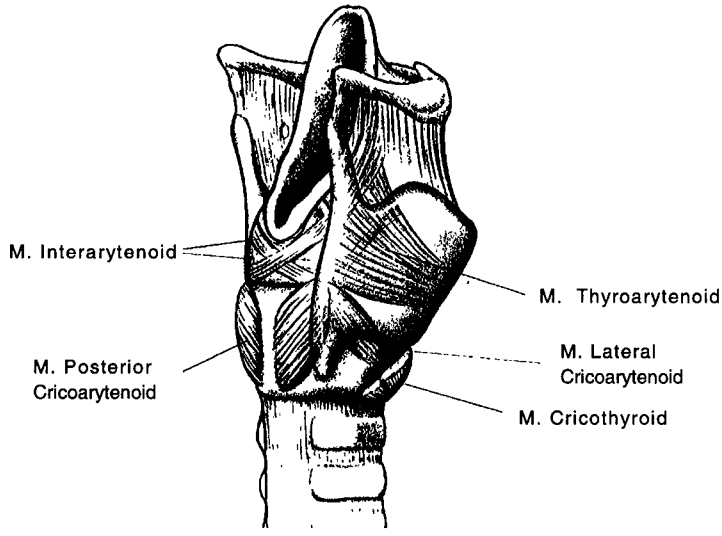

Figure 2.2: Intrinsic laryngeal muscles (from Fink[16])

of the lungs, capable of sound production over a very wide range of pitch and volume. The vocal folds, which consist of the mucosa ligament and the lamina propria and may be lengthened or shortened, tensed or relaxed, and abducted or adducted, is the key for the larynx to accomplish all its basic functions. The active closure of the vocal folds prevents threatening substances and foreign bodies from entering the larynx. A sudden, active dilation of the vocal folds once the air pressure has developed in the lungs results in an explosive emission of air to expel the foreign substance from the respiratory tract (coughing). During normal breathing, the vocal folds are spaced rather widely apart so the air stream can flow in and out of the lungs without much resistance. To initiate speech, the airway has to be opened just enough for the vocal folds to be set into vibration.

The phonatory function of the human larynx has been the center of research for the past one and a half century. Both theories [109,114] and biomechanical models based on theories were derived as the results of the research. The mathematical models of the human larynx developed for the study of voice production have been mainly models of the vocal folds. There were the Single-Degree-of-Freedom Model[17], the Two-Degree-of-Freedom Model[44], the Sixteen-Mass Model[106,107]and the continuous model[108]. The first model of the human larynx which included the cartilages was suggested by Fink and Demarest in their 1978 book [16]. In this model, it was assumed that the arytenoid cartilages were locked in their approximate position, thus becoming a part of the cricoid cartilage. The only motion in the larynx was the motion at the cricothyroid joints which change the length and tension of the vocal folds. The same model structure was applied to the model of voice fundamental frequency control by Farley [14].

The biomechanical aspect of the nonphonatory functions of the human larynx is still not well understood, although it has been studied for several decades. Few quantitative models have been developed to study the motion at the cricoarytenoid joints[72, 97]. There is continuing controversy over the motion of the arytenoid cartilages. Fink gives a brief historical survey of the debate[15]. Based on observations of the actual laryngeal movement, several hypotheses have been proposed. The earlier view (up to the 1940's) was that the arytenoids rotated about vertical axes[23]. This view was later challenged by researchers. Two other types of motion were then suggested based on anatomical data. These are known as "rocking" and "sliding" [112], as shown in Figure 2.3. The rocking motion corresponds to a rotation about the longitudinal axes

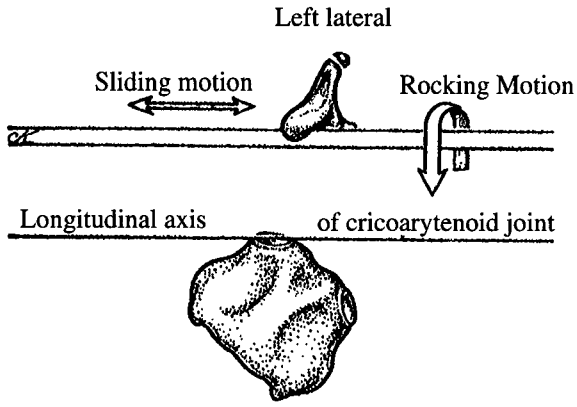

Figure 2.3: The "rocking" and "sliding" of the arytenoid (from Dickson[12])

of the cricoarytenoid joint facets on the cricoid cartilage. The term "rocking" is used to distinguish this motion from the rotation about vertical axes proposed earlier. The sliding takes place along the cylindrical surface of the cricoid facets.

There are several reasons why there is still so much uncertainty about the biomechanics of the larynx. In comparison with more accessible structures, it is very difficult to obtain precise three dimensional motion data from an intact larynx. Because the clinicians/researchers can only see the larynx from one viewing point and the visible surfaces are relatively low contrast, their perception of the motion is mostly two dimensional. The cartilages are completely covered by tissues; their movements cannot be observed directly.

Researchers have tried to resolve the biomechanical questions about the human larynx by means of animal models. For example, the larynx of the dog is often used because of its similar size. Most of the studies performed by Dr. Ingo Titze and his colleagues were on dog larynges [2,3,76,78]. But the differences are still substantial.

The vocal fold tissue of the dog is quite different from the vocal fold tissue of the human. The size and structure of the intrinsic muscles is also different. Therefore, animal studies alone could not definitively decide biomechanical questions about the human larynx such as the motion of the cricoarytenoid joint. Those questions can only be solved by research and experiments on the human larynx.

Building mathematical models of the human larynx which include the skeletal structures, the intrinsic laryngeal muscles as well as the vocal folds and other ligaments/membranes and testing them against experimental data is a first step towards the comprehensive understanding of the biomechanics of the human larynx. The model to be developed should utilize as much information gathered from previous research as possible. The anatomical and mechanical measurements in the following three areas are particularly useful in building the model: (1) laryngeal muscles, (2) laryngeal cartilages and joints, and (3) ligaments and other connective tissues. In the following sections, a comprehensive survey of previous research in these areas is given.

2.2 Intrinsic Laryngeal Muscles

Two kinds of information about the muscles are very important for the purpose of modeling the muscle. First is the anatomical measurements (fiber length, cross-sectional area, origin and insertion, etc.). Second is the mechanical properties of the muscle (contraction time, relaxation time, etc). These parameters will determine the maximum force a muscle can generate and how fast it can do so. Previous studies on the human intrinsic laryngeal muscles were concentrated on their functional anatomy and micro structure. The few anatomical measurements available displayed substantial

variability. The experiments performed to obtain the mechanical properties of the muscles were mainly done on animals.

2.2.1 Structure and Functions

The intrinsic laryngeal muscles may be categorized according to their effect on the shape of the glottis and on the vibration behavior of the vocal folds[126]. There are abductor, adductor and tensor muscles in the larynx. The **abductor** muscles, which separate the arytenoids and the vocal folds for respiratory activities, are opposed by the **adductors**, which approximate the arytenoid cartilages and the vocal folds for phonation and for protective purposes. The glottal **tensors** lengthen the vocal folds.

The anatomical structures and functions of the intrinsic laryngeal muscles have been described in numerous books and papers (e.g. [12,16,126]). The descriptions were more or less the same. The following is a summary:

1. **Posterior Cricoarytenoid** It is the only abductor muscle in the larynx. The large fan-shaped muscle has a broad area of origin from the concavity that covers the lateral half of the cricoid lamina. Its fibers converge to insert onto the arytenoid cartilage by a short tendon that covers the entire superior surface of the muscular process[12](see Figure 2.2).

2. **Thyroarytenoid** The thyroarytenoid is a large muscle that extends anteroposteriorly and makes up the muscular mass of the vocal fold. Its origin is from the deep surface of the thyroid lamina lateral to the attachment of the vocal ligament. Its fibers extend posteriorly to the arytenoid cartilage. It acts as the adductor, tensor of the vocal folds (see Figure 2.2; note that this muscle is

located inside the thyroid cartilage).

3. **Lateral Cricoarytenoid** This is a small muscle that originates from the superolateral rim of the cricoid cartilage. Its fibers extend posterosuperiorly to insert onto the lateral half of the muscular process of the arytenoid cartilage. It acts as an adductor of the vocal folds (see Figure 2.2).

4. **Interarytenoid** This is the only unpaired muscle in the larynx. It extends horizontally across the midline. The attachment, on each side, is to the entire length of the dorsolateral ridge and the dorsomedial surface of the arytenoid cartilage. It acts as a vocal fold adductor (see Figure 2.2).

5. **Cricothyroid** This muscle arises from the superficial surface of the anterior and lateral parts of the cricoid arch by two muscular bellies that lie next to each other. The anterior portion inserts into the inferior border of the anterior half of the thyroid lamina. The posterior portion inserts into the inferior border of the posterior half of the thyroid lamina. The contraction of this muscle would lengthen the vocal folds (tensor). See Figure 2.4 for details.

2.2.2 Anatomical Measurements

There are few reports in the literature on anatomical measurements of human intrinsic laryngeal muscles. The earliest report on the weights of the intrinsic laryngeal muscles was given by Grabower [22] in 1904. In Faaborg-Andersen's 1957 paper [13], the size and weight of four muscle groups were listed. They are cricothyroid, vocalis, transverse arytenoid and posterior cricoarytenoid. Table 2.1 summarizes his results.

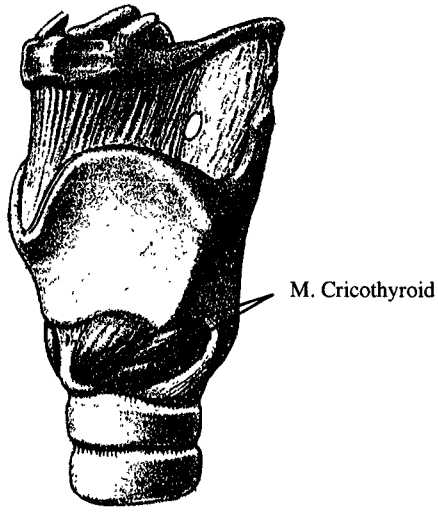

Figure 2.4: Cricothyroid muscle (from Sobotta[100])

Table 2.1: Size of the intrinsic laryngeal muscles (Faaborg-Andersen [13])

	Length (mm)	Breadth (mm)	Thickness (mm)	Cross-sectional area (mm^2)	Volume (mm^3)	Calculated weight (mg)	Weight (mg)
Cricothyroid	15	10	6	60	900	954	940
Vocal	15	4	5	20	300	318	357
Transverse arytenoid	15	7	5	35	525	556	558
Posterior cricoarytenoid	12	10	5	50	600	636	625

In Table 2.1, the sample size used is $n = 4$ (2 males, 2 females). The length, breadth and thickness values were measured at the place where each muscle appeared to be about its average length, breadth and thickness. The cross-sectional area, volume and weight were calculated using the following formula:

- Cross-sectional area = Breadth $\times$ Thickness
- Volume = Length $\times$ Breadth $\times$ Thickness
- Calculated weight = Volume $\times$ 1.06 (muscle density)

The last column in Table 2.1 is the measured weights reported by Grabower [22].

Since the data was based on only 4 samples and the precise locations where the measurements were made were not clear, Faaborg-Andersen's results are difficult to interpret although the calculated weights agree well with the measured weights by Grabower.

Bowden and Scheuer [6] measured the wet and dry weights of all five intrinsic laryngeal muscle groups in 1960. In measuring the wet weights, the blotting technique was used to remove excess fluid. This information was not reported in Faaborg-Andersen's study. The wet weights obtained are listed in Table 2.2.

By comparison, the results by Bowden and Scheuer are lighter than those estimated by Faaborg-Andersen. We think the differences were caused by blotting prior to measurements. Due to larger sample size and the careful processing techniques, Bowden and Scheuer's results are more reliable than those given by Faaborg-Andersen, although the variations from sample to sample were very large.

Table 2.2: Wet weights of the intrinsic laryngeal muscles (Bowden & Scheuer [6])

Muscle	Number of samples	Mean value (mg)	Range (mg)
Cricothyroid	24	696.2	305 – 1194
Thyroarytenoid	22	622.3	217 – 1297
Interarytenoid	12	304.1	141 – 538
Lateral cricoarytenoid	22	251.3	80 – 583
Posterior cricoarytenoid	24	408.2	208 – 655

Table 2.3: Weight of the posterior cricoarytenoid muscle (Zemlin [125])

Muscle	Number of samples	Mean value (mg)	Range (mg)
Posterior cricoarytenoid	20	671.5	449.6 – 843.6

In Zemlin's study [125], the weight measurements of the posterior cricoarytenoid muscles were given. They are listed in Table 2.3. Here blotting prior to measurement was not mentioned.

The dimension measurements of the lateral cricoarytenoid and the posterior cricoarytenoid muscle were published by Lang, et al. [50] in 1986. In 1979, Kuciński et al. [47] measured the dimensions of both the straight and oblique parts of the cricothyroid muscle. Their results are listed in Table 2.4. In Table 2.4, the length of the muscle is defined as the distance between the extremely distant origin and attachment of the muscle, and the breadth of the muscle is defined as the longest transverse dimension perpendicular to the course of the muscle.

In 1984, Zemlin [125] and his colleagues did a morphological study of the posterior cricoarytenoid muscle. Their study indicated that the PCA muscle is composed

Table 2.4: Size of the straight and oblique part of the cricothyroid muscle (Kuciński et al. [47])

Muscle part		Number of samples	Length (mm)	Breadth (mm)
straight	Left	40	13.5	8.7
part	right	40	14.1	8.1
Oblique	Left	40	20.0	9.3
part	right	40	20.0	9.3

of two separate muscle bundles. One is superior-medial and consists of oblique fibers, and the other is lateral and consists of vertically directed bipennate fibers. The two bundles have different sizes of fasciculation and different insertions on the muscular process of the arytenoid cartilage. The muscle mass of each bundle was measured and given in the paper. Zemlin's results are summarized in Table 2.5.

The structure of the thyroarytenoid muscle is a center of controversy. Some investigators claimed that it could be divided into two groups anatomically (Goerttler 1950 [21]; Wustrow 1952 [120]), while others did not agree (Sonesson 1960 [102]). Sonesson and Wustrow claimed that the muscle fibers run parallel to the vocal ligament while Goerttler thought that they arise from the muscular process of the arytenoid cartilage and insert into the vocal ligament. Zenker [127] found that many fibers end within the muscle and are connected with each other there.

In summary, the available anatomical measurements of the laryngeal muscles are very limited. They are mainly weight measurements. The weight data given by Bowden and Scheuer is probably the best we can find in terms of sample size and measuring techniques, but there is substantial variability in the data. No conclusions

Table 2.5: Mean percentage volume and weight of the lateral bundle of the posterior cricoarytenoid muscle (by Zemlin[125])

Side	Mean (%)	SD	Range
Weight			
Right side	67.92	4.99	64.83 – 71.01
Left side	68.18	8.69	62.81 – 73.55
Combined	68.95	6.59	64.87 – 73.03
Volume			
Right side	68.99	4.77	66.03 – 71.95
Left side	68.15	8.42	62.93 – 73.37
Combined	68.57	6.67	64.44 – 72.70

can be made about muscle length and cross sectional area given so few measurements. As for muscle attachments, the only papers found were the studies published by Mossallam et al. [70,71]. They contain detailed descriptions and measurements on muscle attachments on the arytenoid cartilage which can be used in determining where to attach the muscle on the arytenoid cartilage. But similar information for the attachments on the cricoid and thyroid cartilages was not found.

2.2.3 Mechanical Properties

Functional characteristics of the individual laryngeal muscles have been studied by examining contraction properties of the muscles. This can be done by recording the mechanical force or displacement caused by the contraction of the muscle. A single twitch contraction takes place as a response to a single stimulation applied either

directly to the muscle or to the muscle nerve. When both of the muscle endings are fixed, thus keeping the muscle length constant, muscle tension is increased by an isometric contraction of the muscle. When one end of the muscle is pulled by a constant external force and the muscle is stimulated, the muscle length is decreased by an eccentric contraction. In the literature, the main mechanical properties of the laryngeal muscles measured were the **contraction time**, the **relaxation time**, the **fusion frequency** and the **tetanus-twitch ratio**. The time from the beginning to the peak of the twitch contraction is called contraction time, and from the peak to the end of the contraction, relaxation time. The minimum frequency of stimulation to obtain complete tetanus of the muscle is called the fusion frequency. The ratio between maximum tetanus tension and maximum twitch tension (in isometric contraction) is called the tetanus-twitch ratio.

Almost all of the studies reported on the mechanical properties of the intrinsic laryngeal muscles so far have been done on animals.

Mårtensson and Skoglund [62] measured contraction time (C.T.) in eccentric contraction, fusion frequency (F.F.) and tetanus-twitch ratio (Te/Tw) of the laryngeal muscles of the dog, cat, rabbit, monkey and sheep (Table 2.6). According to Mårtensson and Skoglund, for the animals studied, the contraction of the adductor muscles of the larynx, i.e. the thyroarytenoid and the lateral cricoarytenoid, is very fast and is surpassed only by the external eyeball muscles. This result is consistent with histochemical data presented in the next section. Among the intrinsic laryngeal muscles, the cricothyroid and the posterior cricoarytenoid are relatively slow. They claimed that fast contraction of the adductor muscles is important in closing the glottis

Table 2.6: Contraction properties in animal intrinsic laryngeal muscles (Mårtensson and Skoglund [62])

Muscle	specimen	C.T. (*msec*)	H.R.T (*msec*)	F.F. (*spc*)	Te/Tw
cricothyroid	dog	35		> 300	5:1
	cat	15-20		–	–
	monkey and rabbit	25-30		–	–
	sheep	50-60		–	–
thyroarytenoid	dog	14		> 400	10:1
	cat	9-13		–	–
	monkey and rabbit	8-10		–	–
	sheep	15-20		–	–
lat. cricoarytenoid	dog	16		–	–
post. cricoarytenoid	dog	30		–	–

fast enough for effective protection of the respiratory organ against foreign bodies and that the capacity for quick changes in muscle tension is also useful for the regulation of voicing.

Hast also examined the mechanical properties (in isometric contraction) of the cricothyroid and the thyroarytenoid muscles of the dog and other animals (Hynan gibbon, rhesus macaque, squirrel monkey and cat) [27,29,30]. The results are listed in Table 2.7, where H.R.T represents the half relaxation time. His data for the dog were similar to those of Mårtensson and Skoglund. He concluded that the experimental results obtained from the dog's larynx, which is anatomically and physiologically closer to the larynx of primates, would be more valuable for the study of the human

Table 2.7: Contraction properties in animal intrinsic laryngeal muscles (Hast [30])

Muscle	specimen	C.T. (*msec*)	H.R.T (*msec*)	F.F. (*spc*)	Te/Tw
cricothyroid	Hynan gibbon	39	36	43	3.4:1
	rhesus macaque	36.4	23.2	49	4.4 : 1
	squirrel monkey	18.8	13.6	83	4.6 : 1
	dog	39	32.3	45	4.2 : 1
	cat	52.8	42.4	37	3.7:1
thyroarytenoid	Hynan gibbon	16	17	95	5.9:1
	rhesus macaque	14	14.4	112	7.1 : 1
	squirrel monkey	13.2	14	116	6.0 : 1
	dog	14	18	114	6.2 : 1
	cat	22	20	73	5.0:1

larynx. Hirose et al. did similar studies using cats [39] (Table 2.8). Their data for the cricothyroid and the thyroarytenoid were similar to those of Hast. A summary of the contraction properties presented in the 60's by several authors can be found in Sawashima's paper [90].

The most recent study of the mechanical properties of the intrinsic laryngeal muscles in dogs was done by Sato and Hisa in 1987 [88] (Table 2.9). In their experiments, the contraction properties of the cricothyroid, the thyroarytenoid, the posterior cricoarytenoid and the lateral cricoarytenoid muscles were measured as opposed to just those of CT and TA muscles as in Hast's studies. Therefore the data is more complete.

Although a lot of experiments have been performed in this area, almost all of them were done on dogs and other animals. To obtain the contraction properties of

Table 2.8: Contraction properties in cat intrinsic laryngeal muscles (Hirose et al. [39])

Muscle	C.T. (*msec*)	H.R.T (*msec*)	F.F. (*spc*)	Te/Tw
cricothyroid	44	41	44	4.3 : 1
thyroarytenoid	21	27	≥ 100	7.5 : 1
post. cricoarytenoid	22	29	≥ 100	3.4 : 1

Table 2.9: Contraction properties in canine intrinsic laryngeal muscles (Sato & Hisa [88])

Muscle	C.T. (*msec*)	H.R.T (*msec*)	F.F. (*spc*)	Te/Tw
Cricothyroid	38	31.7	40	4.5 : 1
Thyroarytenoid	14	16	95	7.1 : 1
Post. cricoarytenoid	42	37.2	45	3.8 : 1
Lat. cricoarytenoid	21	22.5	90	6.8 : 1

human laryngeal muscles, the differences between human laryngeal muscles and those of the animals must be examined. The survey presented in the next section is an attempt to establish such connections.

2.2.4 Histochemical Characteristics

Numerous studies have been done on the characteristics of the laryngeal muscles. The results indicated that adult human laryngeal muscles differ from other skeletal muscles in a number of fundamental ways. Concerning muscle fiber size, it was seen that the mean fiber diameter was smaller in laryngeal muscles than in limb skeletal muscles. In skeletal muscle, the mean fiber diameter usually ranges from 60 to 70 μm, as against 40 to 50 μm only in laryngeal muscles [84]. The variability in the size of fibers of the laryngeal muscle was also greater[84]. Detailed histochemical analysis of human intrinsic laryngeal muscles has been reported by Teig et al. [105], Rosenfield et al. [83], Sadeh, et al. [84], Malmgren & Gacek [64], Lacan Saint Guily et al. [48], Brøndbo et al. [9], Happak et al. [26] and Claassen & Werner [11]. In Table 2.10, the average percentile distribution of the fiber types in human laryngeal muscles reported by the investigators mentioned above is summarized. The mean fiber diameter is given in Table 2.11.

Histochemical studies of animal laryngeal muscles can be found in the papers published by Sahgal and Hast [85,86] (Rhesus monkeys), by Braund [7] (dogs) and by Happak [26] (sheeps). Their results are summarized in Table 2.12. Smaller fiber sizes have also been observed in dog laryngeal muscles compared with skeletal limb muscles of dogs of comparable sizes. The major difference between human and animal laryngeal

Table 2.10: Average percentile distribution of the fiber types in human laryngeal muscles

Author		CT	TA	PCA	LCA	IA	SCM[a]
Teig et al.	n	7	7	7	7	7	
(1978) [105]	Type I	47	35	67	40	46	
	Type II	53	65	33	60	54	
Sadeh et al.	n	2	2	2	2		
(1981) [84]	Type I	49,42	47,42	55,56	58,35		
	Type IIA	39,50	39,48	31,38	34,48		
	Type IIB	12,8	14,10	14,6	8,17		
Malmgren &	n			10			
Gacek	Type I			52			
(1981) [64]	Type II			48			
Rosenfield	n	3	3	3	3	3	
et al.	Type I	41,38,36	37,58,65	62,72,53	50,39,36	40,41,50	
(1982) [83]	Type II	59,62,64	63,42,35	38,28,47	50,61,64	60,59,50	
Lacan Saint	n	3	4	4	2	2	
Guily et al.	Type I	35-48	23-40	60-75	29,39	30,24	
(1983) [48]	Type II	47-60	60-77	25-40	61,71	70,76	
Brøndbo et al.	n			6			6
(1986) [9]	Type I			57 (37-72)			39 (15-58)
	Type IIA			36 (28-43)			38 (20-56)
	Type IIB			7 (0-23)			23 (3-64)
Happak et al.	n	12	12	12		12	
(1989) [26]	Type I	43	44	65		44	
Claassen &	n	4	9	11	4	8	
Werner	Type I	44	53	67	50	56	
(1992) [11]	Type IIA	54	36	22	35	37	
	Type IIB	2	5	5	15	1	

[a]Skeletal Muscle – Sternocleidomastoid.

Table 2.11: Mean fiber diameter of human laryngeal muscles (in μm)

Author		CT	PCA	LCA	TA	IA
Sadeh et al.	n	2	2	2	2	
(1981) [84]	Type I	40.0,39.9	41.0,45.6	54.0,40.4	42.9,57.0	
	Type II	43.5,47.5	40.0,58.3	54.1,40.0	39.5,60.3	
Rosenfield	n	3	3	3	3	3
et al.	Type I	36.22	34.87	30.72	32.84	34.79
(1982) [83]	Type II	33.37	35.56	36.92	35.68	37.65
Happak et al.	n	12	12		12	12
(1989) [26]	Type I	41.1	41.4		44.8	36.7
	Type II	40.0	45.5		48.5	40.2

muscles is the fiber composition of the posterior cricoarytenoid (PCA) muscle. In human PCA, all the studies have shown the dominance of type I fibers over type II fibers (the ratio of type I/type II is always greater than 1), while in animals, the reverse is true. Since the ratio of type I/type II fibers is directly related to the maximal speed of contraction of the muscle, the discrepancy between human and animal PCA implies that the contraction properties obtained from animal PCAs cannot be applied directly to human model.

In summary, the studies have indicated that there were certain differences (1) between laryngeal muscles and skeletal limb muscles in human, and (2) between human and animal laryngeal muscles. But the results of these studies were not conclusive. The muscle fiber components varied greatly from individual to individual. Even though the data provided us with some information about the fiber components of each muscle, the mechanical properties of the muscle cannot be drived from the available information. More accurate and consistent measurements from the human larynx are needed. Before

Table 2.12: Mean fiber diameter of animal laryngeal muscles (in μm) and percentile ratio of type I over type II fibers

Species		CT	PCA	LCA	TA	IA
Rhesus monkey	n	4	4		4	
(Sahgal & Hast [86])	Type I	28.0	21.8		30.6	
	Type II	28.7	26.5		47.4	
	I/II	0.63	0.54		0.43	
Rhesus monkey	n					
(Sahgal & Hast [85])	I/II	0.43	0.64	0.14	023	
Dog	n	10	10	10	10	
(Braund [7])	Type I	38.20	32.05	33.38	29.39	
	Type II	43.25	38.95	38.59	33.85	
	I/II	0.68	0.69	0.18	0.04	
Sheep	n	6	6		6	6
(Happak [26])	Type I	43.4	33.1		31.1	29.3
	Type II	39.2	34.9		37.0	30.6
	I/II	1.37	0.83		0.35	0.59

those measurements become available, we prefer to use mechanical properties of the human limb muscle.

2.3 Laryngeal Cartilages, Joints and Motion

A review of the literature reveals only a few studies of the laryngeal joints and cartilage dimensions. Earlier studies on cartilage dimensions and ligaments of the larynx were carried out by Balboni [4,5], Minnigerode [69], Mayet and Mundnich [66]. More recent work on the subject was reported by Malinowski [63], Maue and Dickson [65], Sellars [95], Lang [49] and Ajmani [1].

In Malinowski's investigation, the shape, dimensions and process of calcification of the laryngeal cartilages in relation to sex and age in the Polish population were studied. Detailed measurements of the thyroid, cricoid and arytenoid cartilages were given based on a sample size of 97 individuals (42 women and 55 men).

Similar measurements were made by Maue and Dickson based on 20 samples (10 women and 10 men). In addition to the cartilage dimensions, Maue and Dickson also measured the dimensions of the cricoarytenoid joint facets on both the cricoid and the arytenoid cartilages as well as some intercartilage distances between the thyroid and the cricoid. Some of their findings about the joint facets are quite interesting and useful. Maue and Dickson found that the cricothyroid joint facets were so variable in size, shape, configuration, and even presence that it was not possible to quantify their dimensions accurately, while the cricoarytenoid joint facets were well defined, consistent, and bilaterally symmetrical in all cases. There was noticeable variability among cartilages in their facet shape and configuration, however. As for the shape of

the joint facets, in over 90% of the larynges they examined, the cricoarytenoid facets on the cricoid were flat along their major axes and convex along their minor axes, with the length of the minor axis approximately 60% of that of the major axis. The cricoarytenoid facets on the arytenoids were consistently flat along an axis parallel to the longitudinal axis of the cricoarytenoid facet of the cricoid cartilage, and concave along the axis corresponding to the short axis of the cricoarytenoid facet of the cricoid cartilage. The facet of the arytenoid cartilage thus fits smoothly over the convex surface of the cricoarytenoid facet of the cricoid cartilage.

In Sellars and Keen's study [95], the cricoarytenoid joints of 45 larynges were dissected and examined with respect to the ligaments, articulating surfaces and movements. Regarding the arytenoid facet, they observed that it is concave and forms the inferior surface of the muscular process of the arytenoid cartilage. The longer axis of this facet is placed, when the arytenoid is at rest, at right angles to the long axis of the cricoid facet. In this long axis, it is concave, and is longer than the width of the cricoid facet with which it articulates. The concavity is deepest in the middle of the facet. The short axis of the arytenoid facet is both parallel to and shorter than the long axis of the cricoid facet. The length of these two axes can differ by up to 2.5 mm in the same joint. The cricoid facet was studied in detail and measured. In contrast to the findings by Maue and Dickson, they found that not only were the appearances in different larynges often quite dissimilar, but that in many cases the two facets of one cricoid were asymmetrical in appearance. In 30 specimens (17 males and 13 females), the following measurements were recorded: (a) length of the facet, (b) breadth of the facet at its mid-point, (c) medial breadth, at a point midway between the medial

(upper) end of the facet and its midpoint, (d) the medial arc taken as the length of a piece of inextensible thread stretched across the curvature of the facet between the ends of the medial breadth measurement (c), (e) lateral breadth, at a point midway between the lateral (lower) end of the facet and its midpoint, and (f) the lateral arc, taken as in measurement (d).

Lang et al. [49] made measurements of the thyroid cartilage dimensions, while Ajmani [1] measured the dimensions of all three cartilages using a total of 40 specimens (28 males and 12 females).

Since the movement of the two arytenoid cartilages is the only factor which is relevant to the opening (abduction) and closing (adduction) of the vocal folds, the motion at the cricoarytenoid joint has become a focus of research. Besides the work mentioned above, studies on the functional anatomy of the cricoarytenoid joint in human larynges have been reported by Snell [99], Sonesson [101], Von Leden and Moore [112], Frable [18], Takase [104] and Sellars [96,97]. All of these investigators have obtained similar results and pointed out a misconception in some textbooks which describe a rotatory movement of the arytenoid cartilage around the vertical axis of the joint surface. According to their studies, the articular facet on the upper posterior surface of the cricoid cartilage forms a prominence which serves as the convex surface of a cylinder joint. The axis of the cylinder, which defines the longitudinal dimension of the joint, runs in the direction from dorsomediocranial to ventrolaterocaudal. The facets of the joints in the left and the right cartilages are not always symmetrical: they often show some difference in size and in direction of the longitudinal axis. The arytenoid facet of the joint is located in the lateral part of the cartilage on the under-

surface of the muscular process. This facet has a concave surface which is well adapted to the convex surface of the facet on the cricoid cartilage. The transverse dimension of the arytenoid facet is larger than that of the cricoid, while its longitudinal dimension is smaller. Results of the measurements of the joint facets and the angle of the joint axis made by the above investigators were summarized by Sawashima [90].

The main claim made by the above-mentioned authors is that the structure of the cricoarytenoid joint permits the arytenoid cartilage two principal types of motion. One of them, the main type, is a rotating motion around the longitudinal axis of the joint; the other is a longitudinal sliding motion parallel to the axis. Von Leden and Moore described another type of motion, though very limited in its extent, around the attachment of the posterior cricoarytenoid ligament to the cricoid lamina. The longitudinal sliding motion of the arytenoid cartilages is very limited and of little importance for changing the glottal aperture. According to Sonesson, maximum excursion of this is 2 *mm.*, which is allowed by the difference in longitudinal dimensions of the joint surfaces of the cricoid and arytenoid cartilages. Sellars also described a third type of motion of the cricoarytenoid joint: twisting to bring the vocal process together. This motion is in agreement with the one suggested by Von Leden and Moore.

Sato [89] and his colleagues investigated the distribution of the elastic cartilage in the arytenoids. Among the laryngeal cartilages, only the arytenoid cartilage is composed of two types of cartilage, i.e., elastic and hyaline cartilage. These two types of cartilage have very different properties, so their distribution in the arytenoid and its possible functional significance have become an area of research. Sato's investigations were performed histologically in two serial sections of the arytenoid: horizontal and

coronal. The results can be summarized as follows. Elastic cartilage is found not only at the tip of the vocal process but at the superior portion of the arytenoid cartilage from the vocal process to the apex. The vocal process bends at the elastic cartilage portion during adduction and abduction. The sides of the arytenoids come into contact mainly at the elastic cartilage portion.

2.4 Laryngeal Ligaments and Other Connective Tissues

The most studied ligament in the larynx is the vocal ligament because of its important role in phonation. The vocal fold (both vocal ligament and vocalis muscle) structure has been studied by many researchers. According to the histology studies done by Hirano [37] and Hirano and Kakita [38], the most important feature of the vocal fold is that it consists of multiple layers, each having different mechanical properties. Most of the experiments reported in the literature in studying the mechanical properties of the vocal fold were done without separating the vocalis muscle and the vocal ligament. Quantitative evaluations have been made with the use of many different methods.

Using excised human larynges, Van den Berg and Tan [110] removed the external tissue from the intact laryngeal structure, dissected all tissue above the vocal folds, and stabilized the structure to a vertical bar. By using a predetermined force applied to the thyroid cartilage, they elongated the vocal folds, thus simulating cricothyroid contraction. The extensibilities of both the folds and the vocal ligaments were measured in this way.

Hast [28] made in situ active-contraction length-tension measurements on dogs using electrical stimulation of the recurrent laryngeal nerve and, in the process of

reporting his data, included a single passive length-tension curve for one dog.

Kakita, Hirano and Ohmaru [45] used excised dog larynges from which they dissected the vocal folds and made separate force-displacement measurements on the epithelium, lamina propria and muscle. Their preparations remained attached to small portions of the thyroid and arytenoid cartilages. The tissues were hung vertically from the thyroid cartilage, known weights were applied to the arytenoid cartilage, and the amount of elongation was measured using a microscope. They normalized their data with respect to the cross-sectional area, length, and mass of the tissue sample, and presented their results in the form of Young's modulus, the differentiated Young's modulus, and shear modulus.

Perlman et al. did similar studies for canine vocal fold tissue [76,77,79]. But because the vocal ligament in the human vocal fold does not exist in the canine vocal fold, their results can not be applied directly to modeling of the human larynx.

Many researchers investigated the mechanical properties of the vocal folds in the medial-lateral directions. Kaneko et al. [46] assessed the overall stiffness of the vocal folds by measuring stress-strain relations at the mid-portion, when the vocal fold was pulled medially by a string. Using square-pillar frontal sections of human and canine vocal folds, Yokoyama et al. [121] have also measured the stress-strain relations of vocal fold tissue. In the study by Haji and his colleagues[24], the stress-strain relations obtained at different points on the vocal folds of a freshly excised human larynx were reported.

Besides the vocal ligaments, there are other ligaments connecting the four major laryngeal cartilages. According to an anatomy book [23], the ligaments connecting

the arytenoid cartilages to the cricoid are two capsular ligaments and two posterior cricoarytenoid ligaments. The capsular ligaments are thin and loose capsules attached to the margin of the articular surfaces. The posterior cricoarytenoid ligaments attach to the superior rim of the cricoid lamina between the two cricoarytenoid facets and extend anteriorly to the medial surfaces of the arytenoid cartilages. These two ligaments and the vocal ligaments act as guy wires [12]. The ligaments connecting the thyroid cartilage to the cricoid are three in number - the cricothyroid membrane, and the capsular ligaments. The cricothyroid membrane is composed mainly of elastic tissue. It consists of three parts, a central, triangular portion and two lateral portions. The central part is thick and strong, narrow above and broadening below. The lateral portions are thinner and lie close under the mucous membrane of the larynx. They extend from the superior border of the cricoid cartilage to the inferior margin of the vocal cords. The capsular ligaments enclose the articulations of the inferior cornus of the thyroid with the cricoid cartilage on each side.

Few quantitative studies can be found in the literature for non-vocal ligaments and connective tissues of the larynx except for some descriptions about where they are located based on observations during dissections. There are numerous studies on nonlaryngeal ligaments reported in the literature, however. Many experimental methods have been developed to measure the mechanical properties, i.e., the stress-strain behavior and viscoelastic and plastic properties, of ligaments [51,117]. In 1986, Woo and his colleagues studied the effects of freezing on the tensile behavior of ligaments [118]. Their results showed that freezing at -20^oC for up to three months had no effect on the ligament properties. These research results can serve as guidance for

the experiments which we may need to do in the future to evaluate the mechanical properties of laryngeal ligaments.

2.5 Conclusions

The following conclusions can be made from the literature survey:

- There was no existing dynamical model of the human larynx that describes the movement of the arytenoid cartilages. A few existing models of the cricoarytenoid joint were mainly built to interpret the observations of the dissections and were not connected to any muscle actions and real motion data.

- Anatomical data of the human laryngeal muscles is very limited. Among the available data, the variations were large. Very few studies of the mechanical properties of the human laryngeal muscles have been done. Therefore, we have to model the human laryngeal muscles based on what's available and make reasonable estimates for what is not available.

- There were a few quantitative studies of the human laryngeal cartilages. The main measurements taken were the cartilage dimensions and cricoarytenoid joint facet dimensions. The studies performed on the joint anatomy and its possible motion were mainly descriptive. Two types of motion of the arytenoid were agreed upon by many authors: (1) "rocking", and (2) "sliding" (although there was disagreement about how much it can slide). No detailed joint surface measurement has been made. There was no quantitative analysis done to link the joint anatomy and the observed motion. Our research concentrated on filling in

these gaps, which is a necessary step towards building a good joint model.

- The vocal ligament is the only ligament in the larynx that has been studied extensively. The study of other ligaments are still at the level of dissecting and describing. From the modeling point of view, the mechanical properties of the ligament, i.e. the stress-strain behavior and viscoelastic and plastic properties are the most relevant ones. There are well established experimental methods and tools to measure these properties once they are identified and dissected out. This is something that has to be done in the future so their roles in movement of the arytenoids can be better understood.

- Although the laryngeal cartilages may be modeled as rigid bodies, they are different from bones. The tip of the vocal process of the arytenoid bends at its extremal positions (maximum adduction and abduction). We have to keep this in mind when studying and interpreting the modeling results.

Chapter 3

Static Analysis of the Motion at the Cricoarytenoid Joint

3.1 Introduction

As is evident from the literature review in Chapter 2, the gross anatomy of the human cricoarytenoid joints has been studied by many researchers by means of dissection. Although the shapes of the joint facets have been described and their dimensions measured, no quantitative analysis has been performed which links the joint geometry to the motion of the arytenoids. The conclusion of the qualitative studies is that the most likely motion at the cricoarytenoid joint, allowed by the joint geometry, is a "rocking" motion. A "sliding" motion is possible (some claimed that it is very limited[101]). The "rocking" motion of the arytenoid is often described as the rotation of the arytenoid about an axis parallel to the long axis of the cricoarytenoid joint facet on the cricoid cartilage. This description implies the assumption that the cricoarytenoid joint is approximately a cylindrical joint and its motion can be approximated by a

pure rotation about one axis. The goal of the research described in this chapter is to perform a quantitative study of the joint anatomy and establish a relationship between the anatomy and the motion. In section 2 the 3D digitization and reconstruction of the joint facets is discussed. Based on the measurement data, a static motion analysis of the cricoarytenoid joints using optimization techniques is presented in section 3. Finally, in section 4, a comparison between the vocal process trajectories predicted by the optimization procedure and those obtained from the experiments of Selbie et al. [93] is given.

3.2 Analysis of the Joint Geometry

A three dimensional digitization of the entire joint facet was performed to obtain quantitative information about the joint facets. The resulting data was processed, and 3D color pictures of the facets were displayed on the Silicon Graphics' IRIS workstation.

3.2.1 3D Surface Digitization Technique

Digitizing the cricoarytenoid joint facet is a challenging problem in itself because of the small size and the wetness of the surface. Many advanced digitization techniques (those depending on surface reflections) do not work well with a wet surface[68]. After researching various options and comparing the cost, we decided to design our own digitization procedure using a milling machine. The table of the mill can be moved in three orthogonal directions to an accuracy of 0.02 mm. The position of the table can be used to determine the xyz coordinates of a point in 3D space.

Tools Required:

- A milling machine (This works better if it has digital readouts, in which case the machine's backlash is automatically eliminated).
- A dividing head. This is not required if the digitization only involves a small area of the cartilage.
- An indicator/probe with a sharp tip that can fit into the mill's tool chuck and be tightened.
- A cartilage holder. A piece of aluminum cylinder with two pins fastened to it was used in our experiment. The cartilage is held in place by inserting the pins into it.

Experimental Procedure:

The digitization experiment was performed in the Engineering Machine Shop at the University of Maryland under the supervision of a mechanic. The milling machine used is ACER's ULTIMA-3VK Vertical Turret Milling Machine with ACU-RITE's MillMate $x - y$ axis digital readout. The resolution of the mill table is 0.025 mm (0.001 in) in each direction. The indicator used is a dental tool (Stimulator) made by John O. Butler Company. The dividing head used is a very old one and the model and maker could not be identified. The measuring procedure is the following:

1. Mount the dividing head on the mill's table.
2. Mount the cartilage on the aluminum cylinder with the facet fully exposed. The two pins that hold the cartilage prevent it from moving (mainly rotating) during the experiment.

3. Mount the aluminum cylinder (along with the cartilage) into the clamp of the dividing head. The reason for using the dividing head is that we would like to be able to rotate the cartilage to obtain the best angle to do the measurements.

4. Mount the special indicator/probe into the mill's tool chuck. This indicator is used to make contact with the facet surface.

5. Move the mill's table so that the indicator's tip is in contact with the joint facet, then record the 3D coordinates of the contact point by reading out the table's xyz position.

6. Repeat step 5 by moving the table in a grid pattern until the entire area of the facet is covered.

The cricoarytenoid joint facets from two sets of cartilages were digitized using the above procedure (each set has four facets, two on the arytenoids and two on the cricoid). The cartilages were provided by the Voice and Speech Section of the NIH. They came from two male larynges (both in their 70's) preserved in formalin. The larynges were first sent to Duke University for MRI scans. After the MRI was completed, the cartilages were carefully dissected out and kept in formalin before the digitization took place. The joint facet area and some chosen landmark points to be digitized were physically marked on the cartilage. On each facet, 150 to 250 points were measured. These points were not evenly spaced, the distance between the points was from 0.127 mm (0.005 ins) to 0.381 mm (0.015 ins). Fewer points were measured in the flat areas and more in the rough areas. This is an advantage of digitizing by hand. Besides the points on the articulation facets, some landmark points on the

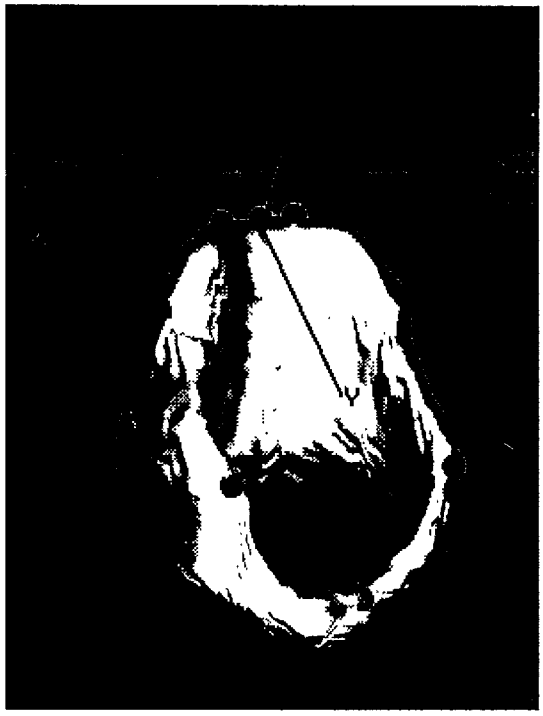

Figure 3.1: Position of the landmark points on the cricoid cartilage

corresponding cartilages were also measured. On the cricoid seven landmark points were measured, three on the top back of the ring, two on the top front of the ring and one on each side. On the arytenoid, two landmark points were measured, one at the tip of the apex and the other at the tip of the muscular process. Figure 3.1 is a reconstructed 3D picture of the cricoid cartilage (Selbie[94]) with the positions of those landmark points shown as black dots. Since the facet data was obtained separately from cartilage data (from MRI scan), there was no other reference between the two data sets. These landmark points were used later to fit the joint facet pictures on to the corresponding cartilage pictures to determine the approximate locations of the joint surfaces on the cartilages.

The digitization procedure can also be applied to the case where the entire

surface of a small irregular shaped object is to be digitized. Two whole arytenoid cartilages were digitized using the above procedure. The experiment was performed at the engineering machine shop of the University of Maryland. The situation becomes more complicated when the entire object is to be measured because the object has to be remounted at least a couple of times in order to cover its entire surface. In other words, different "views" of the object were obtained first, and then these views were put together using coordinate transformations. To define the coordinate transformation between view 1 and view 2, at least four reference points (A, B, C and D) must be marked and measured under both views. The only requirement for these points is that they are not co-planar. The measurement results are used to define the coordinate transformation between view 1 and view 2.

First define an orthogonal coordinate system fixed in the body of the measured object using the four reference points mentioned above in the following manner: a) choose point A as the origin of the coordinate system. b) choose the direction of the vector AB as the direction of the x axis. c) choose the plane defined by A, B and C as the x-y plane. d) choose the normal vector of the ABC plane as the z axis such that the angle between the normal vector and the vector AD is less than 90 degrees (i.e. the vector AD and the positive z axis are on the same side of the ABC plane). e) choose the y axis on the ABC plane such that it is orthogonal to the x axis and the directions of the x, y and z axes satisfy the right hand rule.

Second, find the transformation between the reference frame under which the data set is obtained and the fixed body coordinate system. This transformation is completely defined by the measurements of the four reference points and is given by

$$\begin{bmatrix} u \\ v \\ w \end{bmatrix} = T_2 T_1 \begin{bmatrix} x - x_A \\ y - y_A \\ z - z_A \end{bmatrix} \tag{3.2.1}$$

where (u, v, w) represents the fixed body frame and (x, y, z) the measurement frame. The transformation matrix T_1 is an orthogonal matrix defined as

$$T_1 = \begin{bmatrix} \cos\alpha\cos\beta & \sin\alpha\cos\beta & \sin\beta \\ -\sin\alpha\cos\gamma + \cos\alpha\sin\beta\sin\gamma & \cos\alpha\cos\gamma + \sin\alpha\sin\beta\sin\gamma & -\cos\beta\sin\gamma \\ -\sin\alpha\sin\gamma - \cos\alpha\sin\beta\cos\gamma & \cos\alpha\sin\gamma - \sin\alpha\sin\beta\cos\gamma & \cos\beta\cos\gamma \end{bmatrix} \tag{3.2.2}$$

where

$$\begin{aligned} \alpha &= \tan^{-1}\left(\frac{y_B - y_A}{x_B - x_A}\right) \\ \beta &= \tan^{-1}\left(\frac{z_B - z_A}{\sqrt{(x_B - x_A)^2 + (y_B - y_A)^2}}\right) \\ \gamma &= \tan^{-1}\left(\frac{n_C}{-m_C}\right) \\ n_C &= -(x_C - x_A)\cos\alpha\sin\beta - (y_C - y_A)\sin\alpha\sin\beta + (z_C - z_A)\cos\beta \\ m_C &= -(x_C - x_A)\sin\alpha + (y_C - y_A)\cos\alpha \end{aligned}$$

After obtaining the matrix T_1, we can transform the coordinates of point D into frame (u, v, w)

$$\begin{bmatrix} u'_D \\ v'_D \\ w'_D \end{bmatrix} = T_1 \begin{bmatrix} x_D - x_A \\ y_D - y_A \\ z_D - z_A \end{bmatrix} \tag{3.2.3}$$

The matrix T_2 can be determined by the sign of w'_D. If w'_D is is positive, let $T_2 = I$, otherwise let

$$T_2 = \begin{bmatrix} 1 & 0 & 0 \\ 0 & \cos\pi & \sin\pi \\ 0 & -\sin\pi & \cos\pi \end{bmatrix} = \begin{bmatrix} 1 & 0 & 0 \\ 0 & -1 & 0 \\ 0 & 0 & -1 \end{bmatrix} \tag{3.2.4}$$

The complete transformation matrix is given by $T = T_2 T_1$.

Given two sets of data measured under different reference frames, once the transformation matrix between each reference frame and the fixed body frame is determined, say by matrices T and T', then the transformation matrix between the two reference frames is easily obtained, which is $T^{-1}T'$.

Two arytenoid cartilages were digitized using the 3D digitization technique and the coordinate transformation method given above. Figure 3.2 is the wireframe picture of one of the arytenoid cartilages reconstructed based on the measurement data. The data was obtained from two different views and put together using the transformation method. The first set of data was obtained while the arytenoid cartilage was held at the base. Due to the fact that the bottom surface can not be reached by the indicator during the experiment, the entire base surface including the articulation facet could not be measured for this particular orientation of the cartilage. The second set of data was obtained while the arytenoid was held at the lateral part between the apex and the muscular process. Again, a part of the surface was missing from the data. The idea was to combine both data sets to get a complete picture of the arytenoid.

3.2.2 Estimation of the Measurement Error

The measurement error of the above digitization procedure comes from three sources: (1) Equipment error (the resolution of the milling machine in this case), (2) Human

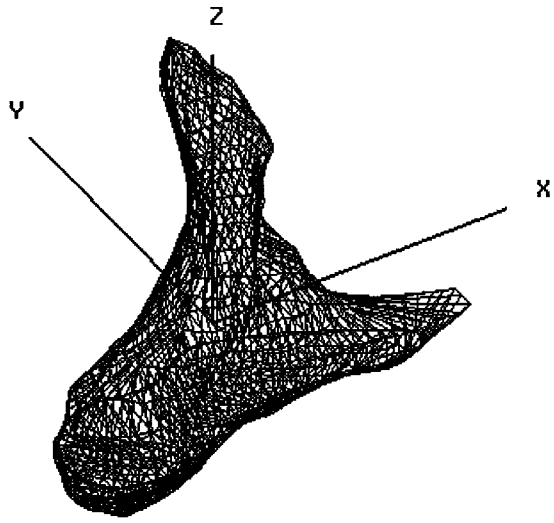

Figure 3.2: 3D wireframe picture of a human arytenoid cartilage

error (making judgement about the contact between the indicator and the cartilage surface), and (3) The error introduced by the coordinate transformation (when the entire cartilage is digitized). For the joint surface measurement, only the first two types of errors apply. The resolution of the mill is 0.025 mm (0.001 in), which implies that the systematic errors of the above digitization procedure introduced by the machine are very small. Then the accuracy of the procedure depends mainly on how accurately the operator can determine the contact point between the tip of the indicator and the cartilage surface. Since the contact was judged by human eyes, random errors were introduced. This type of error can be reduced by the carefulness of the operator. Several steps were taken to minimize the human error. First, the visibility of the contact area was improved by using high intensity lighting and positioning the cartilage at the best viewing angle (using the dividing head to allow rotation). Second, each

point was measured several times to make sure the readings could be repeated within a certain limit. Third, the experiment was performed by two people. The first one operated the milling machine and determined when the contact occurred. The second person read and recorded the data after a contact was declared. This person also determined whether a measurement should be repeated by comparing the consecutive measurements and whether a smaller step size should be taken by comparing the value of the current point with the value of its neighbor.

To estimate the human error, 16 randomly selected points on the joint surfaces (6 on the cricoid facet, 10 on the arytenoid facet) were measured repeatedly. For each point, two out of three coordinates of the mill table were fixed, the table was moved along the third direction (x-axis) until the tip of the indicator touched the cartilage surface, then the reading of this x-value was recorded. Each point was measured 10 times, all results were recorded. The mean error and the standarded deviation were then calculated using the data[113].

$$\bar{E} = \frac{1}{NM} \sum_{i=1}^{N} \sum_{j=1}^{M} |x_{ij} - \bar{x}_i| \tag{3.2.5}$$

$$SD^2 = \frac{1}{NM - N} \sum_{i=1}^{N} \sum_{j=1}^{M} (x_{ij} - \bar{x}_i)^2 \tag{3.2.6}$$

where N is the total number of points; M is the number of measurements for each point; x_{ij} is the value of ith point, jth measurement, and $\bar{x}_i$ is the mean value of point i. Table 3.1 shows the computation results.

From Table 3.1 we can see that the measurement of the cricoid facet is more accurate than that of the arytenoid facet. This is because the joint surface is concave

Table 3.1: Mean error and standard deviation for the digitization procedure

Joint Surface	N	M	Mean Error (mm)	SD (mm)	Error Range (mm)
Cricoid	6	10	0.014	0.020	-0.038 - 0.064
Arytenoid	10	10	0.027	0.036	-0.094 - 0.084
Combined	16	10	0.022	0.031	-0.094 - 0.084

on the cricoid cartilage and easier it to see when the contact occurred. The average dimension of the 8 joint surfaces digitized was approximately 5.0 mm, which implied that the mean error and the standard deviation are less than 1%. The worst case error is within 2%.

3.2.3 3D Reconstruction of the Cartilages and Joint Facets on the IRIS

Modern computer graphics technology provides us with ways of visualizing objects that were previously impossible. With the digitized facet data, the joint surface can be reconstructed in 3D and its features can be studied in detail.

The facet data was processed first in the following ways: (1)A rectangular mesh was collected. (2)A triangular mesh was generated by dividing each rectangle into two triangles. There are two ways to divide a rectangle into two triangles. We chose to connect the two opposite vertices with the smaller distance between them. (3)The surface normal vector at each vertex of the triangular mesh (i.e. at each data point) was calculated by averaging all the normal vectors of the surface triangles which share

Figure 3.3: Picture of a reconstructed cricoarytenoid joint facet

the same vertex.

Next, a computer software was developed on the IRIS workstation using the C programming language which reads in the triangularized data and the surface normals and displays a 3D color picture of the corresponding object, which in our case is the joint articulation surface. Figure 3.3 shows a shaded rendering of a cricoarytenoid joint facet on the right side of the cricoid.

Finally, the facet pictures were "fit" onto the corresponding pictures of the cartilages. To do this, the reconstructed cartilage picture (Selbie[94]) was first displayed on the computer screen, then the reconstructed joint surface picture along with the landmark points (measured using the mill) were displayed on the same screen. The landmark points were physically marked on the cartilage before the digitization of the joint surface took place, but they were not marked on the cartilage picture reconstructed from the MRI scan(Selbie[94]). Because there was no absolute reference between the two data sets, the "fit" between them is an approximation. The posi-

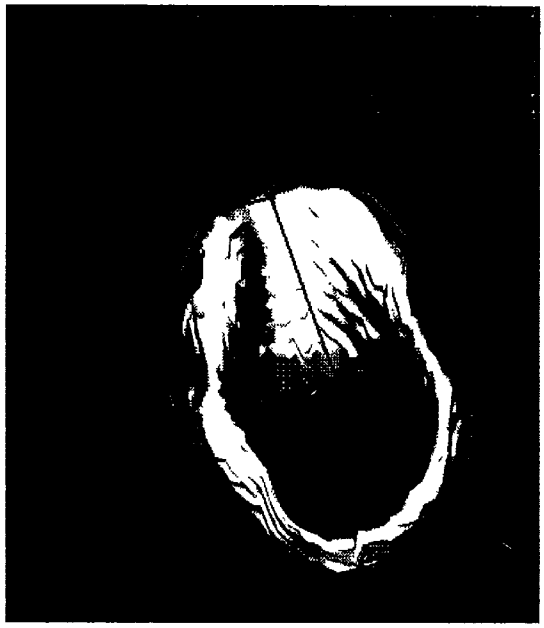

Figure 3.4: Picture of a reconstructed cricoid cartilage (Selbie[94]) with its joint facets

tion of the joint surface picture was manually adjusted until all the landmark points were placed at the approximate "right" place on the cartilage, judged by human eyes. This procedure was used to fit both the arytenoid facet and the cricoid facet picture onto their corresponding cartilage pictures reconstructed from MRI data (Selbie[94]). Figure 3.4 shows the picture of a cricoid cartilage with the facet picture (dark area) superimposed on it. See Section 3.3.5 for a sensitivity study of this "fitting" method.

3.3 Motion Analysis Using Optimization Techniques

The digitization of the joint facets allows us to predict the relative motion between the two joint surfaces quantitatively. The observations of the cricoarytenoid joint facets have shown that it is not cylindrical. However, two of the descriptions that have been given for the movement of the arytenoids involve motion about an axis of rotation.

If such a rotation is reasonable, we should be able to locate an axis such that the resulting rotation of the arytenoid about the axis is, at least, close to the real motion of the arytenoid. In this section, based on the assumption that the major motion at the cricoarytenoid joint is a rotation, the precise location of the best rotation axis is determined using the joint geometry data obtained in the previous section. The feasibility of a rotation about this axis is then studied.

3.3.1 Problem Formulation

To simplify the problem, only the rotation motion is considered. The cricoarytenoid joint is approximated by a pin joint. The joint axis can be represented by a straight line in 3D space. A straight line in 3D space can be defined by the intersection of two planes. For a given line, there are an infinite number of choices for such planes. Two special planes were chosen such that the resulting representation for the straight line has minimum number of parameters. One such special plane is the one parallel to the y axis and the other one is parallel to the x axis. Any line which does not lie in a plane parallel to the $x-y$ plane can be uniquely defined by the intersection of these two planes using four parameters (k_x, d_x, k_y, d_y) as follows:

$$\begin{aligned} x &= k_x z + d_x; \quad -\infty < k_x, d_x < \infty \\ y &= k_y z + d_y; \quad -\infty < k_y, d_y < \infty \end{aligned} \tag{3.3.1}$$

In the above definition, the orientation or slope of the planes is determined by parameters k_x and k_y. Parameters d_x and d_y determine the location of the planes with respect to the origin of the selected coordinate system. Figure 3.5 shows how the position and orientation of a plane parallel to the y axis varies as a function of

parameters d_x and k_x. Figure 3.6 shows an example of a line defined by two planes of the form (3.3.1).

Definition (3.3.1) leaves out a class of lines corresponding to $k_x, k_y = \pm\infty$, i.e. those which lie in a plane parallel to the $x-y$ plane. This class of lines can be defined using three parameters (k_z, d_z, z_0) as:

$$\begin{aligned} y &= k_x x + d_z; \quad && -\infty < k_z, d_z < \infty \\ z &= z_0; && -\infty < z_0 < \infty \end{aligned} \tag{3.3.2}$$

The second class of lines is treated separately from the ones defined by (3.3.1). For the coordinate system chosen to represent the joint surface data, it is very unlikely that the primary motion axis lies on the $x-y$ plane. Therefore in this chapter we refer to a line which has a representation of the form (3.3.1) unless otherwise specified. Those represented by (3.3.2) can be treated similarly if necessary.

Given representation (3.3.1), the problem becomes to find a set of parameters k_x, d_x, k_y, d_y such that the joint axis defined by (3.3.1), using the parameters, is anatomically feasible and, for the range of motion of the arytenoid, gives the best performance under a certain criterion. By anatomically feasible we mean that when the arytenoid rotates around this axis, within the normal range of motion, the real joint will not dislocate and the cartilages will not jam.

3.3.2 Performance Measure

There are many ways in which a criterion can be defined to measure the performance of the pin/cylinder joint model. The question is, which one is most realistic in the

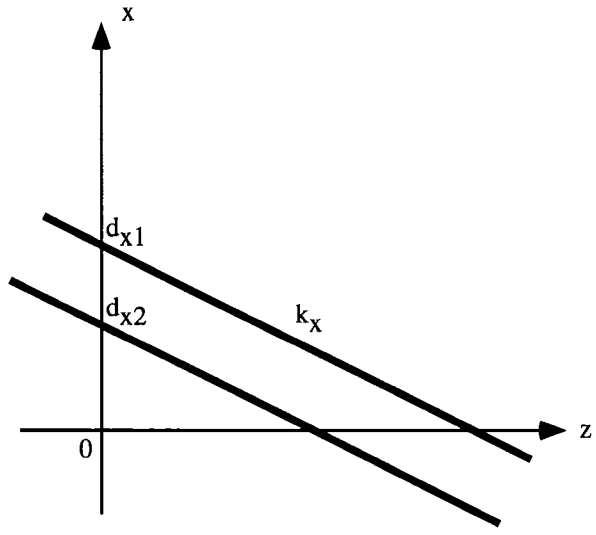

(a) Position of the plane as a function of d_x.

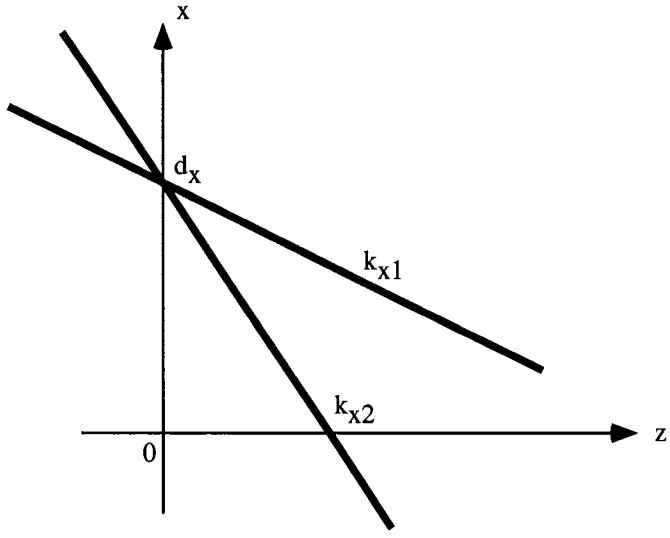

(b) Position of the plane as a function of k_x.

Figure 3.5: The position and orientation of a plane parallel to the y axis varies as a function of d_x and k_x

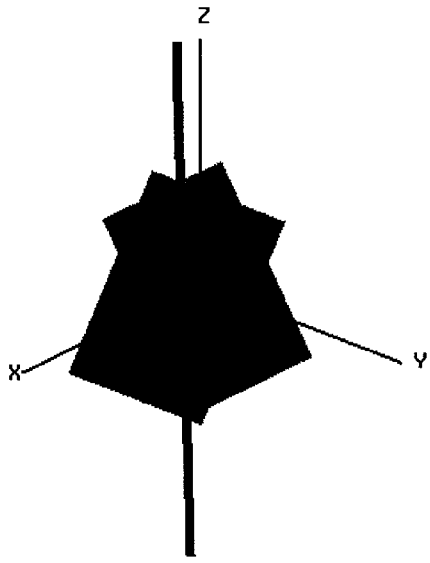

Figure 3.6: A line defined by the intersection of two planes

sense that it reflects what is actually happening in the human cricoarytenoid joint. It also depends on what information is available to us to make the evaluation. As far as the joint geometry is concerned, the only measurements available are the digitized joint facets of the cricoarytenoid joint on both the cricoid and the arytenoid cartilage and their relative position (approximation) obtained by fitting the digitized data to the MRI pictures of the cartilages, as described in the previous section. Therefore, one reasonable criterion to use would be the minimum variation in distance between the two joint surfaces as the arytenoid traverses its full range of motion. In other words, it is the minimum variance criterion. Under this criterion, the resulting joint axis will produce a motion for which the gap between the cricoid and the arytenoid joint facets is the most uniform one. The rationale for this choice is that, if the joint facets were ideal cylinders, they would fit perfectly, and the variation in distance between the two surfaces would be zero. But the real joint surfaces are not cylinders, they are more or

less elliptical. When one such surface moves on top of the other one, the variation in distance between them is no longer zero. A large variance would imply more squeezing of the fluid lubricants filling the joint gap and therefore more motion resistance. If a joint is able to move almost freely, this motion resistance must be small, i.e., the variance must be small for a realistic joint to work properly.

To precisely define this performance measure, it is necessary to define the distance between the two joint surfaces and the variance associated with it.

Suppose the cricoid facet consists of N_c discrete 3D points and at each point there is an associated surface normal vector. The surface normal is obtained by averaging the normals of the surface triangles for which the given point is one of their vertices. For a given joint axis, the arytenoid will rotate around it and the motion range will be between θ_1 and θ_2. The distance is defined as follows: Let the rotation angle be $\theta_k = \theta_1 + k\Delta\theta$, $k = 0, ..., K$, $\Delta\theta = (\theta_2 - \theta_1)/K$. For each data point on the cricoid facet, draw a radial line along the direction of the surface normal at that point, determine a point on the line where it crosses the arytenoid facet (this point is obtained using a trilinear interpolation of three vertices of the corresponding surface triangle) , then define the distance at that point to be the distance between the two points and denote it by $r_{ki}(k = 0, ..., K; i = 0, ..., N_c - 1)$, provided that there exists such a point. If not, it means that there is no arytenoid facet encounted along the surface normal passing through that point. In this case, we simply ignore the point and move on to the next point on the cricoid facet. Let the total number of points for which a distance can be defined be N_k. Note that a negative distance r_{ki} implies that interdigitation between the two facets has occured. For each $\theta_k \in (\theta_1, \theta_2)$, repeat the

above calculation, and define the average distance for the given joint axis to be

$$\bar{r} = \frac{1}{N} \sum_{k=0}^{K} \sum_{i=0}^{N_k} r_{ki} \tag{3.3.3}$$

where $N = \sum_{k=0}^{K} N_k$, and the variance associated with it is

$$Var = \frac{1}{N-1} \sum_{k=0}^{K} \sum_{i=0}^{N_k} (r_{ki} - \bar{r})^2 \tag{3.3.4}$$

Var is a function of the parameters k_x, d_x, k_y, d_y which define the joint axis.

By minimizing the variance given by (3.3.4), a joint axis can be located which produces the most uniform gap while the arytenoid rotates through its range of motion about this axis. But this process will not guarantee that there is no interdigitation between the two surfaces associated with the resulting axis. In order to penalize for the interdigitation due to inappropriate choice of the axis parameters, a cost function that is different from the variance is defined.

$$Cost = \frac{1}{N-1} \sum_{k=0}^{K} \sum_{i=0}^{N_k} (\hat{r}_{ki} - \bar{r})^2 \tag{3.3.5}$$

where $\hat{r}_{ki} = r_{ki}$ if $r_{ki} \geq 0$, and $\hat{r}_{ki} = 100 r_{ki}$ if $r_{ki} < 0$.

Applying this cost function instead of the variance (3.3.4), the optimization process will always move toward the direction of reducing interdigitation. It will eliminate those "bad" axes first due to their high cost, and then select the best one among the "good" ones. Once the process moves into the subspace consisting of those "good" axes, it is equivalent to the one using the minimum variance criterion.

Once the cost function is defined, the problem of finding the best joint axis under the minimum variance criterion becomes an unconstrained optimization problem: Find $u \in R^4$, such that $Cost(u)$ is minimized, where $u = (k_x, d_x, k_y, d_y)^T$.

3.3.3 Optimization Algorithms

In the previous sections we have formulated our problem as a multidimensional unconstrained optimization problem. There are well established theories and algorithms for solving this type of problem. Some of them will be discussed briefly in this section for the purpose of choosing an appropriate algorithm to solve our problem.

Consider optimization problems of the form

$$\begin{aligned} &\text{minimize} \quad f(u) \\ &\text{subject to} \quad u \in R^4 \end{aligned} \tag{3.3.6}$$

There are two kinds of solution points to problem (3.3.6): local minimum points and global minimum points. In formulating and attacking problem (3.3.6) we are, by definition, explicitly asking for a global minimum point of f in R^4. Practical reality, however, both from the theoretical and computational viewpoint, dictates that we must in many circumstances be content with a relative minimum point (local minimum). In deriving necessary conditions based on the differential calculus, for instance, or when searching for the minimum point by a convergent stepwise procedure, comparison of the values of nearby points is all that is possible and attention focuses on relative minimum points. Global conditions and global solutions can, as a rule, only be found if the problem possesses certain convexity properties that essentially guarantee that any relative minimum is a global minimum. Thus, by solving problem (3.3.6), we usually mean that we are finding a local minimum point.

Since most of the multidimensional minimization problems in reality can not be solved analytically, iterative methods are used in searching for the solutions. At each iteration, in general, two steps are involved: (1) determine a search direction

according to a fixed rule, and (2) find the point along this direction which minimizes the objective function (line search). The newly found point is then used as the starting point of the next iteration.

One of the oldest and most widely known methods of solving (3.3.6) is the **Steepest Descent** method[59]; it requires the gradient $\Delta f(u)$ of the objective function $f(u)$. The method is defined by the iterative algorithm

$$u_{k+1} = u_k - \alpha_k \Delta f(u_k) \tag{3.3.7}$$

where α_k is a nonnegative scalar minimizing $f(u_k - \alpha \Delta f(u_k))$. In words, from the point u_k we search along the direction of the negative gradient $-\Delta f(u_k)$ to a minimum point on this line; this minimum point is taken to be u_{k+1}. The method guarantees the descent in objective function at each iteration. Its disadvantage is that the speed of convergence can be very slow, especially near the solution.

The method with fastest convergence rate is **Newton**'s method. Its idea is to approximate $f(u)$ locally by a quadratic function, and this approximate function is minimized exactly. The method has very desirable properties if started sufficiently close to the solution point. Its order of convergence is two[60]. Newton's method requires the second partial derivatives of $f(u)$ (Hessian matrix); it also requires modification before it can be used at points that are remote from the solution (by introducing line search). The main concern with this method for us is the need to evaluate, store and invert the Hessian matrix, which makes it unpractical to use in our problem.

Somewhere between the method of steepest descent and Newton's method, there is a class of other methods. They are motivated by the desire to accelerate the typically slow convergence associated with steepest descent while avoiding the information re-

quirements associated with the Hessian matrix as required by Newton's method. One of the methods which belongs to this class is the **Conjugate Gradient** method. This method was invented initially to solve quadratic problems, but later generalized to solve nonquadratic problems as well[35]. The basic idea is not to have the algorithm follow the direction of the new gradient, but rather, a direction that is somehow constructed to be conjugate to the old gradient, and to all previous directions traversed. This choice of directions would improve the speed of convergence[60]. In the case where the Hessian matrix is available, the method becomes the pure form of Newton's method. No line searching is required at any stage. The introduction of line search can avoid the direct use of the Hessian matrix, but at the cost of the speed of convergence. One of the important conjugate gradient methods with line search is the Polak-Ribiere method[80]. For an n dimensional problem, the complete algorithm (using restarts) is:

- Step 1. Given u_0, compute $g_0 = \Delta f(u_0)$ and set $d_0 = -g_0$.
- Step 2. For $k = 0, 1, ..., n-1$:
  (a) Set $u_{k+1} = u_k + \alpha_k d_k$, where α_k minimizes $f(u_k - \alpha \Delta f(u_k))$.
  (b) Compute $g_{k+1} = \Delta f(u_{k+1})$.
  (c) Unless $k = n-1$, set $d_{k+1} = -g_{k+1} + \beta_k d_k$, where

$$\beta_k = \frac{g_{k+1}^T g_{k+1}}{g_k^T g_k}$$

.

- Step 3. Replace u_0 by u_n and go back to Step 1.

From the above review of the optimization algorithms, we think that the algorithm best suited for our case is the steepest descent or the conjugate gradient method. The reason for making the choice is that our problem is nonquadratic and there is no gradient or Hessian information available. The best we can do is to estimate the gradient using the finite difference method. Also, the convergence speed is not a major concern here.

3.3.4 Best Joint Axis

Computer software has been developed to solve problem (3.3.6) using the Conjugate Gradient algorithm with line search. Some C-language functions in the "Numerical Recipes in C [81]" were used in the simulation. Calculations were performed for the joint facets of the right side cricoarytenoid joint. The solution depends on the initial positions of the joint surfaces and the initial guess for the axis parameters. The initial positions of the joints were estimated from the MRI pictures which was the cadaver position. The main factor in the initial position is the gap between the two facets. Due to the inaccuracy of the MRI picture at the location of the joint facets, the joint gap obtained from the MRI picture is not an accurate measure of the actual joint gap of the cricoarytenoid joint. Different initial joint gaps were tested during the simulation and results were compared.

In order to test different joint gaps, another optimization process was designed to locate the best direction vector so that when the two facets were moved closer along this direction, the changes in variance along the path were minimal. In other words, this optimal direction allows us to move the facets closer while keeping the uniformity

of the gap between them. To formulate this optimization process mathematically, let's define the direction vector first. Suppose $(u\ v\ w)$ is a direction vector; it must satisfy the following condition:

$$u^2 + v^2 + w^2 = 1 \tag{3.3.8}$$

Any direction vector can be defined by two parameters (a, b) as follows:

$$\begin{aligned} u &= a \\ v &= b \\ w &= \sqrt{1 - (a^2 + b^2)}, \end{aligned} \tag{3.3.9}$$

where $a^2 + b^2 \leq 1$.

When moving a point $(x_0\ y_0\ z_0)$ along the direction $(u\ v\ w)$ by amount Δt, the resulting new position of the point is given by

$$\begin{aligned} x_1 &= x_0 + u\Delta t \\ y_1 &= y_0 + v\Delta t \\ z_1 &= z_0 + w\Delta t. \end{aligned} \tag{3.3.10}$$

For a given direction vector defined as above, the arytenoid facet can be moved along this direction by amount Δt to a new position. Let the movement range be between T_1 and T_2, and let $t_j = T_1 + j\Delta t$, $j = 0, \ldots, J, \Delta t = (T_2 - T_1)/J$. For each t_j, a variance in distance can be calculated using equation (3.3.4) with $K = 0$; we call it V_j. The cost function which measures the changes in variance along the path can then be defined as

$$C(a, b) = \sum_{j=0}^{J} (V_j - \frac{1}{J} \sum_{m=0}^{J} V_m)^2. \tag{3.3.11}$$

By minimizing $C(a,b)$, an optimal direction can be determined so that when the arytenoid facet is moved closer to the cricoid facet, the uniformity of the gap between them will be kept.

The difference between minimizing $C(a,b)$ and the cost function (3.3.5) defined in section 3.3.2 is that this is a constrained optimization problem:

$$\begin{aligned} &\text{minimize} \quad C(a,b) \\ &\text{subject to} \quad a^2+b^2 \leq 1 \end{aligned} \tag{3.3.12}$$

Problem (3.3.12) can be converted to the unconstrained problem of form (3.3.6) using the penalty method[60]. Introduce a penalty function into the cost function

$$P(a,b) = [max(0, a^2+b^2-1)]^2 \tag{3.3.13}$$

The resulting unconstrained problem has a cost function:

$$\tilde{C}(a,b) = C(a,b) + \mu P(a,b) \tag{3.3.14}$$

where μ is a positive constant (penalty coefficient, taken to be 100).

The penalty function P has a minimum value 0 only when the inequality constraint is satisfied. The unconstrained minimization problem can be solved in the same way as solving problem (3.3.6).

The cost functions defined by (3.3.5) and (3.3.14) were constructed solely from the measurement data, i.e., no smoothing of any kind was performed on the data; they are not nice smooth functions. Figure 3.7 is a plot of the variance (3.3.4) as a function of k_x only; the three other parameters are fixed. It can be seen that the function has a lot of small wiggles, especially when it is far from the solution. At those points, the partial derivatives of the cost function are not defined. However, this will

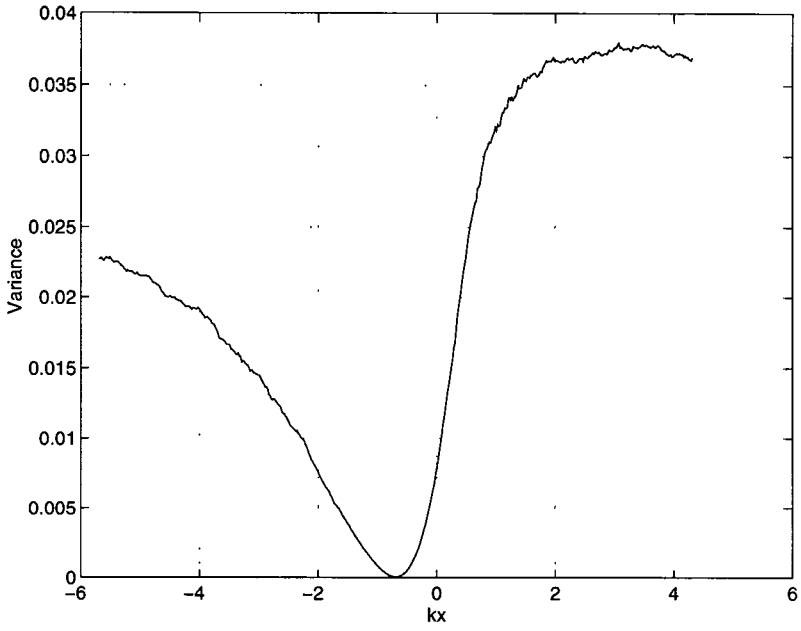

Figure 3.7: The variance as a function of k_x

not affect the algorithm much because the derivatives were estimated using the finite difference method so we will always have a direction to move along. The problem introduced by the lack of smoothness is the additional local minimum points of the cost function. The optimization algorithm can get stuck at any local minimum point. This problem exists even if the cost function is smooth. There are two ways to prevent this from happening. The first one is to start the algorithm from a good initial point in the parameter space (close to the solution). This requires some prior knowledge of the solution. Another way is to restart the algorithm after it converges from a point which is slightly different from the solution point (by adding a small random vector to the solution) in hope of jumping out of the local minimum. The second method is especially important in our situation. Both measures were taken in our computation.

The initial guesses of the joint axis were based on the knowledge obtained from the dissections, i.e., the "rocking" axis is parallel to the long axis of the cricoarytenoid joint facet on the cricoid, and the rotation axis, if it exists, is vertical to the joint facet.

The local minimum points introduced by the lack of smoothness of the cost function can be eliminated if the joint surfaces are smoothed prior to optimization. The performance of the optimization algorithm will be improved a great deal, once the small wiggles shown in Figure 3.7 disappear. However, it is generally better to minimize the processing of the data so the following results were obtained without smoothing the joint surfaces.

Results for Cartilage # 1

Optimization was performed using the measurement data of the right side cricoarytenoid joint facets. Three different starting joint gaps were tested. The first is at 0.63 mm, which is estimated from the MRI reconstruction of the cartilages. The other two gaps tested were 0.31 mm and 0.23 mm respectively. The motion range of the arytenoid was taken to be from -25^o to 25^o, with 0^o corresponding to the MRI (initial) position. This is the maximum range possible before the arytenoid falls off the cricoid cartilage.

The optimal direction vector used to move the facets closer (reducing the average joint gap) was:

$$\begin{aligned} x &= 0.310566 \\ y &= 0.128398 \\ z &= 0.941840 \end{aligned} \tag{3.3.15}$$

Table 3.2: Best "rocking" axis for Cartilage #1

Joint Gap (mm)	d_x (mm)	d_y (mm)	k_x	k_y	Final Cost (mm^2)
0.63	0.201968	0.0475546	-0.709527	-0.674101	4.877400e-05
0.31	0.186906	0.037207	-0.697890	-0.667660	4.901473e-05
0.23	0.179963	0.032212	-0.691917	-0.663541	4.984633e-05

To locate the best "rocking" axis, an initial guess of the joint axis parameters was made based on the assumption that it is parallel to the long axis of the cricoid facet. The four initial parameters and the associated cost are:

- Initial Parameters (for joint gap of 0.63 mm):

$$\begin{aligned} d_x &= 0.330604 \\ d_y &= 0.017307 \\ k_x &= -0.547773 \\ k_y &= -0.767629 \end{aligned} \tag{3.3.16}$$

- Initial Cost:

$$Cost = 7.126755e - 05 \tag{3.3.17}$$

Table 3.2 shows the solutions found by the optimization processes for three different initial joint gaps. The result corresponding to the average joint gap of 0.63 mm was obtained using the above initial guess. The results corresponding to an average joint gap of 0.31 mm were obtained using the final results of gap 0.63 mm as its initial conditions, and were in turn used as initial conditions for a joint gap of 0.23 mm. The

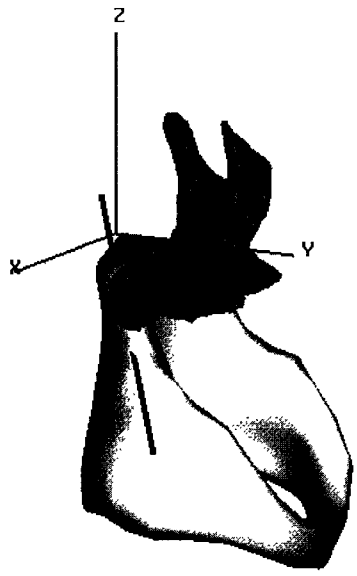

Figure 3.8: The location of the optimal "rocking" axis. Note that the axis passes through the cricoid cartilage below the joint facet

location of the optimal "rocking" axis obtained by the optimization algorithm for joint gap of 0.23 mm is shown in Figure 3.8.

To test the hypothesis that the arytenoid can rotate about an axis vertical to the joint facet, an initial axis that was vertical to the joint facet was used to start the simulation. The four initial parameters and cost are:

- Initial Parameters (for joint gap of 0.63 mm):

$$\begin{aligned} d_x &= 1.313803 \\ d_y &= 0.704306 \\ k_x &= 1.025626 \\ k_y &= 0.350486 \end{aligned} \tag{3.3.18}$$

Table 3.3: Best "vertical" axes for Cartilage #1

Joint Gap (mm)	d_x (mm)	d_y (mm)	k_x	k_y	Final Cost (mm^2)
0.63	2.659252	-0.412402	0.958763	0.625911	6.383532e-05
0.31	3.259868	-0.963002	0.9584173	0.626829	6.253566e-05
0.23	3.284337	-1.002707	0.938015	0.645088	6.425745e-05

- Initial Cost:

$$Cost = 1.642674e - 04 \tag{3.3.19}$$

Table 3.3 shows the solutions found by the optimization processes for three different initial joint gaps. The result corresponding to the average joint gap of 0.63 mm was obtained using the above initial guess. The results corresponding to an average joint gap of 0.31 mm were obtained using the final results of gap 0.63 mm as its initial conditions, and were in turn used as initial conditions for a joint gap of 0.23 mm. The location of the best "vertical" axis obtained by the optimization algorithm for joint gap of 0.23 mm is shown in Figure 3.9.

Results for Cartilage # 2

Optimization was performed using the measurement data of the right side crico-arytenoid joint facets. Two different starting joint gaps were tested. The first is at 0.52 mm, which is estimated from the MRI picture of the cartilages. The other one is 0.35 mm. The motion range of the arytenoid was taken to be from 0^o to 45^o, with 0^o corresponding to the MRI (initial) position.

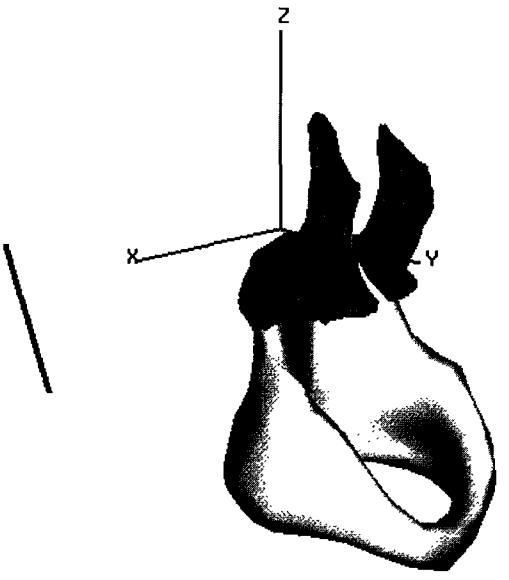

Figure 3.9: The location of the best "vertical" axis

The optimal direction vector used to move the facets closer (reducing the average joint gap) was:

$$\begin{aligned} x &= 0.789724 \\ y &= 0.002353 \\ z &= 0.613458 \end{aligned} \tag{3.3.20}$$

To locate the best "rocking" axis, an initial guess of the joint axis parameters was made based on the assumption that it is parallel to the long axis of the cricoid facet. The four initial parameters and the cost are:

Table 3.4: Best "rocking" axis for Cartilage #2

Joint Gap (mm)	d_x (mm)	d_y (mm)	k_x	k_y	Final Cost (mm^2)
0.52	0.219657	-0.128644	-1.830611	-2.024060	3.313791e-04
0.35	0.171039	-0.178575	-1.836661	-1.983561	3.629360e-04

- Initial Parameters (for joint gap of 0.52 mm):

$$\begin{aligned} d_x &= 0.244800 \\ d_y &= -0.537862 \\ k_x &= -1.403628 \\ k_y &= -2.947076 \end{aligned} \tag{3.3.21}$$

- Initial Cost:

$$Cost = 5.231973e - 04 \tag{3.3.22}$$

Table 3.4 shows the solutions found by the optimization processes for two different initial joint gaps. The result corresponding to the joint gap of 0.52 mm was obtained using the above initial guess, and was used as initial condition for a joint gap of 0.35 mm.

To test the hypothesis that the arytenoid can rotate about an axis vertical to the joint facet, an initial axis that was vertical to the joint facet was used to start the simulation. The four initial parameters and cost are:

Table 3.5: Best "vertical" axes for Cartilage #2

Joint Gap (mm)	d_x (mm)	d_y (mm)	k_x	k_y	Final Cost (mm^2)
0.52	1.178532	0.343202	0.952091	0.125826	4.047163e-04
0.35	1.633068	0.070628	1.329215	-0.090091	6.743874e-04

- Initial Parameters (for joint gap of 0.52 mm):

$$\begin{aligned} d_x &= 1.891221 \\ d_y &= 0.354464 \\ k_x &= 0.793872 \\ k_y &= 0.864431 \end{aligned} \tag{3.3.23}$$

- Initial Cost:

$$Cost = 6.959176e - 04 \tag{3.3.24}$$

Table 3.5 shows the solutions found by the optimization processes for two different initial joint gaps. The result corresponding to the joint gap of 0.52 mm was obtained using the above initial guess, and was used as initial condition for a joint gap of 0.35 mm.

Discussion

The results listed in Table 3.2 through Table 3.5 all correspond to feasible rotation axes of the arytenoid as far as the joint surface geometry is concerned. Several consistent observations were made based on these results:

1. For both cartilages tested, the "rocking" axis is the optimal axis of the cylindrical joint model of the cricoarytenoid joint.

2. Although a feasible axis was found for the rotation about an axis vertical to the joint facet, this solution is only a local minimum point of the cost function. Therefore it is not the optimal joint axis.

3. The vertical axis found by the optimization process does not pass through the joint but rather is located outside the cartilage. The resulting motion of the arytenoid rotating about this axis looks more like sliding than rotation.

4. The absolute "vertical" axis refered in the literature is NOT a solution to the optimization problem.

5. For different joint gaps, the solutions differ only slightly, provided that the facets were moved closer along the optimal direction.

Besides the rocking and the vertical axes, other initial joint parameters were used during the simulation to test the optimization algorithm as well as ensure that the results obtained for the rocking axis were not some local minimums of the cost function. With larger joint gap (e.g. 0.63 mm), it seems that the algorithm always converges to a feasible axis, although the final costs are larger than the one corresponding to the rocking axis given in Table 3.2 and Table 3.4. But as the joint gap becomes smaller, the chances of getting such feasible axes for the normal range of motion becomes smaller as well. For example, for Cartilage #1, when the joint gap is at 0.20 mm, a feasible rocking axis with motion range from -25^o to 25^o can still be found, but for the same to happen for the vertical axis, the motion range has to be reduced to -12^o

to 12^o. The smallest starting gap (with no interdigitation) found is 0.19 mm. At this distance even the motion range for rocking has to be limited in order to find a feasible rocking axis. This result is not against common sense, when a joint is heavily loaded, its flexibility will be significantly reduced. One reason behind this is that when the joint is pressed hard, the joint spacing becomes smaller. Therefore its motion range becomes limited. Of course, loading will also change the shape of the joint facets.

All the estimates obtained so far (from MRI and laryngeal slices) have indicated a spacing (joint gap) between 0.1 mm and 0.6 mm in the cricoarytenoid joint. To verify whether the estimation is reasonable, we checked the standard recommendations for the clearance limit in mechanical bearings. The clearance limits for loose-running fits between plain cylindrical parts recommended by the ANSI B4.1-1967 (R1979) standard is between 0.1 and 0.4 mm. Since the cricoarytenoid joint is not an ideal cylinder, the two joint surfaces cannot fit as well as those in a mechanical bearing; a larger average distance is expected here. Therefore, the estimated joint gap is reasonable. The initial joint gaps obtained from the MRI pictures were slightly larger (0.63 mm and 0.52 mm). The subsequent ones tested in the simulation were well within the range of the estimation.

The characteristics of the cost function (3.3.5) near the solutions were also studied. 3D surface plots and the corresponding 2D contour plots were made for the cost function of Cartilage #1 by varying two of the four parameters at a time. Figures 3.10 - 3.15 are the plots associated with the rocking axis, i.e. the cost function in the neighborhood of the optimal rocking axis given in Table 3.2. Figures 3.10 - 3.12 correspond to the joint gap of 0.63 mm. Figures 3.13 - 3.15 correspond to the joint gap

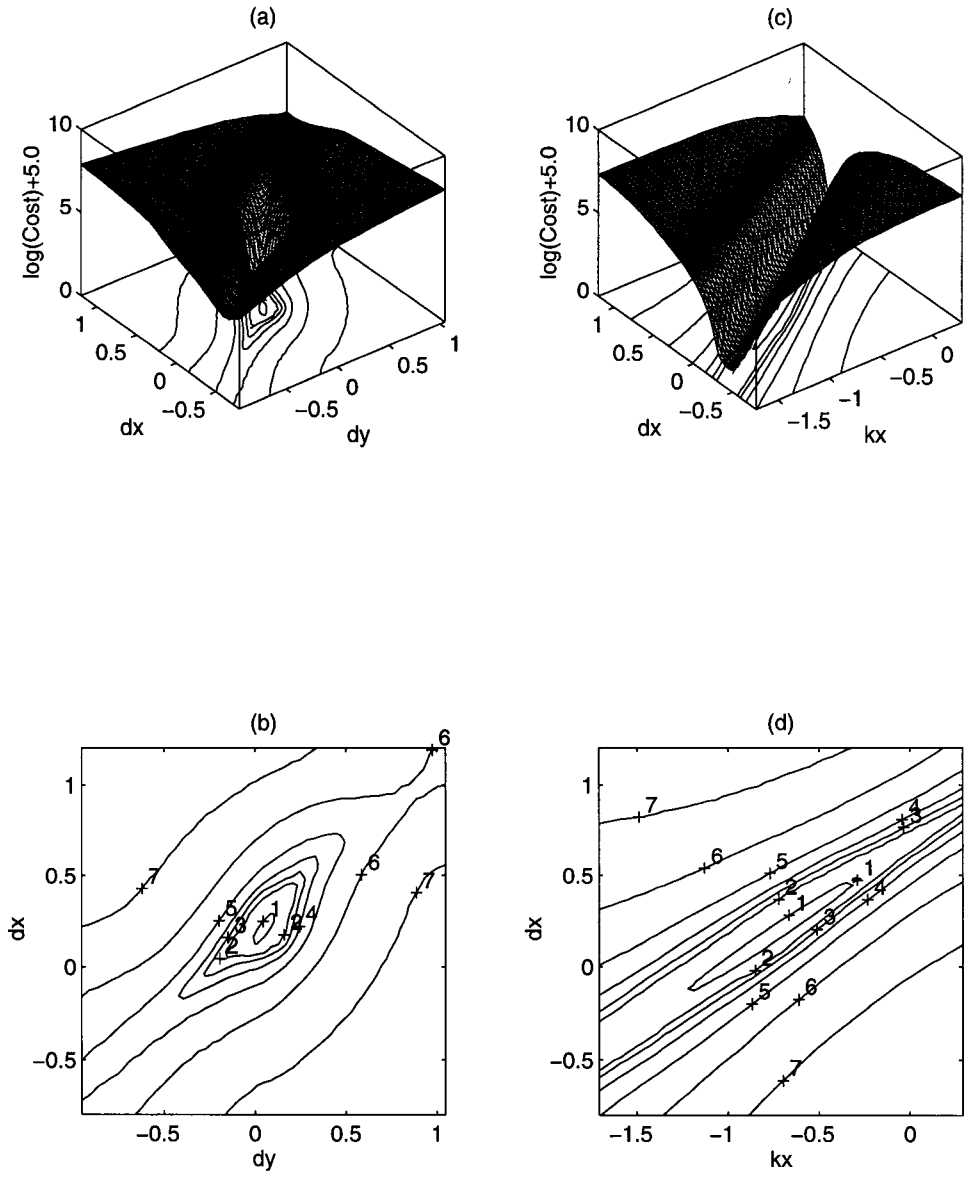

Figure 3.10: Surface and contour plot of the cost function for Cartilage #1 in the neighborhood of the optimal rocking axis (joint gap = 0.63 mm). (a)(b): Cost vs. d_x and d_y; (c)(d): Cost vs. d_x and k_x

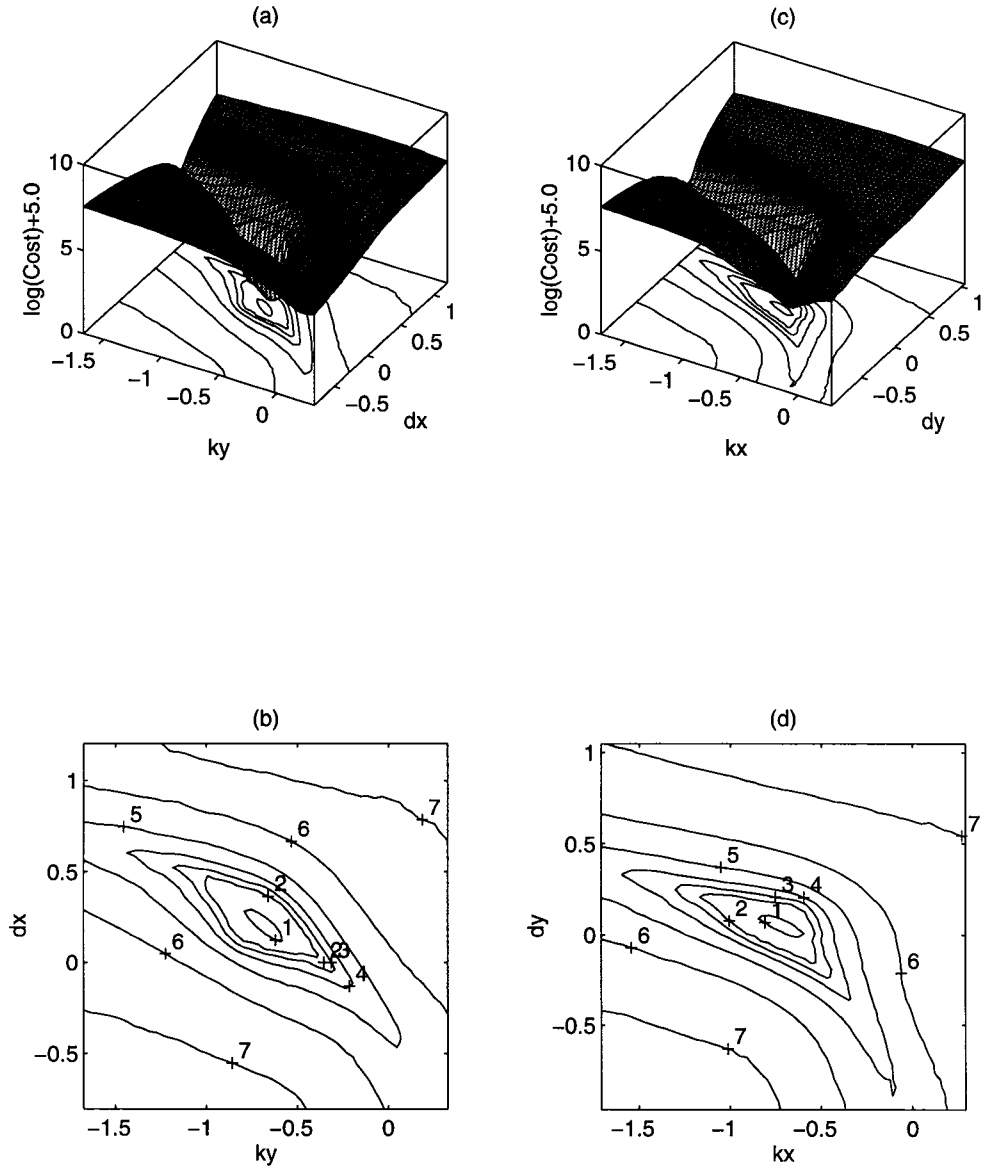

Figure 3.11: Surface and contour plot of the cost function for Cartilage #1 in the neighborhood of the optimal rocking axis (joint gap = 0.63 mm). (a)(b): Cost vs. d_x and k_y; (c)(d): Cost vs. d_y and k_x

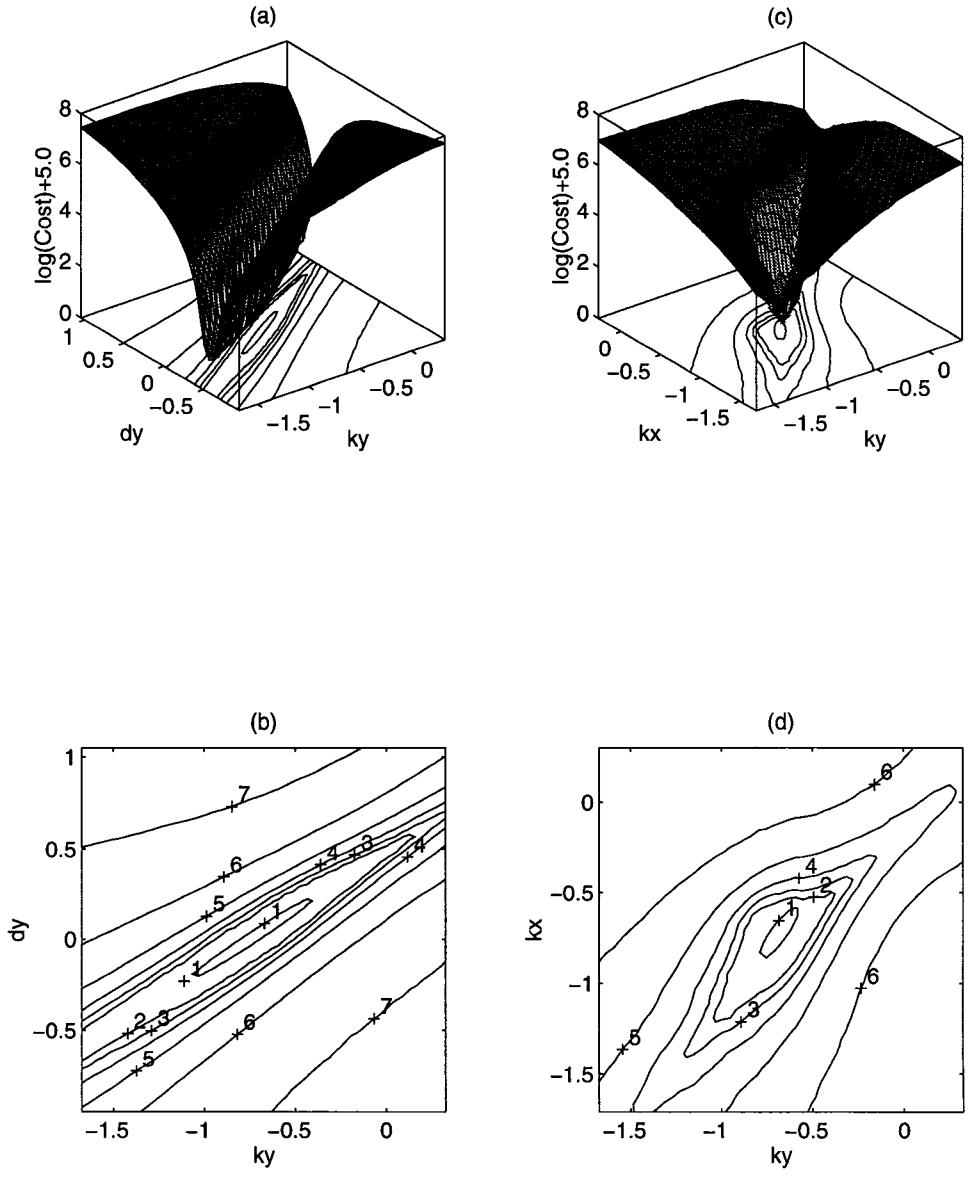

Figure 3.12: Surface and contour plot of the cost function for Cartilage #1 in the neighborhood of the optimal rocking axis (joint gap = 0.63 mm). (a)(b): Cost vs. d_y and k_y; (c)(d): Cost vs. k_x and k_y

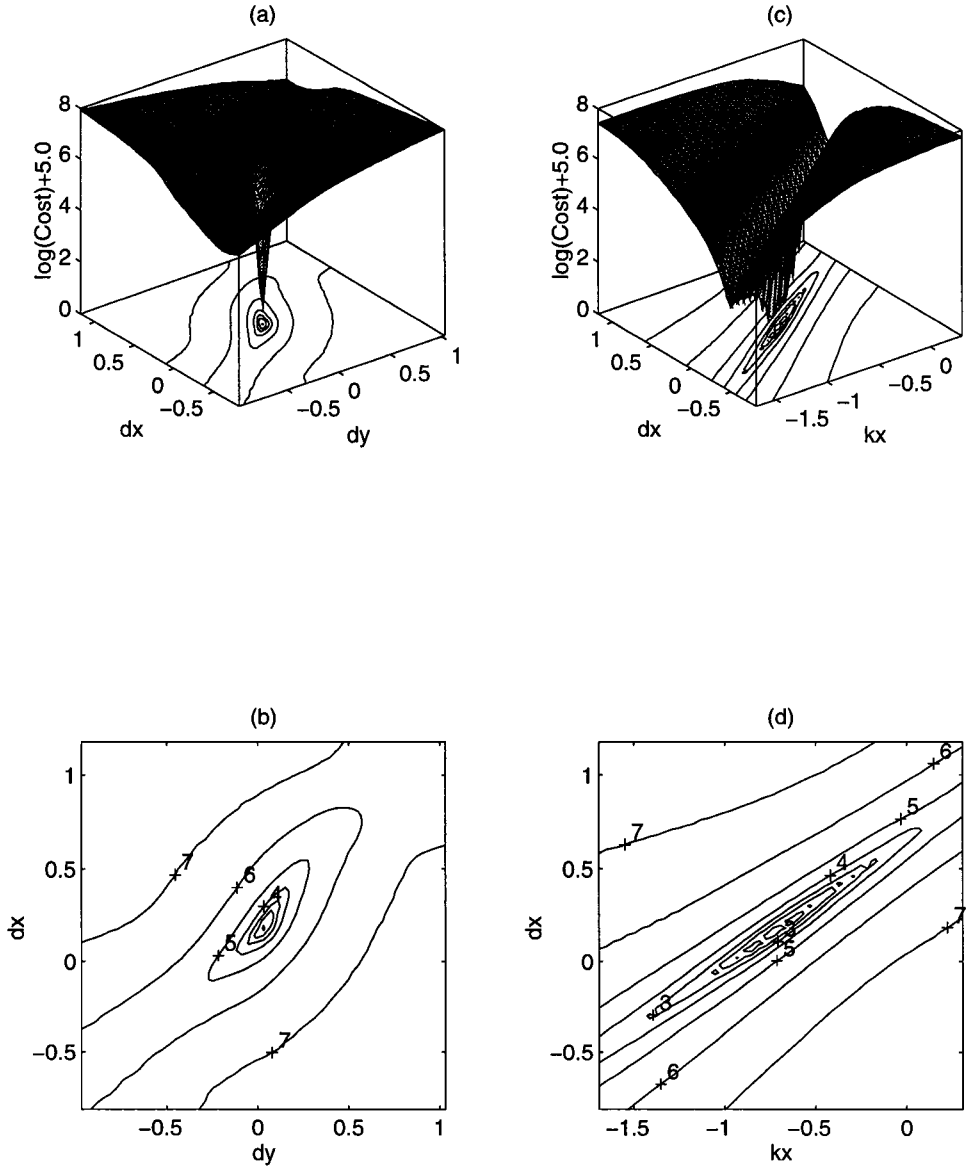

Figure 3.13: Surface and contour plot of the cost function for Cartilage #1 in the neighborhood of the optimal rocking axis (joint gap = 0.23 mm). (a)(b): Cost vs. d_x and d_y; (c)(d): Cost vs. d_x and k_x

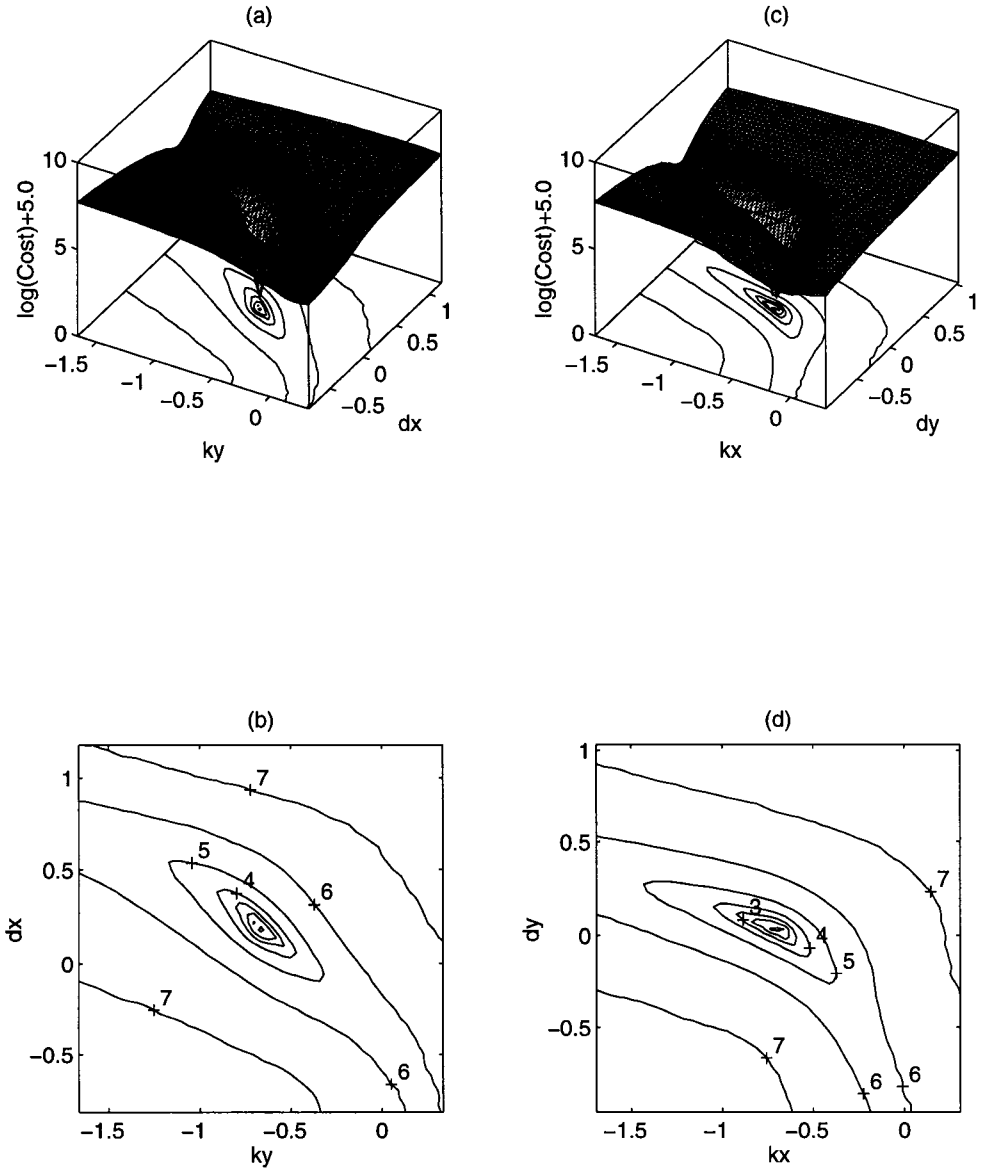

Figure 3.14: Surface and contour plot of the cost function for Cartilage #1 in the neighborhood of the optimal rocking axis (joint gap = 0.23 mm). (a)(b): Cost vs. d_x and k_y; (c)(d): Cost vs. d_y and k_x

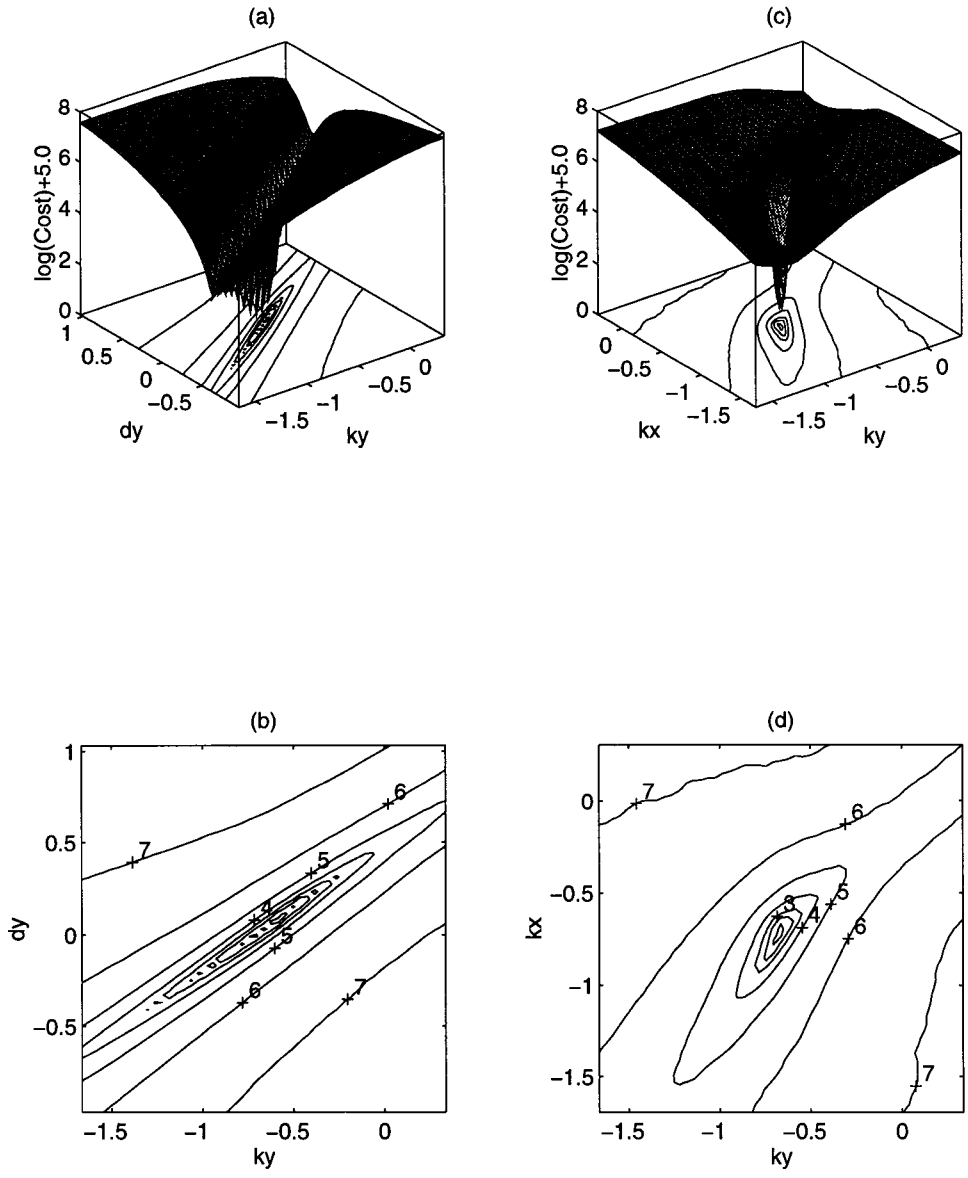

Figure 3.15: Surface and contour plot of the cost function for Cartilage #1 in the neighborhood of the optimal rocking axis (joint gap = 0.23 mm). (a)(b): Cost vs. d_y and k_y; (c)(d): Cost vs. k_x and k_y

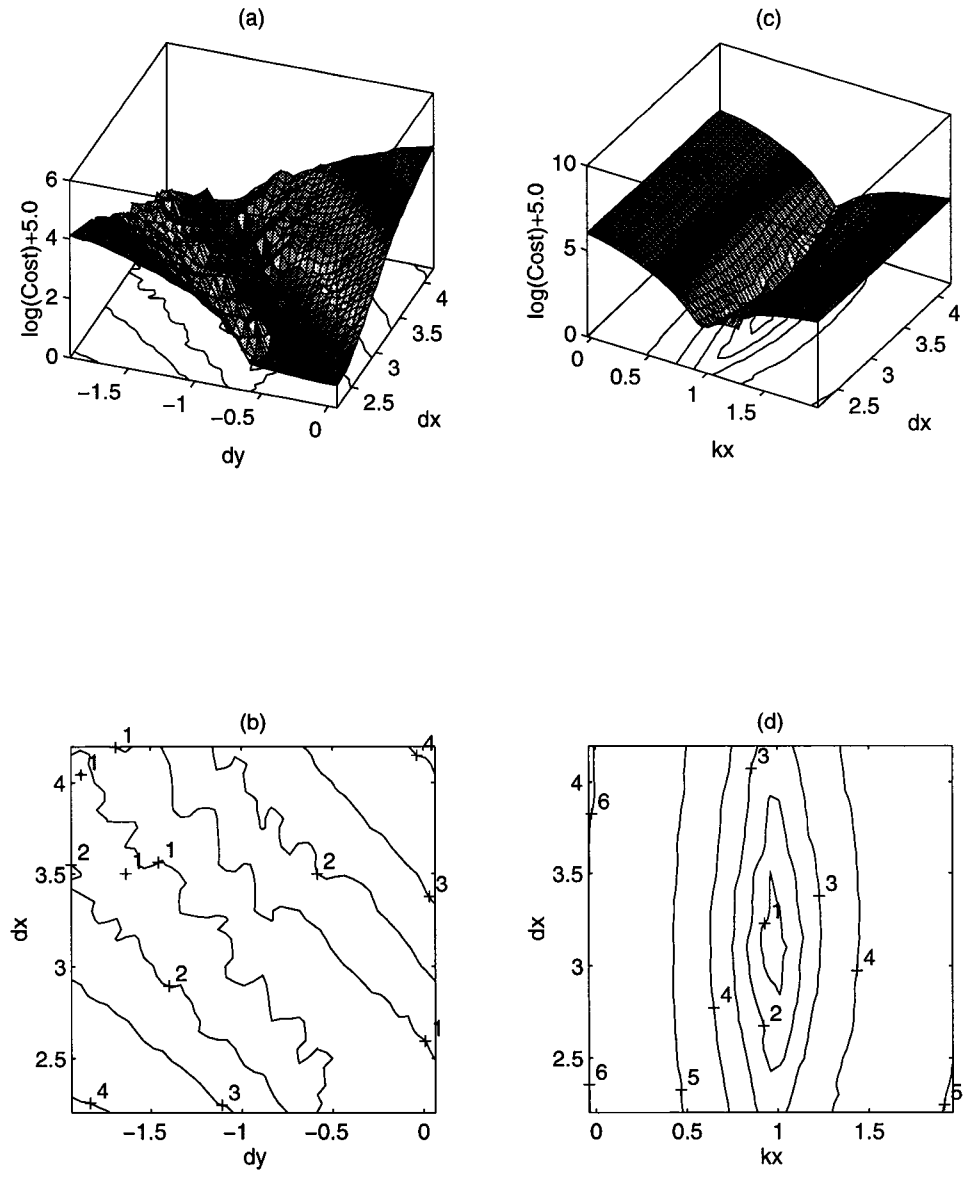

Figure 3.16: Surface and contour plot of the cost function for Cartilage #1 in the neighborhood of the best vertical axis (joint gap = 0.23 mm). (a)(b): Cost vs. d_x and d_y; (c)(d): Cost vs. d_x and k_x

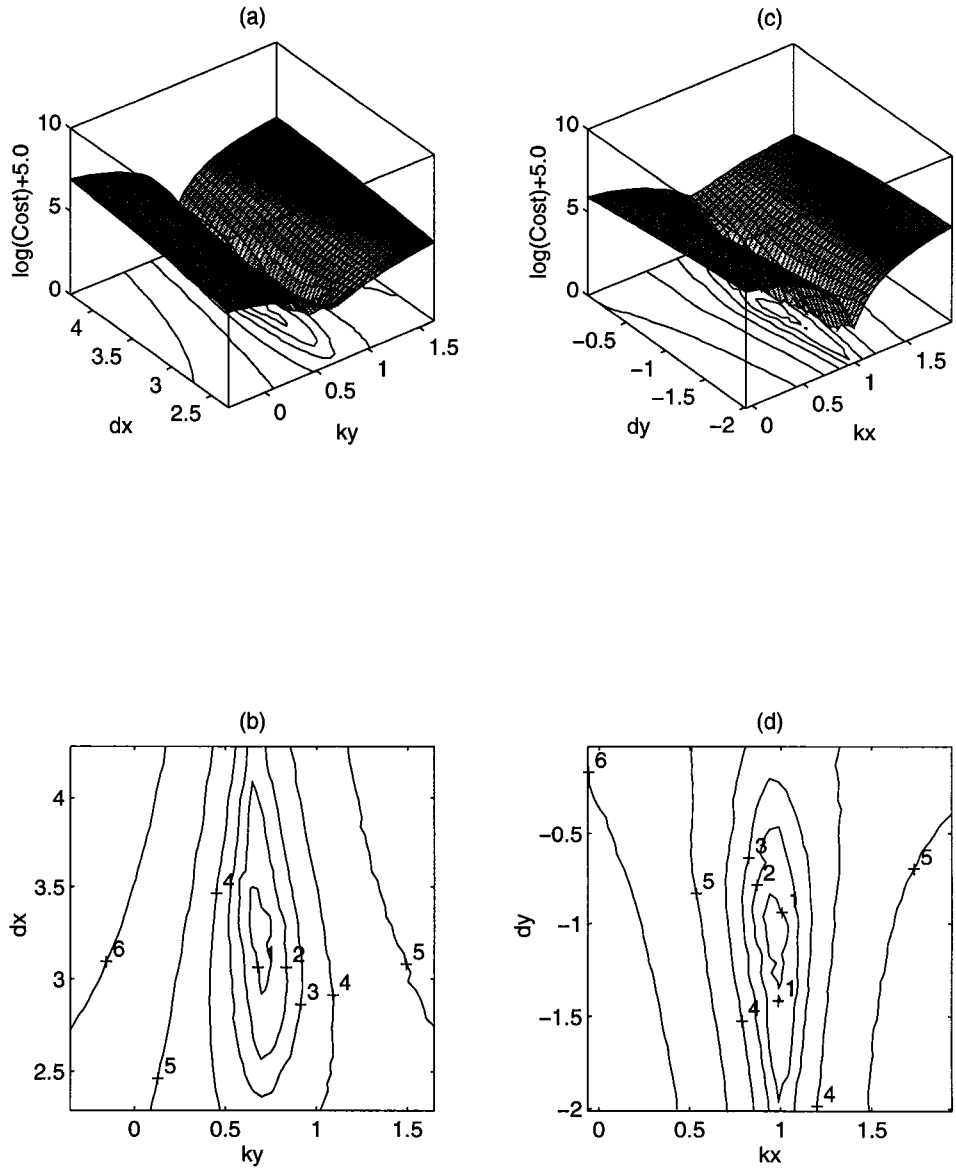

Figure 3.17: Surface and contour plot of the cost function for Cartilage #1 in the neighborhood of the best vertical axis (joint gap = 0.23 mm). (a)(b): Cost vs. d_x and k_y; (c)(d): Cost vs. d_y and k_x

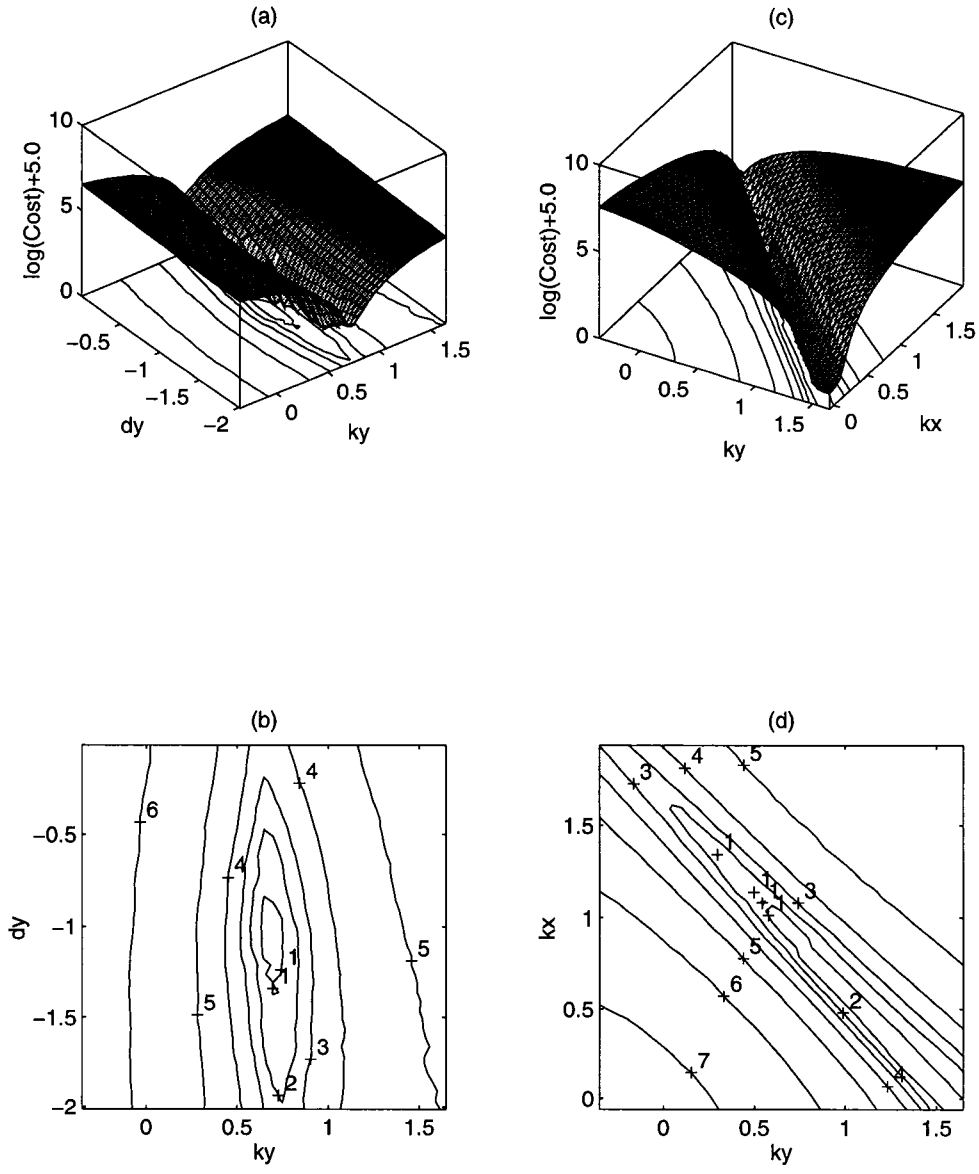

Figure 3.18: Surface and contour plot of the cost function for Cartilage #1 in the neighborhood of the best vertical axis (joint gap = 0.23 mm). (a)(b): Cost vs. d_y and k_y; (c)(d): Cost vs. k_x and k_y

of 0.23 mm. Figures 3.16 - 3.18 are the plots associated with the vertical axis given in Table 3.3 with joint gap of 0.23 mm. In each figure, plot (a) and (c) are the surface plots and (b) and (d) are the contour plots of the cost function as two parameters vary in the neighborhood of their final values, while the other two are fixed at their final(optimal) values. In these figures the cost function was plotted using a log scale rather than linear scale because the minimum value is too small (at the level of 10^{-5}) to show on the linear scale. From the surface plots associated with the rocking axis we can see that near the solution, the cost function is quite smooth, just like the one predicted by the one dimensional plot (Figure 3.7). Within the range of the plots, there are no obvious local minimum points. The solution point (at the center of each plot) is well defined in the sense that the value of the cost function at this point is much smaller than the values of its surrounding points in four out of six plots. In two plots (Figure 3.13(c) and Figure 3.15(a)), there exists a deep valley, which corresponds to the feasible axes. The existence of this valley implies that we can move one of the planes (change the two parameters in a linear fashion) while keeping the other one fixed without causing interdigitation between the two facets and a big increase in the variance. This room for maneuver exists because (1) there is still distance between the two facets, and (2) the two joint surfaces do not fit as nicely as an ideal cylinder; in this particular case, the bottom part of the surface fits tighter than the top part; therefore, one end of the joint axis can move slightly while the other end cannot. As the distance between the two surface becomes smaller, this valley becomes more narrow. For the vertical axis, the characteristics of the cost function surfaces are quite different. From Figure 3.16 (a) we can see that, as long as the orientation of the axis is fixed, the axis can be moved (theoretically) all the way to infinity without causing interdigitations

between the two surfaces. The true sliding motion is a rotation about a axis located at infinity. In general, the surfaces shown in Figures 3.16 - 3.18 are much flatter than the ones for the corresponding rocking axis; this was caused by the flatness of the cricoid facet along the direction of its long axis.

Although there is no guarantee that the solutions given in Table 3.2 and Table 3.4 were the global minimums for our problem, no other solutions have been found which have smaller costs after numerous trials from different starting points. So for now it is reasonable to conclude that the rocking axis is the global optimal axis under the minimum variance criterion.

3.3.5 Sensitivity of the Surface Alignment

The cost function J does not only depend on the four axis parameters but also on the relative position between the two joint surfaces of the same joint. As mentioned above, the joint surface alignment was determined by fitting the joint surface pictures onto the cartilage pictures reconstructed from the MRI data (Selbie [94]) using some landmark points. This procedure will introduce some error. The relative position between the two surfaces depends on six parameters: three translations and three rotation angles between the two reference frames that define the two surfaces. To study the effect of the alignment error on the solutions presented in the previous section, we must first define the reference frames and the position parameters. The reference frame on the cricoid facet was chosen in the following way: first select a point on the center of the surface to be the origin; then use the direction of the surface normal at that point to define axis w; the u axis is chosen to be perpendicular to the w axis and its direction

is along the direction of the longitudinal axis of the cricoid facet; the v axis is chosen such that it is perpendicular to the plane defined by u and w, and the directions of the u, v and w axis satisfy the right hand rule. Such a choice of reference frames is shown in Figure 3.19 (left). The local reference frame for the arytenoid facet is obtained by first translating the cricoid reference frame to a point on the center of the arytenoid facet and then rotating this frame about u-axis by an angle a , about v-axis by an angle b and about the w-axis by an angle c. Note that these angles can have arbitrary values since we can select any coordinate system to be the local reference frame for the arytenoid facet. The resulting coordinate system is used as the reference frame for the arytenoid facet (Figure 3.19 (right)). The transformation between the two reference frames is determined by six parameters (u v w a b c). Among them, (u v w) is a vector from the origin of the cricoid frame to the origin of the arytenoid frame expressed in the cricoid coordinate system, and a is the rotation angle of the arytenoid frame about the u-axis of the the cricoid frame; b is the rotation angle of the arytenoid frame about the v-axis of the cricoid frame; c is the rotation angle of the arytenoid frame about the w-axis of the cricoid frame. If we fix the cricoid facet, then the location of the arytenoid facet is uniquely defined by these six parameters.

Once the two reference frames are chosen, the effect of the misalignment between the two surfaces can be studied. To have a general idea about how each of the six parameters will affect the cost function at the solution point, the cost J of Cartilage #1 with a nominal joint gap of 0.31 mm was plotted against each of the six parameters mentioned above. The cricoid facet was fixed and the nominal position of the arytenoid

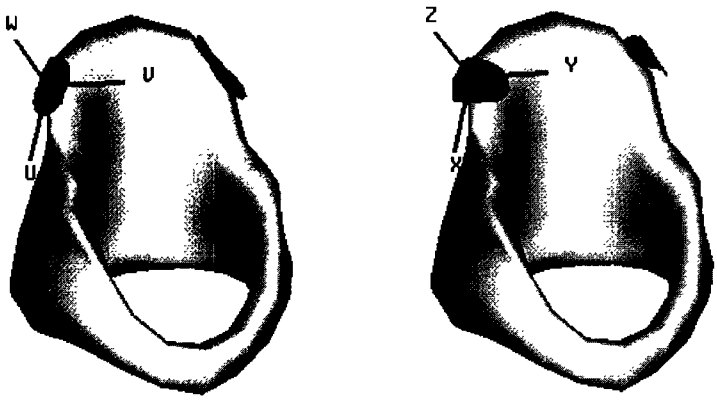

Figure 3.19: Local reference frames for the joint surfaces. Left (U-V-W): cricoid facet; Right (X-Y-Z): arytenoid facet. Cartilage pictures by Dr. Selbie[94].

facet was given by

$$\begin{aligned} u_0 &= -0.004176\ cm \\ v_0 &= 0.072370\ cm \\ w_0 &= 0.018829\ cm \\ a_0 &= 0.017453\ rad \\ b_0 &= 0.017453\ rad \\ c_0 &= 0.017453\ rad \end{aligned} \tag{3.3.25}$$

Figure 3.20 shows how the cost for the optimal "rocking" axis varies as each of the six parameters is moved away from its nominal value. Figure 3.21 is the corresponding plots for the best "vertical" axis. The length of the horizontal interval for these plots is 0.1 cm for the three translation parameters and 0.1 rad for the three rotation angles. Note that the plots for cost vs. v and cost vs. w have much larger vertical scales than the rest of the plots for both figures. This indicates that when the arytenoid facet is moved in these two directions, particularly in the negative w

direction, to a certain point, the two surfaces cross each other resulting in a large increase in cost (the penalty). This holds true for both the rocking and the vertical axes. In other directions, the costs do not change as much within the parameter range studied.

Figure 3.20 and 3.21 give an overall picture of how the relative position of the two joint surfaces will affect the solution. To estimate the sensitivities of the cost function at the solution point, we need to look at the variations of the cost in the neighborhood of the solution point. Suppose F is a function of x, the normalized differential sensitivity S_x^F at point x_0 is defined as[8]

$$S_x^F = \frac{\Delta F/F_0}{\Delta x/x_0}|_{\Delta x->0} \tag{3.3.26}$$

In our case, the cost function J is defined using discrete measurement data; it is not a smooth function. There are many discontinuous points of J at which the partial derivative of J with respect to one or more of the six parameters is not defined. The solution point obtained in the previous section is one such point because the optimization procedure pushed the parameters to a corner of the performance criterion. To see the nonsmoothness of the cost function in the neighborhood of the solution point, the same figures (Figure 3.20 and 3.21) were plotted using a much smaller horizontal scale (10^{-3}). The resulting plots are Figure 3.22 for the "rocking" axis and Figure 3.23 for the "vertical" axis. To estimate the component-wise sensitivities for this discontinuous cost function J, we let ΔJ be the difference between the maximum and minimum value of J in the given interval, and let Δx be the length of the interval. The S_x^J at point x_0 is then calculated according to 3.3.26. The same method was used to calculate the component-wise sensitivities for the four optimal axis parameters d_x,

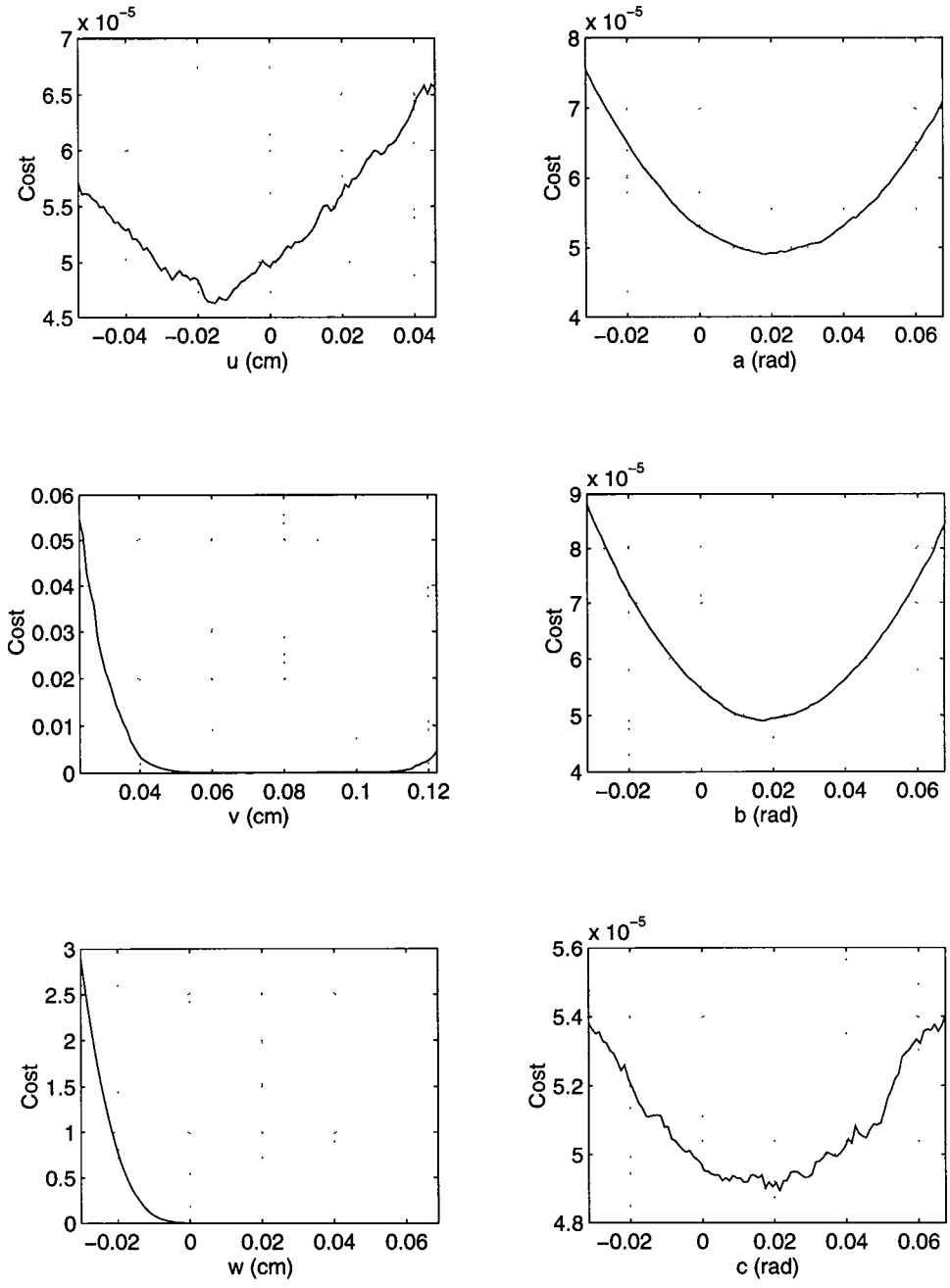

Figure 3.20: The cost function for the optimal "rocking" axis varies as a function of each of the six position parameters.

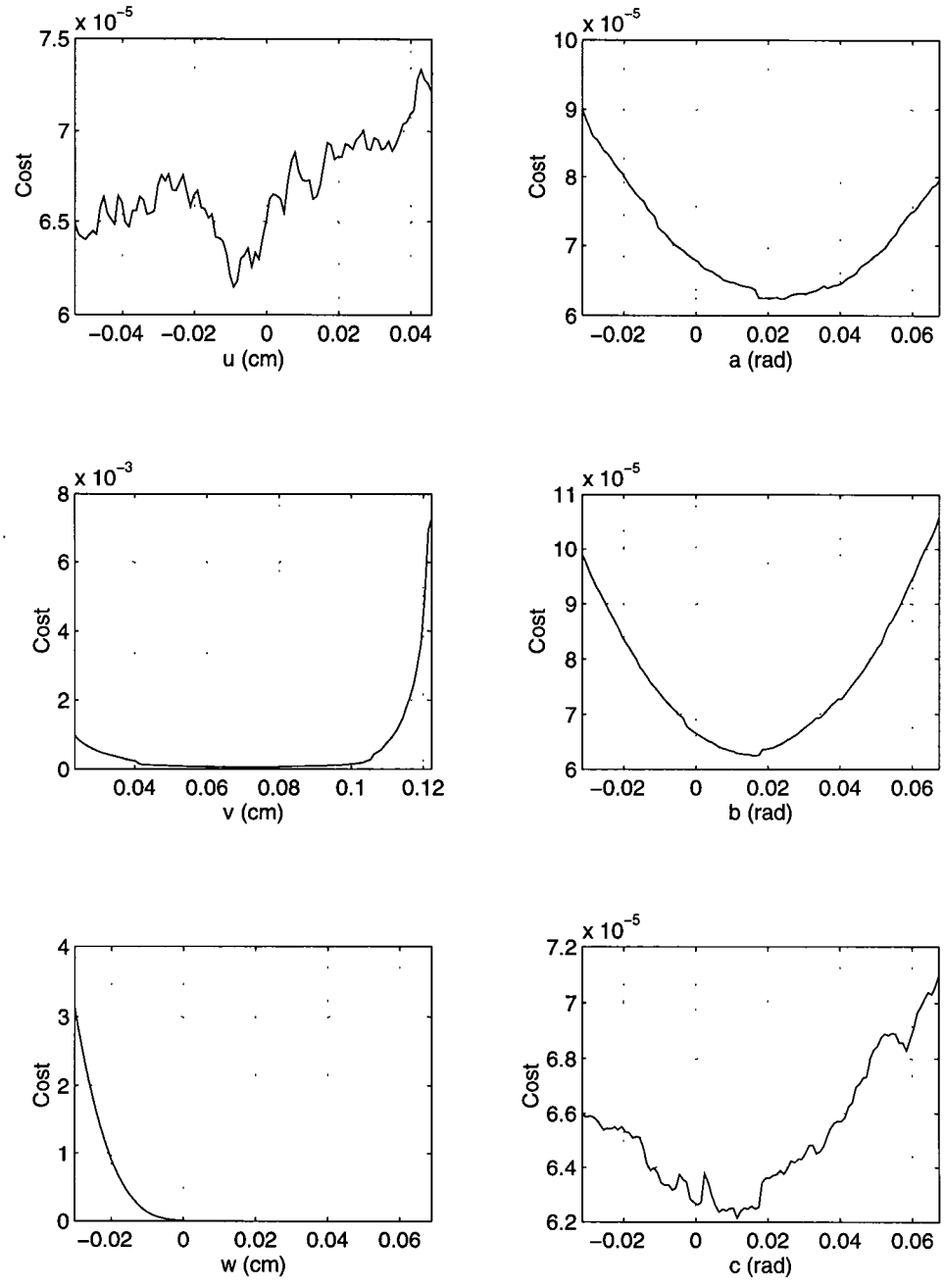

Figure 3.21: The cost function for the best "vertical" axis varies as a function of each of the six position parameters.

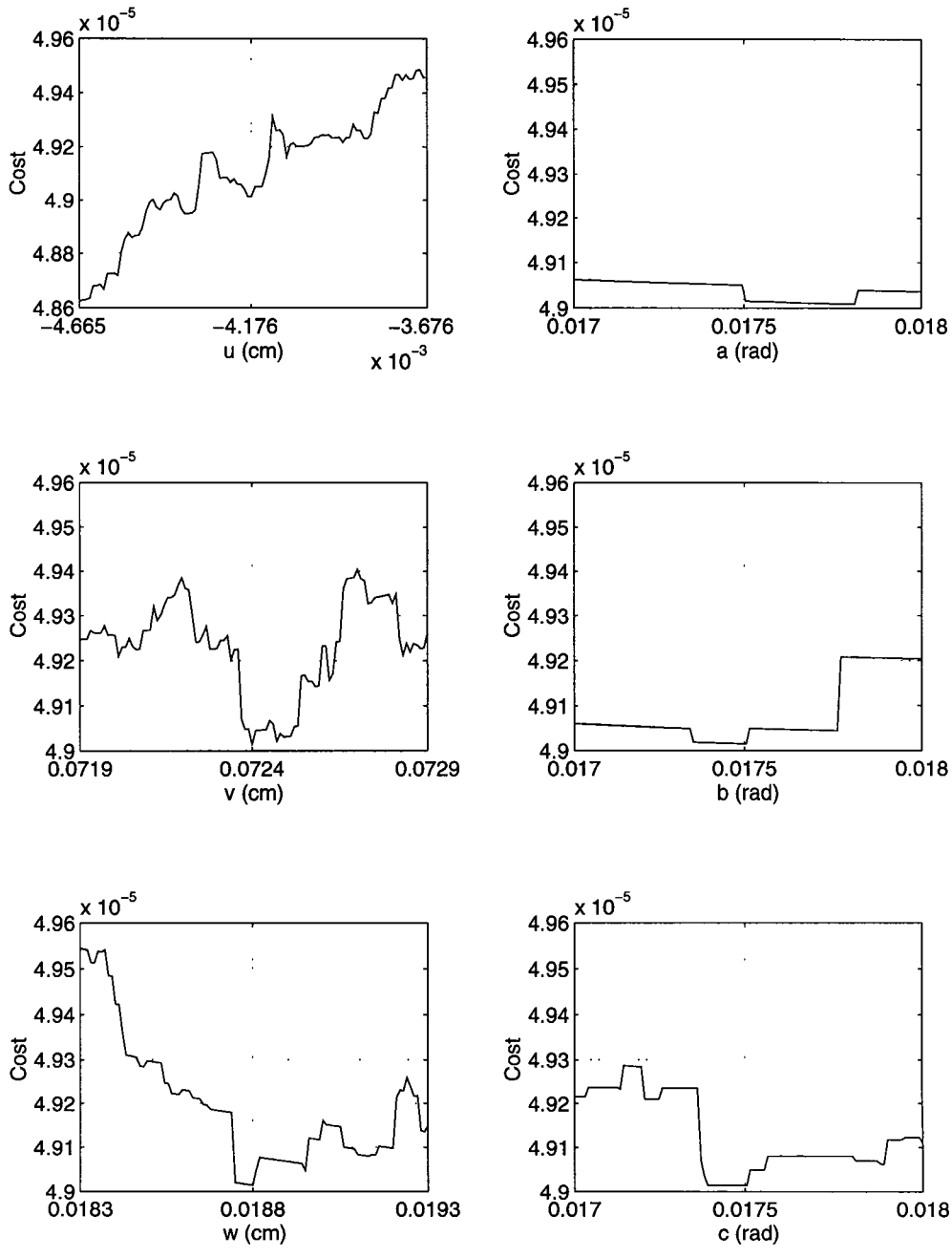

Figure 3.22: The variations of the cost function within a small interval $\Delta x = 10^{-3}$ (the optimal "rocking" axis).

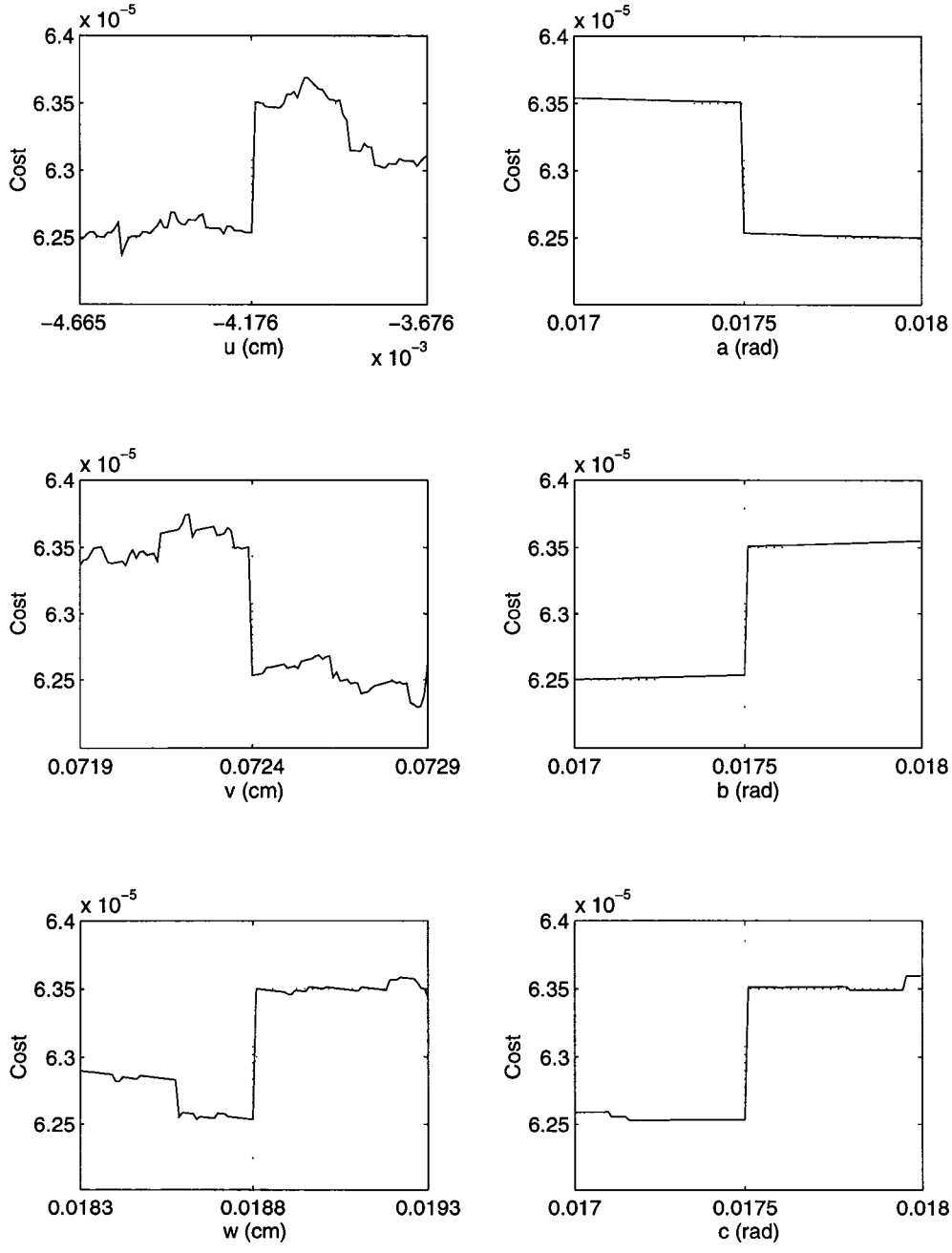

Figure 3.23: The variations of the cost function within a small interval $\Delta x = 10^{-3}$ (the best "vertical" axis).

Table 3.6: Sensitivity results for Cartilage # 1 (rocking axis, $\Delta x = 10^{-3}$)

F	d_x	d_y	k_x	k_y	J
S_u^F	0.03	0.18	0.02	0.01	0.07
S_v^F	0.63	1.17	0.29	0.16	0.57
S_w^F	0.29	0.57	0.14	0.07	0.20
S_a^F	0.01	0.04	0.002	0.002	0.02
S_b^F	0.13	0.16	0.04	0.03	0.03
S_c^F	0.13	0.30	0.04	0.03	0.10

d_y, k_x and k_y. The sensitivity results are listed in Table 3.6 (the optimal "rocking" axis) and Table 3.7 (the best "vertical" axis).

From Table 3.6 and Table 3.7 we can see that in general our results are not very sensitive. This implies that a small surface alignment error made in any one of the six directions will not produce a large difference in the solution (since all but three values in both tables is less than 1.0). Among the three translation parameters u, v and w, the least sensitive direction is the u direction, which is the direction of the longitudinal axis of the cricoid facet. This is further evidence to support the sliding movement of the arytenoid. The directions v and w are the most sensitive directions of all. This can be explained by the fact that for the chosen cricoid facet coordinate system, moving the arytenoid facet in these two directions will eventually cause interdigitation between the two joint surfaces. Among the rotation parameters, the most sensitive one is the rotation around the w axis (measured by angle c). This result is consistent with our findings presented in the previous section, i.e. the arytenoid cannot rotate around an

Table 3.7: Sensitivity results for Cartilage # 1 (vertical axis, $\Delta x = 10^{-3}$)

F	d_x	d_y	k_x	k_y	J
S_u^F	0.05	0.20	0.04	0.03	0.08
S_v^F	0.43	1.29	0.52	0.54	1.65
S_w^F	0.06	0.22	0.16	0.11	0.31
S_a^F	0.06	0.23	0.14	0.12	0.29
S_b^F	0.02	0.09	0.08	0.02	0.29
S_c^F	0.07	0.25	0.14	0.13	0.29

axis that is vertical to the joint facet and passes through the center of the joint.

3.4 Testing Motion Hypotheses Using Vocal Fold Trajectories

A good joint model should produce a movement trajectory that is close to the actual movement trajectory for the arytenoid. One important way to test different motion hypotheses is to check their corresponding movement trajectories and compare them with the experimental results. The best movement axes for "rocking" and "rotating" have been located in the previous section. By rotating the arytenoid cartilage around the solution axes, a 3D movement trajectory can be produced for any point on the cartilage. In order for the trajectories to be comparable with the movement data obtained during experiments, we need to look at approximately the same point on the cartilage and from roughly the same viewing angle. This implies that projection of the 3D trajectory has to be made onto the viewing plane where the experimental trajecto-

ries were observed. Since the arytenoid cartilages are not visible in live experiments, the trajectory data was obtained for some landmarks with easy visibility; they were not the points on the arytenoid cartilage surface. The tip of the vocal process and the apex were chosen for their visibility on the video tape. Movement data was digitized at 60 Hz. This experiment was performed at NIH on a normal female volunteer and the digitization of the movement data was done by Dr. Scott Selbie[93]. The data was normalized with respect to the distance between the mid glottic wall and the anterior commissure.

In order to determine the viewing plane onto which the 3D trajectories of the joint model can be projected, the 3D pictures of the cartilages reconstructed from the MRI scans were rotated on the computer screen until the desired viewing angle (similar to that of the camera) was obtained. The judgement on where to stop the rotation was made by an NIH expert. Suppose that the base of the cricoid cartilage is sitting on the horizontal plane, then the angle between this viewing plane and the horizontal plane is about 20^o to 25^o. This plane was used to compare arytenoid movement trajectories produced by different pin joint models with the experimental data.

Figure 3.24 shows the movement trajectories of the arytenoid vocal processes and superior tips obtained from video (sampled at 60 Hz). The data were collected from five trials of vocal fold adduction for phonation. In Figure 3.24 the circles correspond to the trajectories of the vocal processes of the arytenoids, while the plus signs correspond to those of the superior tip (the apex) of the arytenoids. In Figure 3.25 and Figure 3.26, the movement trajectories of the right arytenoids produced by the pin joint models are superimposed on top of the experimental data. Figure 3.25

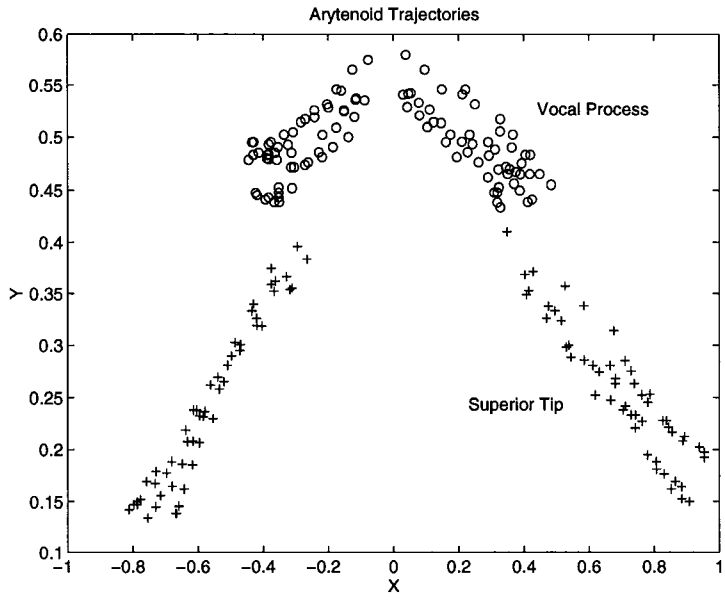

Figure 3.24: Experimental trajectories of the arytenoids (Selbie[93]). The +'s indicate the trajectories of the vocal processes. The o's indicate the superior tips.

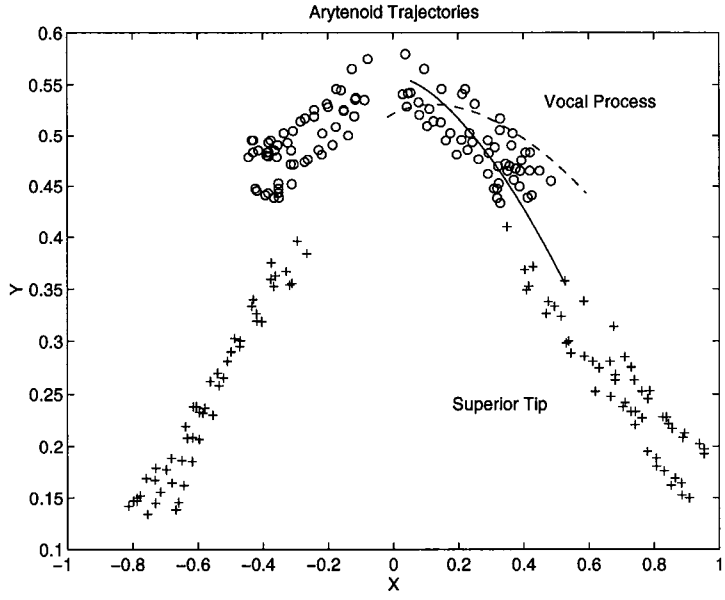

Figure 3.25: Vocal process trajectory of the rocking motion. The dashed line is for Cartilage # 1 and the solid line is for Cartilage # 2.

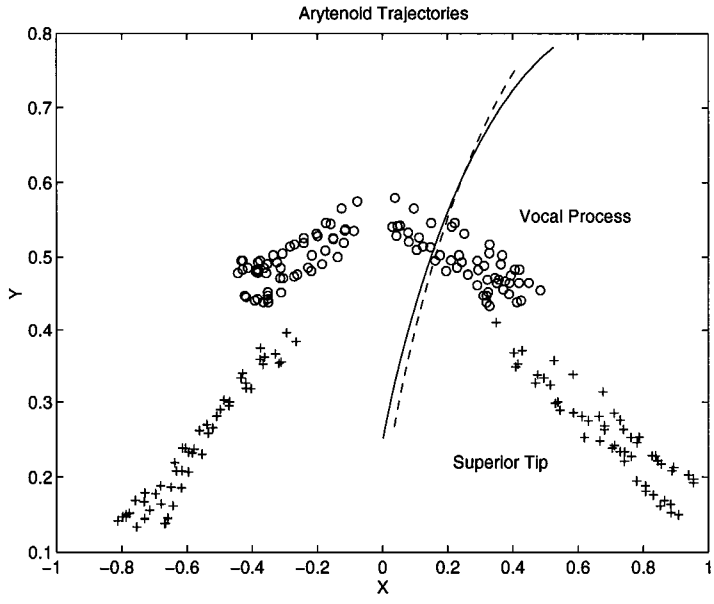

Figure 3.26: Vocal process trajectory of the rotation around the vertical axis. The dashed line is for Cartilage # 1 and the solid line is for Cartilage # 2.

shows the motion trajectory of the vocal process when the arytenoids rotate around the optimal "rocking" axes determined in previous section. Figure 3.26 corresponds to the trajectory of the arytenoid rotating around the vertical axes. By comparison, the "rocking" trajectories fit well with the experimental data while the trajectories for rotation around the vertical axis is totally different. These results show that the hypothesis that the arytenoid rocks around the long axis of the cricoarytenoid joint facet on the cricoid is basically correct. A location and orientation of that axis has been found (as the results of Section 3) which produces a movement trajectory consistent with the recording. The comparison results contradict the hypothesis of rotation about a vertical axis. The conclusion is consistent for both cartilages tested.

3.5 Conclusions

Quantitative measures of the cricoarytenoid joint facets were made by the means of 3D digitization. Based on the measurement data, the problem of finding the best rotation joint axis has been formulated into an unconstrained optimization problem and the variation in distance between the two joint facets is defined as the cost function. By minimizing this cost function, an anatomically feasible joint axis can be determined around which the arytenoid cartilage rotates. Global optimality is not guaranteed by the optimization algorithm. The best we can do is to repeat the calculation with different starting points in the hope that one of them will converge to the global minimum.

The lowest cost joint axis found is a pretty reasonable one. Rotating around this axis will result in the normal motion of "rocking" of the arytenoid. The movement

trajectory of the vocal process produced by the pin joint model using this rocking axis is consistent with the experimental trajectory.

A suboptimal axis was found which corresponds to the axis vertical to the joint facet. This axis is located outside the cartilage and the resulting motion is more like a sliding than a rotating. The trajectory resulting from a rotation about this axis does not agree with the experimental observation of such trajectories. The restriction on the sliding movement of the arytenoid was not imposed by the joint anatomy; it has to come from other structures of the larynx. The ligaments are among the possible candidates.

The absolute vertical axis is not a solution to our optimization problem. This means that this axis is not a good joint axis measured by our performance criterion.

Chapter 4

Muscle EMG Signal Processing

4.1 Role of Muscle EMG in Motion Studies

EMG is the electromyographic recording of the muscular activity. It represents the major changes in currents and voltages that occur whenever muscle fibers are being activated by their motoneurons.

From the biomechanical point of view, the main interest in studying muscle EMG is to understand movement and its neural control rather than the electrical activities in the muscle. This means that we wish to use the EMG as an indication of the neural activities of the muscle, the forces exerted by the muscle and, of the displacements created by those forces. There are two common ways of utilizing the EMG signals in the study of motion. When the movement trajectories can be obtained with reasonable precision, good models of the system (skeletal or cartilage structures, muscles and their attachments, ligaments, tendons and joints) are available and the purpose of the movement can be described precisely then an optimal control model of the task can be created and solved. The optimal control signals can then be compared

with the processed EMG signals to validate the model. Many studies of locomotion use this approach because the movement trajectories of the limb segments are relatively easy to obtain[10,31,33,73]. The second method is to use the information revealed in the EMG to estimate the muscle forces, simulate the result of applying these forces to the system and compare the simulated movement trajectories with the observed ones. In the case of laryngeal motion, both the muscle EMGs and the movement trajectories of the arytenoids are difficult to obtain due to the inaccessibility of the larynx. The second approach is preferred given that there is much more muscle EMG data available than motion data.

Although muscle EMGs have been used extensively in motion studies, the technique has its limitations. Its effectiveness highly depends on the skill with which the electrode has been formed and placed and the appropriateness with which the resulting signals have been filtered, amplified, and otherwise treated. A fundamental problem associated with the method is the so-called muscle "cross-talk". It is difficult to identify an EMG as originating from the activity of one particular muscle. A second major problem is that it is not possible to quantify the relation between EMG and muscle activation with any degree of precision. The amplitude of the EMG signal depends upon the number of motor units contained within the electrical field of the recording electrode. Furthermore, the EMG signal processing technique is very important in the sense of maintaining the information contained in the raw EMG signal as well as correlating it with motion.

4.2 Experiment

The laryngeal EMGs used in this study were data obtained for a study [58] by the Voice and Speech Section, National Institute on Deafness and Other Communication Disorders (NIDCD). Three normal subjects (two females and one male) participated in the study. Detailed experiment procedures can be found in [58]. During each experiment the EMGs of five intrinsic laryngeal muscles were recorded. They are the right thyroarytenoid (RTA), the left thyroarytenoid (LTA), the right cricothyroid (RCT), the left cricothyroid (LCT), and the posterior cricoarytenoid (PCA). The recordings of the first four muscles were made using bipolar hooked wire electrodes [54], and the recording of the PCA muscle was made using a surface electrode inserted through the nasal passage into the hypopharynx which recorded muscle activity through the hypopharyngeal mucosa [19]. Before recording, the location of the electrode in each muscle was verified by asking the subject to perform certain gestures that would produce typical responses if the electrode was in the right muscle. This verification procedure would also minimize the "cross-talk" between muscles. Recordings were obtained in all five muscles simultaneously with signal amplification and band-pass filtering between 100 and 5000 Hz for the bipolar hooked wires and between 50 to 1000 Hz for the surface electrode. Placement of the electrodes was constantly monitored throughout the experiment.

Beside the EMG signals, the changes in glottal opening during each gesture, i.e., the amount of light passing through the glottis, were also recorded. The light was detected with a photoglottographic (PGG) light detector held against the skin below the cricoid cartilage.

For the male subject, the muscle EMGs were recorded while he performed the following phonation gestures repeatedly:

1. Repetition of /*i*/.
2. Repetition of /*si*/.
3. Repetition of /*i*/ in falsetto.
4. /*ah*/ glide from low to high pitch.
5. Prolonged /*i*/ in falsetto.

For each normal subject studied, five maximum muscle activation gestures were recorded including, (1)deep breath, hold, then release, (2)/*ah*/ glide, (3)high pitch sustained /*i*/, (4)falsetto /*i*/ repetitions, and (5) wet swallow. Among the recorded signals of the male subject, the ones for wet swallow contain too much noise due to the artifact of the up and down movement of the larynx, and therefore were ruled out completely. By comparing the remaining four gestures, it was found that for this particular normal control, the /*ah*/ glide produces maximum activations for all five muscles recorded. Therefore, this gesture was used to obtain the peak amplitude for each muscle. The maximum value was calculated by averaging over a 20 *ms* window which was placed around the point where the maximum value occured. The results are listed in Table 4.1

Table 4.1: Peak muscle activation levels of five laryngeal muscles (in μv)

Muscle	RTA	RCT	LTA	LCT	PCA
V_{max}	348.230	106.867	202.331	267.046	22.375

4.3 Sampling and Pre-processing

The EMG signals were digitized from FM tape at 5000 Hz with anti-aliasing filtering at 2000 Hz. After digitizing, a test signal (square wave) was used to calibrate each EMG channel. DC drift for each EMG channel was measured during a period of quiet respiration prior to recording, and was removed from the EMG signal of the corresponding channel so that the resulting EMG signal reflects only the changes in neuron activities associated with the recorded gesture. A full wave rectification was then performed on each EMG channel, followed by noise removal, i.e. the minimum noise level was measured for each channel and subtracted from the rectified EMG of the corresponding channel. The resulting rectified EMG signals were then converted to microvolts. All this processing was done at the NIH using MITSYN (which is a synergistic family of high-level languages for time signal processing) on a PC[Bassick,1993]. The MITSYN stream processing diagrams and macros were provided by the Voice and Speech Section of the NIH. The resulting rectified EMGs are the "raw" EMG signals available for use in the model. Figure 4.1 shows an example of the rectified EMG signals from the male subject performing the repetition of /*si*/ (five times). In Figure 4.1, the acoustic signal is in arbitrary units and all five EMG channels are in microvolts.

How can muscle EMGs like the ones shown in Figure 4.1 be interpreted as

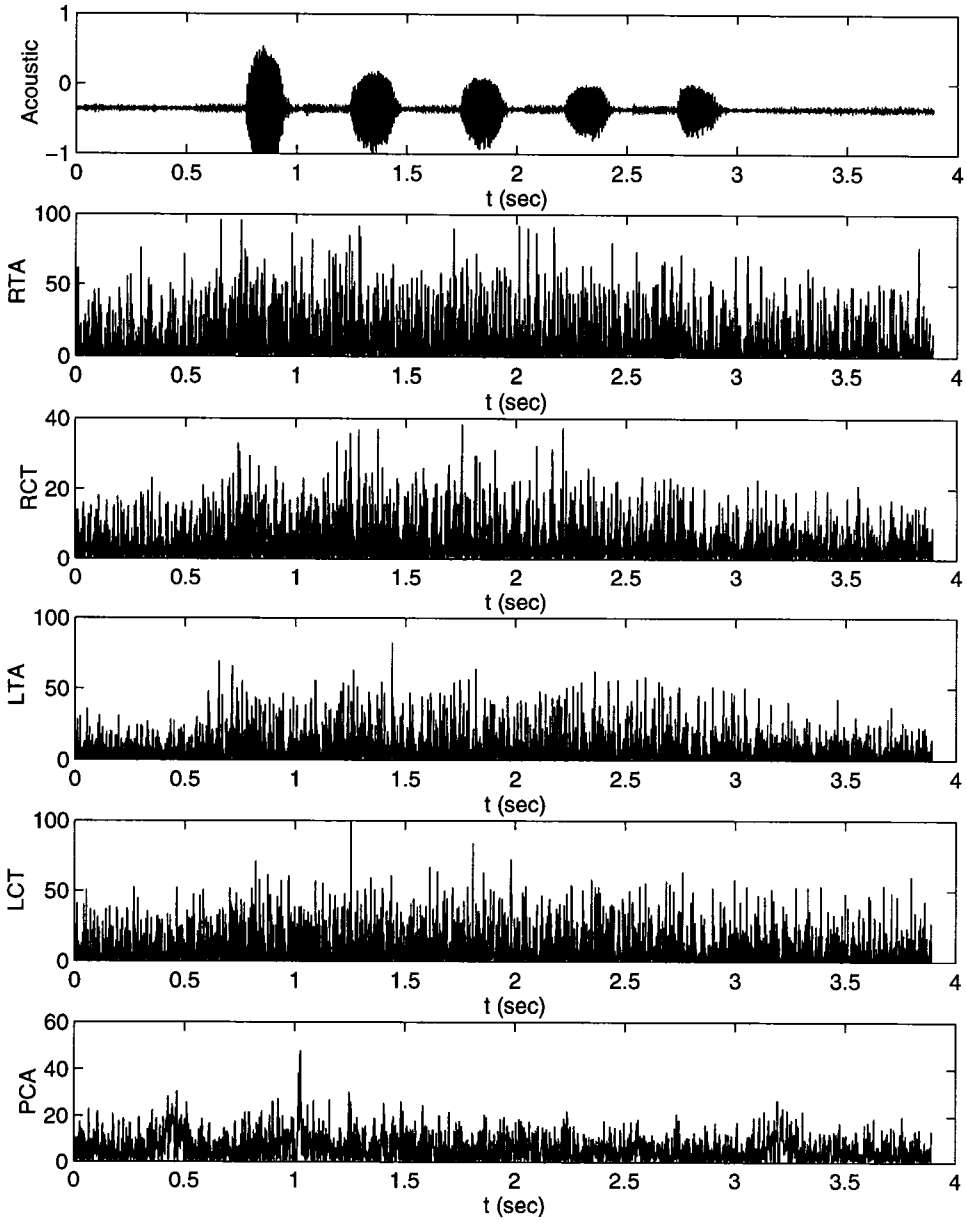

Figure 4.1: Rectified laryngeal EMG signals for the repetition of /*si*/ (sampled at $5000Hz$).

indicators of the mechanical force being generated by the muscles? The muscle force generation process is a much more slowly changing positive-going event that is more or less proportional to the envelop amplitude of the rectified EMG signal. This envelop represents the overall activity level of the motor neurons in the muscle fibers. It indicates how active that particular muscle is under the neural stimulation. Many muscle models use this muscle activation state to estimate the muscle force produced.

The muscle model used to model the laryngeal motion is a so called Hill- type model which will be described in detail in Chapter 5. The model consists of two parts. The first part is the activation dynamics in which a first order nonlinear differential equation is used to describe the relation between the neural input (stimulation) to the muscle and its mechanical activation. The second part is the musculotendeon actuator which generates muscle force as a function of the muscle activation level, fiber length and the rate of contraction. The processed EMG envelop enters the model as an input signal to the activation dynamics which represents the neural stimulation to the muscle. This is a well-established approach [40,41,42,43] that captures the main qualitative features of the relation between EMG and muscle activation. Other approaches can also be found in the literature[111].

4.4 Filter Design and Implementation

There are two important issues to address in processing the "raw" EMG in order to obtain a smoothed envelop signal, (1)keep the amplitude distortion small, and (2)keep the timing of the signal as accurate as possible because it contains the information about coordination between different muscle group's actions. These requirements can

be translated into the filter design specifications, i.e. to obtain the EMG envelop using a low pass filter with maximum flatness in the passband and minimum phase distortion.

4.4.1 Filter Choices

A digital low pass filter was designed to satisfy the above requirements. There were two classes of filters to choose from: (1)the finite impulse response (FIR) filters and (2)the infinite impulse response (IIR) filters. The FIR filters have simple architectures, are always stable, and have the ability to exhibit linear phase versus frequency behavior. The major disadvantage of the FIRs is their inability to achieve sharp magnitude response in the frequency domain. In general, a high-order FIR must be used to achieve sharp frequency response. Unlike the FIR, an IIR filter possesses an impulse response which may persist for all time. It does not exhibit the phase linearity of the FIR but compensates for this shortcoming by providing an improved magnitude frequency response and lower order. Because of its feedback structure, the IIR filter is not guaranteed to be stable. In practical situations, high-Q filters, and those which have nearly a piecewise constant spectral shape, are generally implemented as IIR filters.

To determine which class of filters is most suitable for processing the muscle EMGs, the design requirements need to be analyzed first. The cutoff frequency of the lowpass filter designed was less than $10Hz$, which is the frequency range for most of the movements. Since the laryngeal muscle EMG's were sampled at $5000Hz$, the ratio of the cutoff frequency to the sampling frequency is very small (< 0.002), which means

that the lowpass filter will have a very narrow pass band. A very high order FIR filter is needed in this case in order to obtain a reasonable performance.

Example. Design a lowpass filter with a passband cutoff frequency of $4Hz$, a stopband cutoff frequency of $8Hz$, passband ripple of -3dB, stopband ripple of -20dB, and a sampling frequency of $5000Hz$. The estimated order of the FIR filter is 1138 (An under estimate). A 5th order Butterworth filter will achieve the same performance. The orders were estimated using MATLAB functions **remezord** and **buttord**. Figure 4.2 and Figure 4.3 show the frequency responses of a linear-phase FIR filter of order 1500 and of a Butterworth filter of order 5. The filters were designed using MATLAB functions **remez** and **butter**. The reason for using the log scale for the frequency axis is that the bandwidth of the filter is too narrow to be noticed on a linear scale covering 0 to half of the sampling frequency ($2500Hz$).

If a lower order FIR filter is desired, downsampling of the original EMG signal is necessary. However before downsampling, we must lowpass filter the signal first to prevent aliasing. The more filtering we use, the more distortion will be introduced into the the original signal. Therefore downsampling is not a good idea. By comparison, the IIR filter is clearly a better choice.

Among the classic optimal IIR filters (Butterworth, Chebyshev, etc.), the Butterworth filter provides the maximum flatness in the passband (no ripples) which implies the minimum amplitude distortion, and is therefore better suited for our situation. The phase distortion caused by the IIR filter can be eliminated using the "forward-backward" filtering technique. The signal sequence is passed through the filter in the forward direction first, the filtered (output) sequence is then reversed and

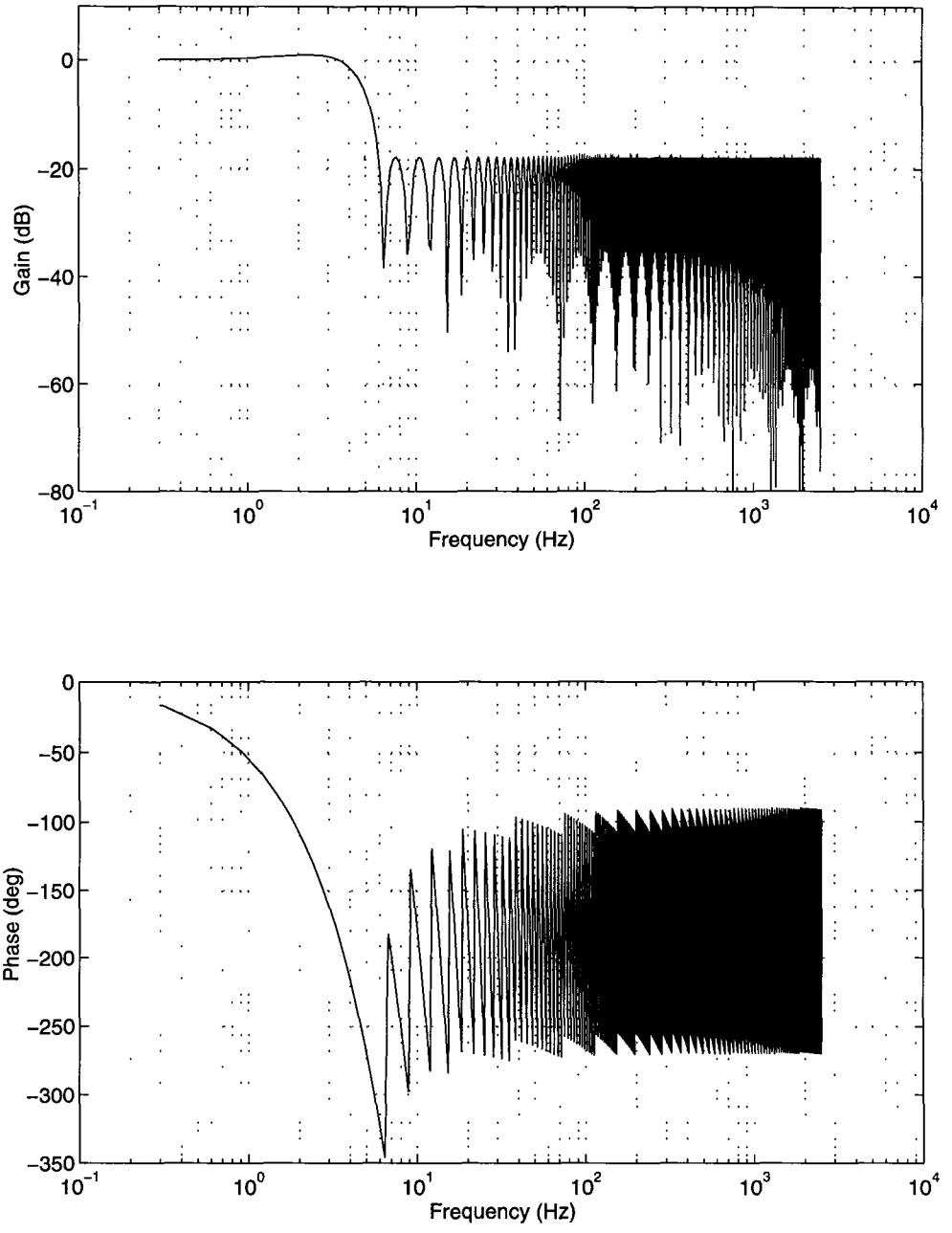

Figure 4.2: Frequency response of a linear phase FIR filter of order 1500

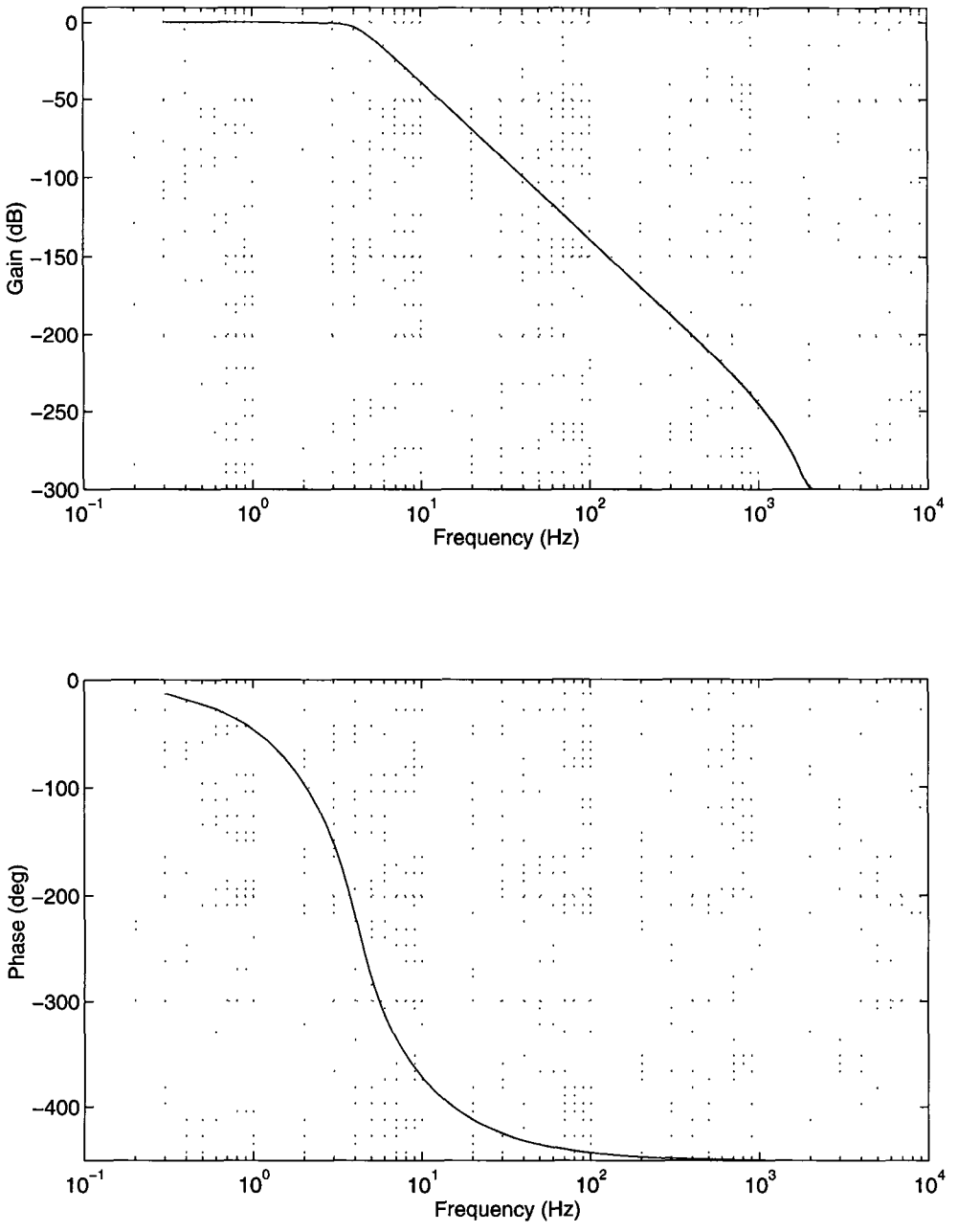

Figure 4.3: Frequency response of a Butterworth filter of order 5

run back through the same filter again. The resulting sequence has precisely zero-phase distortion and double the filter order. Using this technique, we only need a 3rd order Butterworth filter to achieve the performance mentioned in the above example.

Mathematically, the forward-backward filtering technique is equivalent to passing the input signal through an equivalent filter whose order is twice that of the original filter and whose phase shift is zero. Suppose $H(z)$ is the z-transform of the impulse response of the original filter, then the z-transform of the equivalent filter, $H_e(z)$, is given by $H_e(z) = H(z)H(z^{-1})$. It can be shown that $H_e(z)$ has zero phase shift.

4.4.2 Spectrum Analysis of the Muscle EMGs

The choice of the cutoff frequency f_c will affect the envelopes produced. The higher f_c is, the more frequency components will be included in the envelope. Different researchers use different cutoff frequencies in their research. For example, David Winter [115] used a lowpass filter with $f_c = 3Hz$ to process the EMG signals of the medial hamstrings and soleus muscles during walking. To filter the kinematic data associated with walking, Winter sets the cutoff frequency at 6 Hz based on the spectrum analysis of the raw data. In order to choose a reasonable cutoff frequency for our lowpass filter, we must know what are the frequency components of interest. A spectrum analysis of the laryngeal muscle EMGs was performed for this purpose. For the "raw" EMGs shown in Figure 4.1, the corresponding spectra are obtained by performing the fast Fourier transforms (FFT) of the original signals. The spectra are plotted in Figure 4.4.

From Figure 4.4 we can see that besides the DC component, there is clearly a

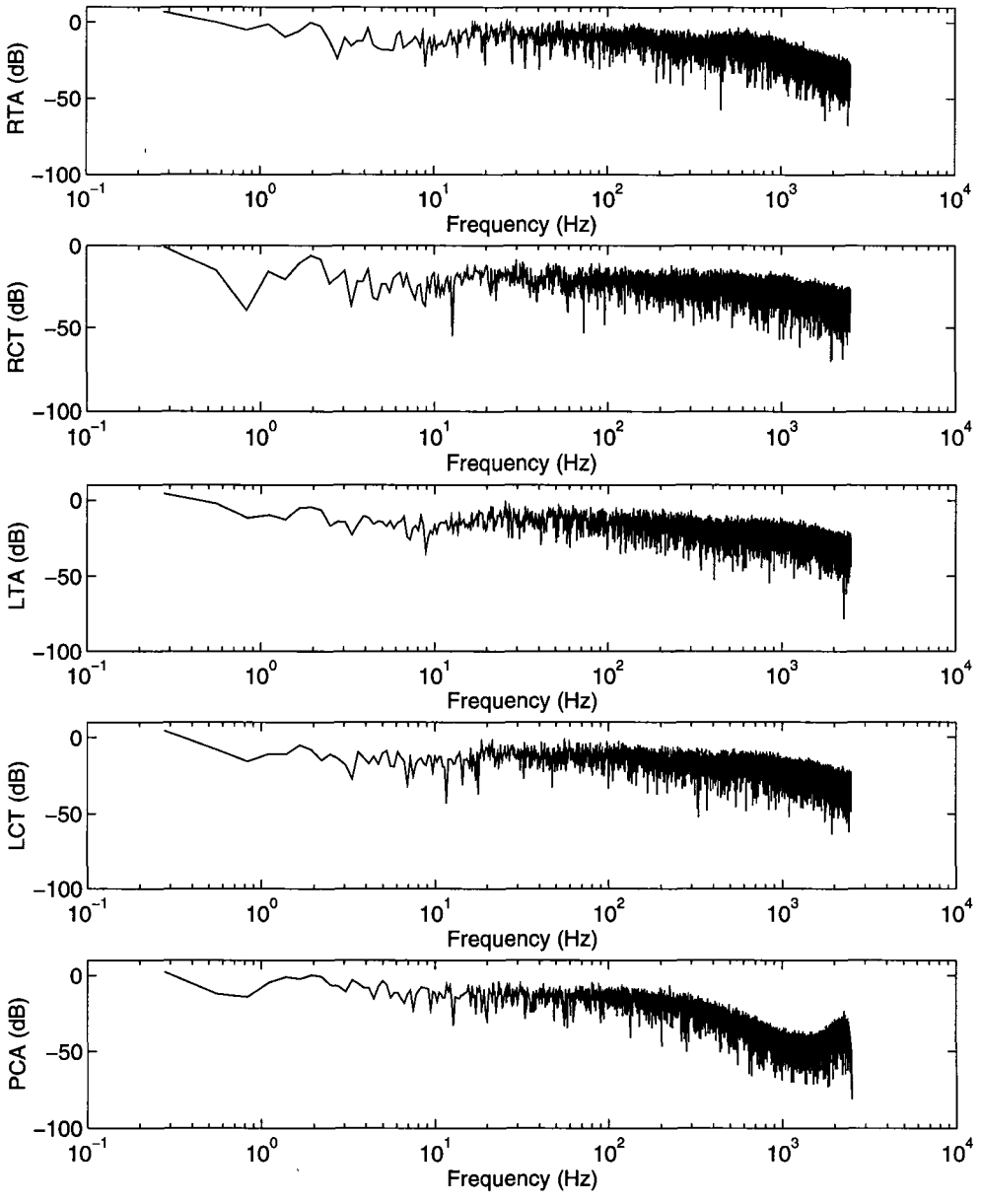

Figure 4.4: Spectra of the laryngeal EMGs (for the repetition of /*si*/).

peak at around $2Hz$ for every muscle recorded. This component corresponds to the repetition frequency of the vocal gesture $/si/$, which is also the movement frequency of the arytenoid cartilages. This frequency is the one we are most interested in. There are other peaks at around 4, 6, and $8Hz$. If the cutoff frequency of the lowpass filter is taken to be $8Hz$, most of the low frequency peaks will be kept in the resulting envelopes.

4.4.3 Filter Design

Based on the research described in the previous sections, the forward- backward Butterworth lowpass filter is chosen to process the laryngeal muscle EMGs. Two filters were designed using MATLAB:

Filter 1:

- Order $N = 3$
- Cutoff frequency $f_c = 4.5Hz$
- Equivalent filter bandwidth $W = 4Hz$
- Transfer function

$$H(z) = \frac{b_1 + b_2 z^{-1} + b_3 z^{-2} + b_4 z^{-3}}{a_1 + a_2 z^{-1} + a_3 z^{-2} + a_4 z^{-3}} \tag{4.4.1}$$

Where

$[b_1\ b_2\ b_3\ b_4]$=[0.2530 0.7590 0.7590 0.2530]$\times 10^{-7}$, and

$[a_1\ a_2\ a_3\ a_4]$=[1.0000 -2.9882 2.9756 -0.9883].

Filter 2:

- Order $N = 3$
- Cutoff frequency $f_c = 9.3Hz$
- Equivalent filter bandwidth $W = 8Hz$
- Transfer function

$$H(z) = \frac{b_1 + b_2 z^{-1} + b_3 z^{-2} + b_4 z^{-3}}{a_1 + a_2 z^{-1} + a_3 z^{-2} + a_4 z^{-3}} \tag{4.4.2}$$

Where

$[b_1\ b_2\ b_3\ b_4]$=[0.1994 0.5983 0.5983 0.1994]$\times 10^{-6}$, and

$[a_1\ a_2\ a_3\ a_4]$=[1.0000 -2.9765 2.9534 -0.9768].

The frequency responses of the two filters are shown in Figure 4.5 and Figure 4.6. The bottom plot in each figure is the amplitude response of the equivalent forward-backward filter of order 6. The bandwidths of the equivalent filters are equal to $4Hz$ and $8Hz$ respectively.

4.4.4 EMG Envelopes and Their Spectra

Using the two filters designed above, the laryngeal muscle EMGs were filtered. The signal sequence was passed through the filter twice, first in the forward direction and then in the reverse direction. The phase shift in the output sequence is zero, i.e. the timing of the original signal is perfectly preserved. The resulting envelopes of the EMGs are shown in Figure 4.7 and Figure 4.8.

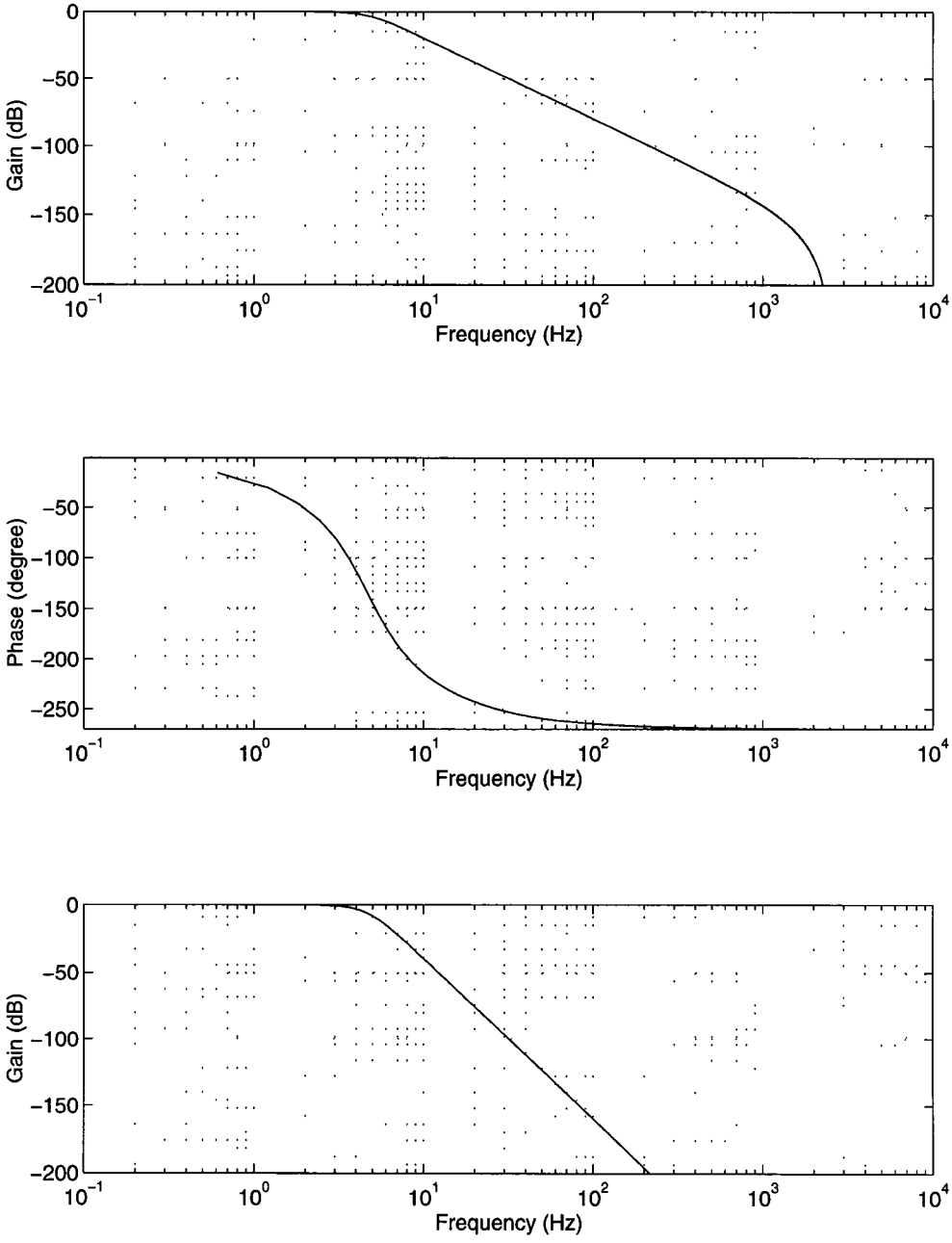

Figure 4.5: Frequency responses of Filter 1 with $f_c = 4.5Hz$

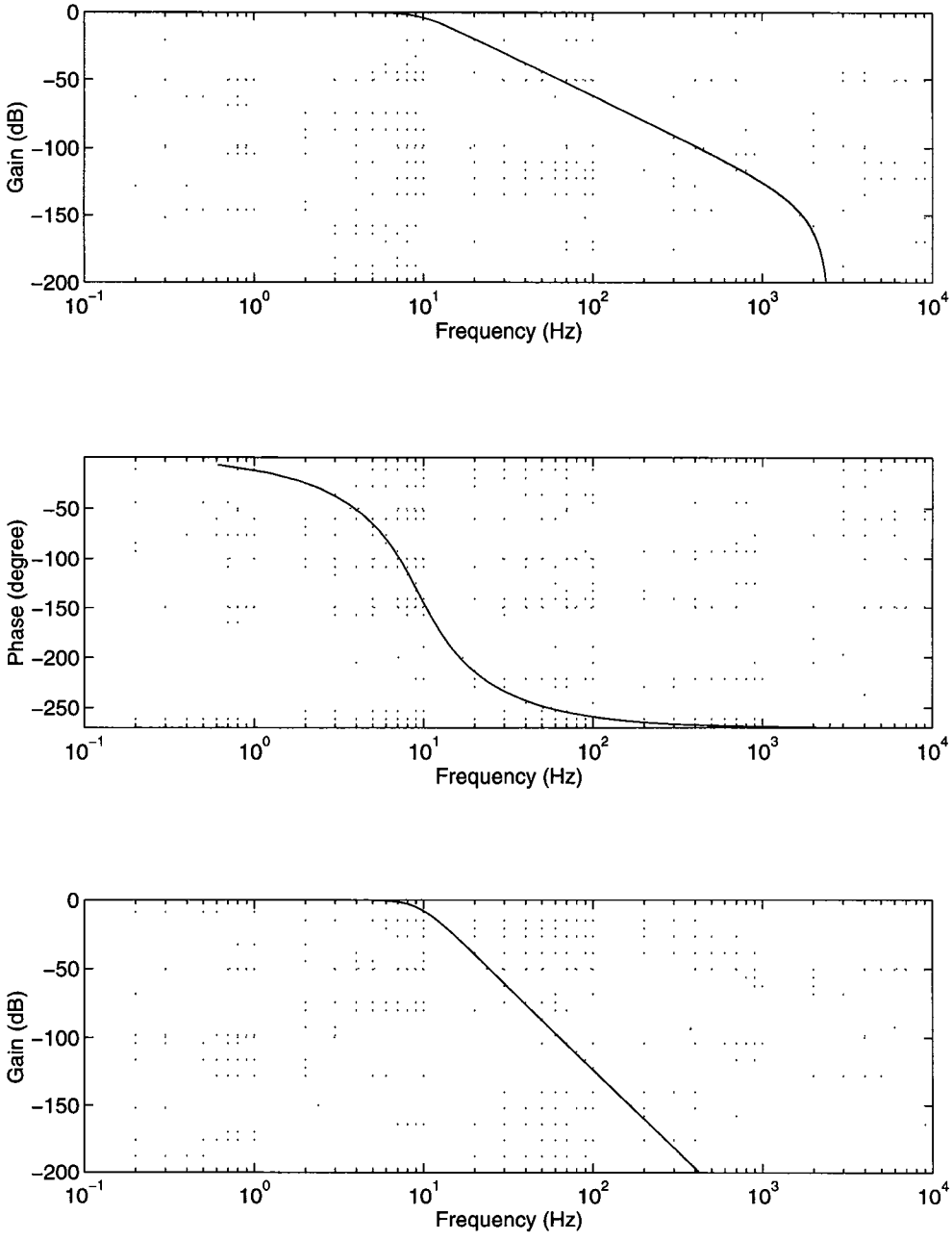

Figure 4.6: Frequency responses of Filter 2 with $f_c = 9.3Hz$

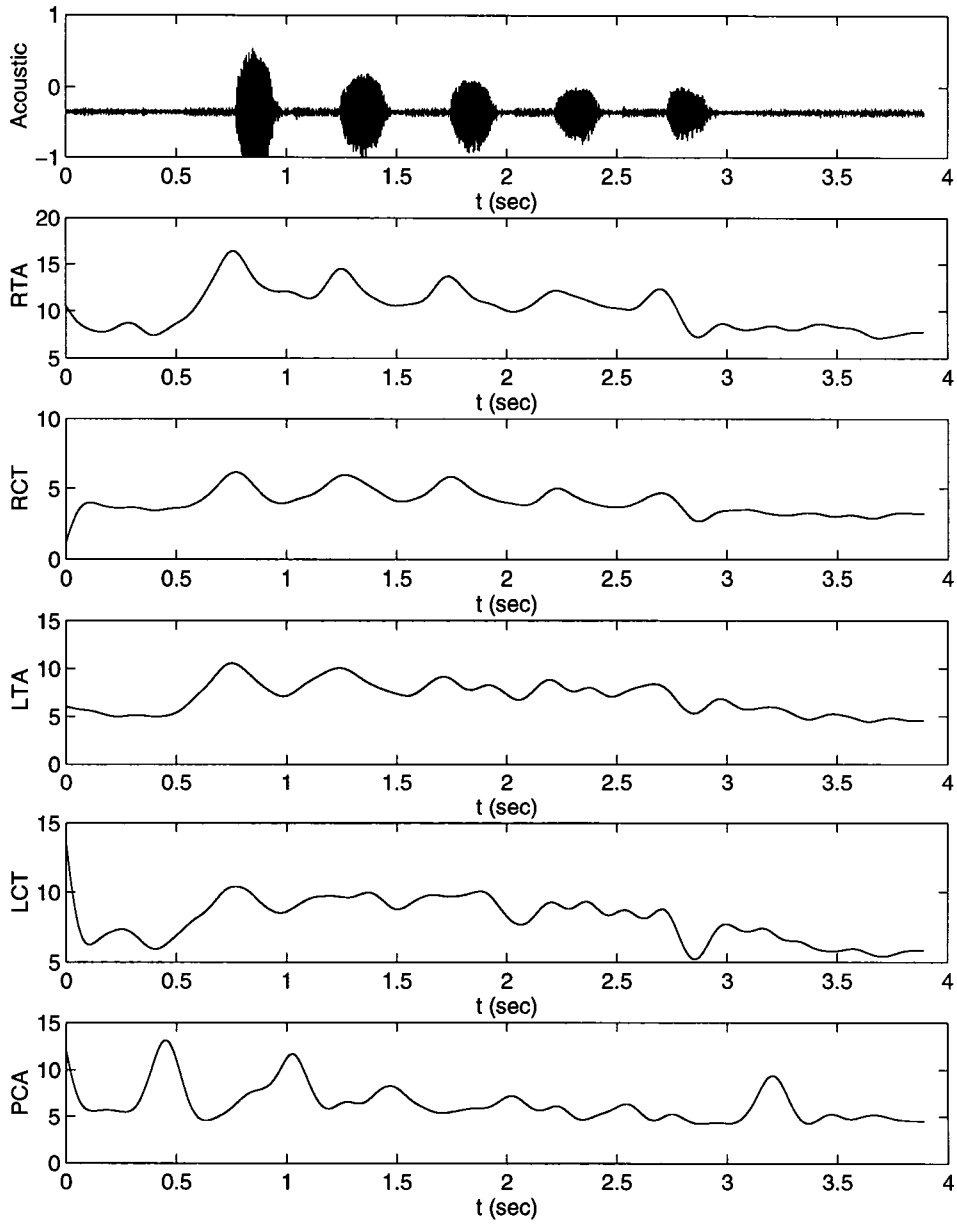

Figure 4.7: EMG envelopes produced by Filter 1.

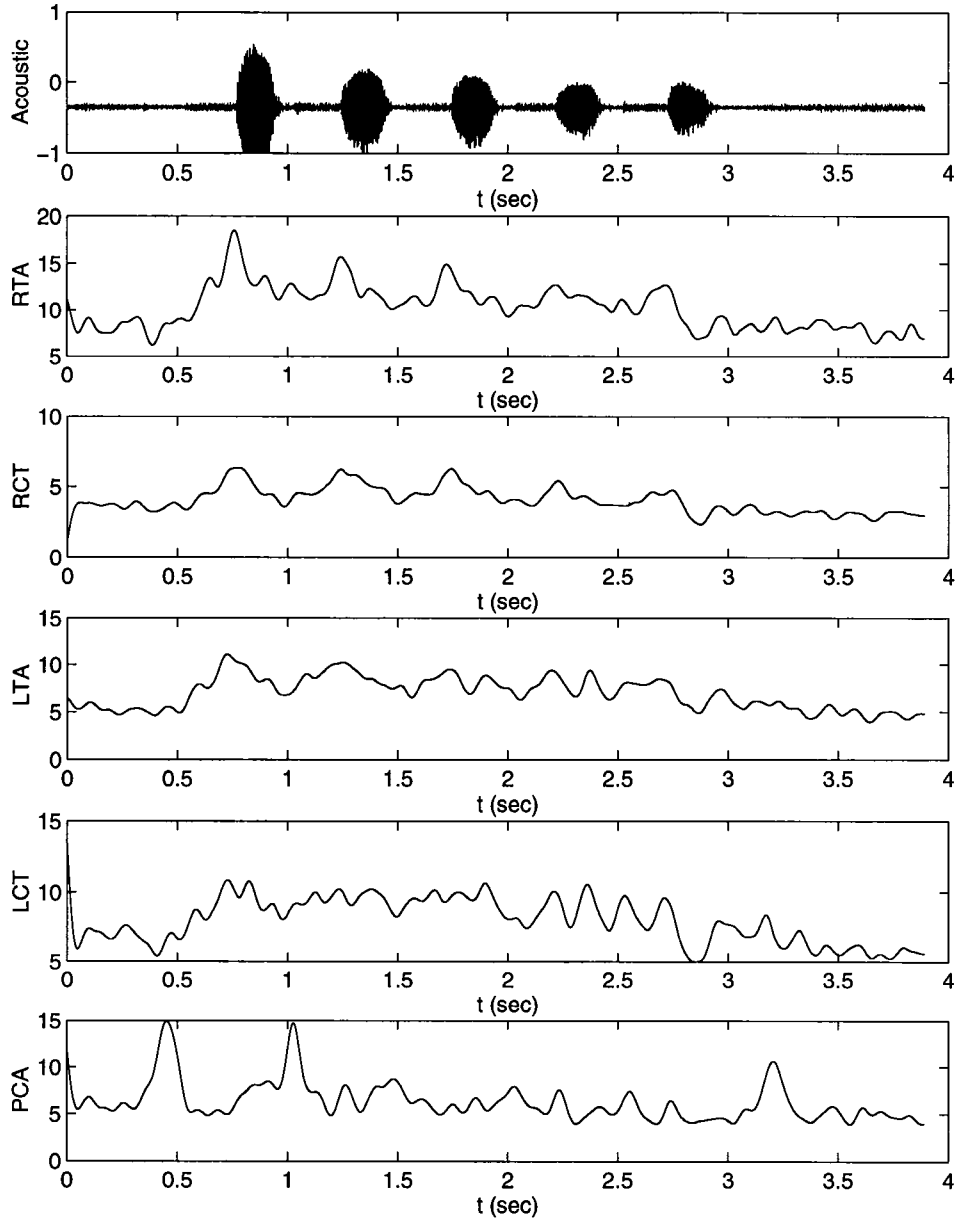

Figure 4.8: EMG envelopes produced by Filter 2.

Discussion

In Figure 4.7 and Figure 4.8, the non-zero cluster of the acoustic signal corresponds to the duration of each /*si*/ performed by the subject. The vocal gesture was repeated five times in 3 seconds. No breath was taken during the gesture. The peaks of the TA and the CT muscles lead the corresponding acoustic signal by about 0.1 second indicating that these adductor muscles were activated prior to phonation to close the vocal folds. This was accomplished by moving the arytenoid cartilages to their approximate positions. The peaks of the PCA muscle occur much before the first cluster of the acoustic signals and a little after each of them. The first peak of the PCA muscle occurred a little before 0.5 seconds, indicating a big breath was taken before the phonation started. The last peak occurred at 3.2 seconds indicating another big breath taken after the phonation. In between, the peaks of the PCA correspond to the partial opening of the vocal folds for producing /*s*/. In other words, the PCA was used for both breathing and speech. Since the PCA is identified as the only abductor muscle of the larynx, any voluntary opening of the vocal folds requires the activation of the PCA muscle.

To see how close the spectra of the output signals are to those of the original ones for the frequency range of interest, the output spectrum of the RTA signal is compared with its original one. Figure 4.9 shows the results. In Figure 4.9(a), the output signal was obtained using Filter 1 and Figure 4.9(b) corresponds to the result of Filter 2. The dotted lines in both figures are the spectrums of the original RTA. By comparison, the output spectra are very close to the input ones in the pass band and attenuated sharply in the stop band. This means that the filters designed produced

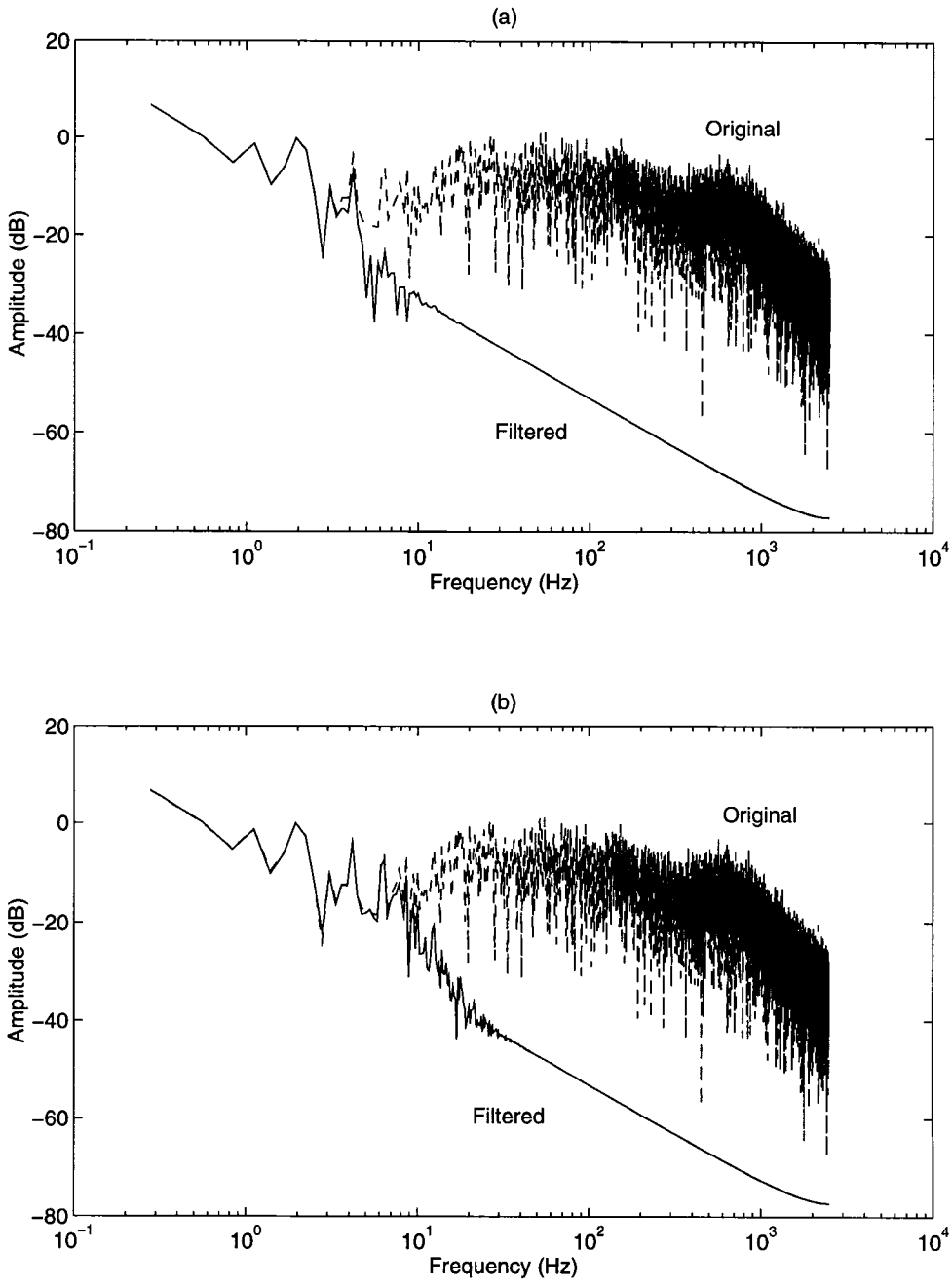

Figure 4.9: Spectra of RTA produced by Filter 1 (a) and Filter 2 (b).

very little amplitude distortions to the frequency components of interest, and the phase distortions are zero. Therefore, all the design requirements have been met.

The filter design and smooth processing mentioned above were performed on a Sun 4 Station using MATLAB. The MATLAB commands used are listed in the Appendix A.

4.4.5 Some Implementation Issues

The disadvantage of the forward-backward filtering technique is the need of reversing the signal sequence twice in order to obtain the right output sequence. From the real time signal processing point of view we wish to run the whole process sequentially, thereby eliminating the need for storage and the time delay associated with it. In some practical situations, it is much easier if the filter can be implemented as a convolutional filter (FIR) (for example in MITSYN).

The Butterworth filter designed can be approximated by a FIR filter by truncating its impulse response sequence to a finite length N. Using this finite impulse sequence to define a FIR filter of order N:

$$H_f(z) = \sum_{i=0}^{N} b_i z^{-i} \tag{4.4.3}$$

The equivalent forward-backward filter to (4.4.3) has a transfer function of

$$H_{fe}(z) = H_f(z)H_f(z^{-1}) \tag{4.4.4}$$

In equation (4.4.4), the second filter $H_f(z^{-1})$ is a non-causal filter and is non-realizable. But the filter $z^{-N}H_f(z^{-1})$ is causal and realizable. The concatenation of the two filters $H_f(z)$ and $z^{-N}H_f(z^{-1})$ produces an equivalent filter with transfer

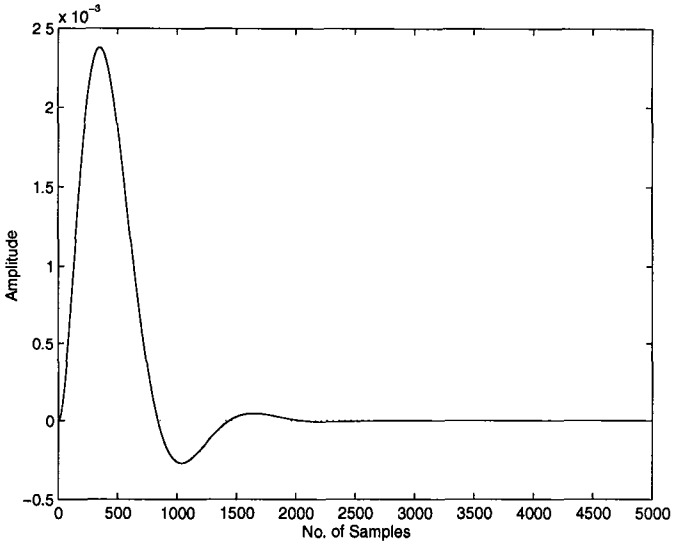

Figure 4.10: Impulse response of the Butterworth Filter 1.

function

$$G(z) = H_f(z)z^{-N}H_f(z^{-1}) = z^{-N}H_f(z)H_f(z^{-1}) = z^{-N}H_{fe}(z) \tag{4.4.5}$$

Filter $G(z)$ has the same amplitude response as the forward-backward Butterworth filter $H_{fe}(z)$. The only difference between the two filters is that $G(z)$ has introduced a constant time delay (by N samples). This time delay is the same for all EMGs that are processed using the same filter, and can be easily corrected; hence, it will not affect the correlations between the EMGs of different muscle groups. Therefore, in practice, if the processing speed is not crucial, it is prefered to implement $G(z)$ instead of $H_{fe}(z)$.

Because the FIR filter $H_f(z)$ is only an approximation of the designed Butterworth filter, we expect some performance degradation when using it. From the impulse

response of the 3rd order Butterworth filter (Filter 1), (Figure 4.10), we can see that the larger N is, the closer the truncated sequence is to the original one; therefore the closer the performance of the FIR filter will be to that of the Butterworth filter. Figure 4.10 indicates that in order for the FIR filter to have a similar performance as the Butterworth filter, N cannot be less than 1500, which is consistent with the estimate given in the Example in Section 4.4.1.

4.5 Comparison of the Filters

Previously at the Voice and Speech Section, National Institute on Deafness and Other Communication Disorders (NIDCD), the EMGs were smoothed using a single pole recursive lowpass filter (lag filter) provided by MITSYN. This filter has two disadvantages compared to the Butterworth filter. First, its gain drops very slowly outside the cutoff frequency so that the unwanted high frequency components remain in the output signal. Second, its phase shift is non-linear so it is difficult if not impossible to correct.

A single pole lag filter has a transfer function of the following form:

$$H(s) = \frac{a}{s+a} \tag{4.5.1}$$

Where $a = 1/\tau$, and τ is the time constant of the filter.

Figure 4.11 shows the frequency response of a 25 Hz lag filter (time constant $\tau = 0.04$). The bandwidth of this filter is around 4.0 Hz. The plots clearly show the nonlinearity in the phase shift and the slow drop in filter gain outside the filter bandwidth.

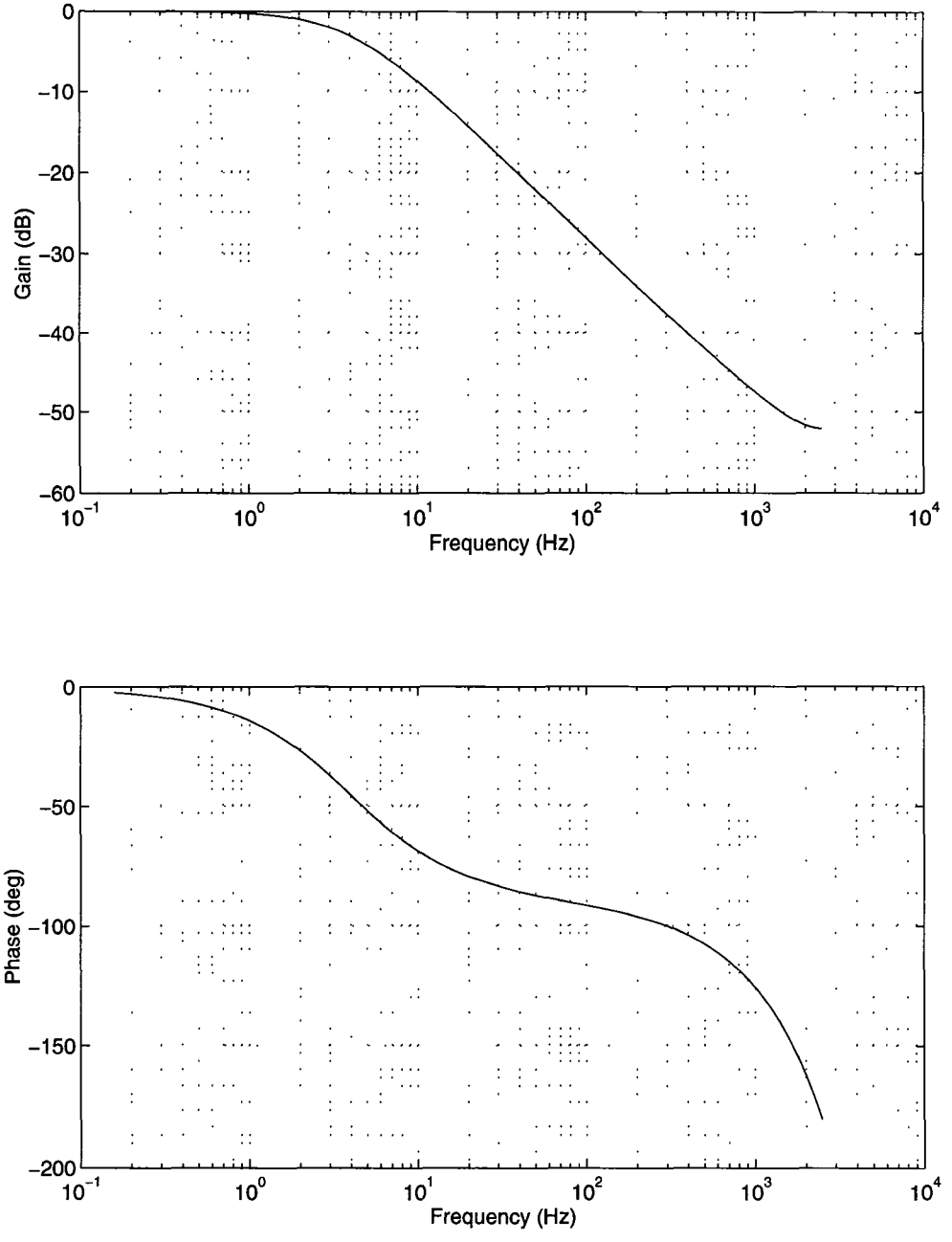

Figure 4.11: Frequency response of a lag filter ($\tau = 0.04\ s$)

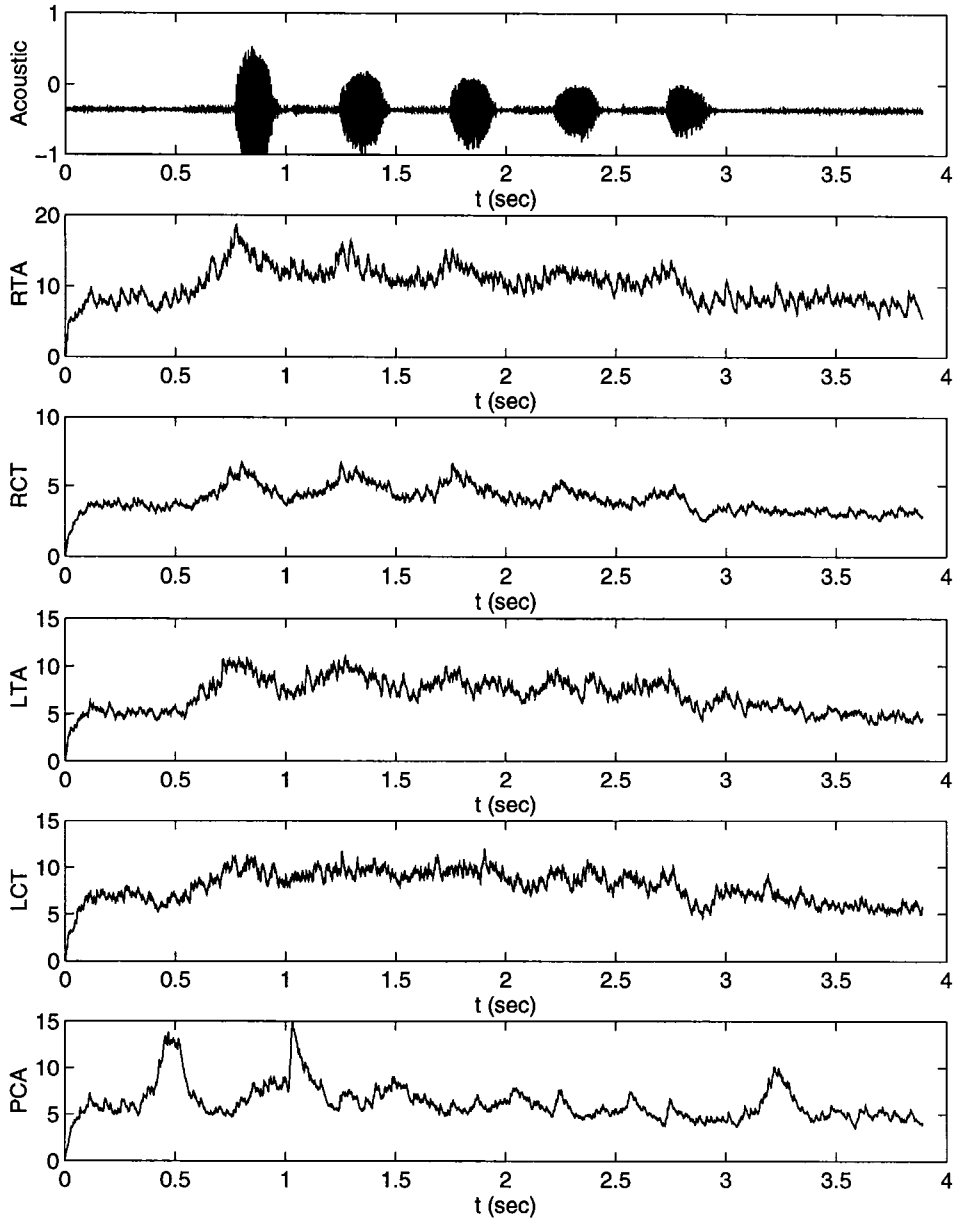

Figure 4.12: EMG envelopes produced by the lag filter

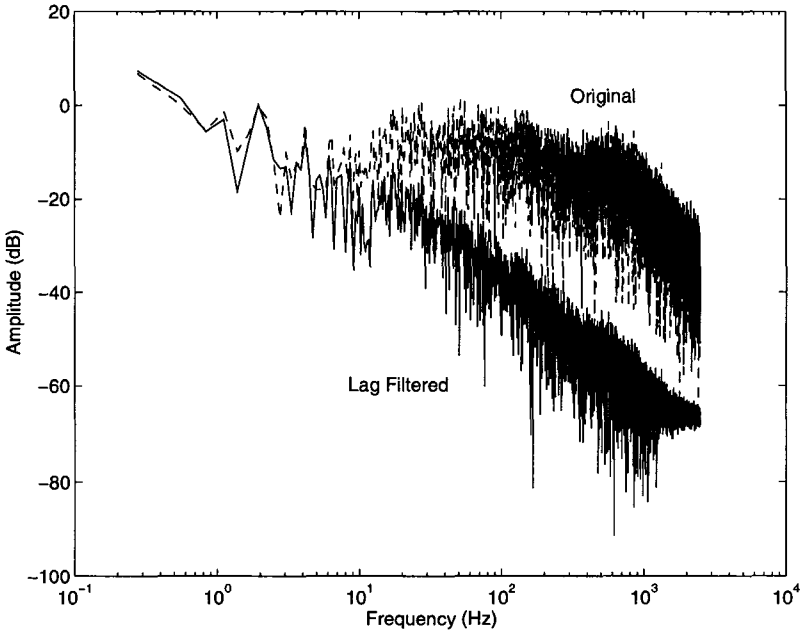

Figure 4.13: Spectra of RTA produced by the lag filter

The smoothed EMG envelopes obtained by applying this lag filter are shown in Figure 4.12. Spectrum analysis of the lag filtered signal (Figure 4.13) showed that there were distortions to the low frequency components of interest and unwanted high frequency components also passed through the filter which is why there were a lot of wiggles in the resulting EMG envelopes in Figure 4.12.

Compared with the forward-backward Butterworth filter designed in Section 4.4, the lag filter is clearly not a good choice for the EMG signal processing.

4.6 Conclusion

Muscle EMG signal plays an important role in study of human movements. The laryngeal muscle EMGs will be used to estimate the muscle forces. In this chapter the experiment performed at the NIH that recorded the laryngeal muscle EMGs was discussed. Signal processing requirements were analyzed and digital filters were designed to process the rectified EMGs. The raw EMG signals were full-wave rectified and lowpass filtered to produce smoothed envelopes, which have been shown to be proportional to the muscle forces. The forward-backward Butterworth filter was designed to process the rectified EMGs. The advantage of this filter over the linear phase FIR and previously used lag filter is that it has a sharp frequency response, zero phase shift and low order. Spectrum analysis has shown that the frequency components of interest were well preserved in the output EMG envelopes obtained using the designed filter.

Chapter 5

A Dynamical Model of the Human Larynx

5.1 Introduction

As stated in Chapter 2, the larynx serves three basic functions in humans. In order of functional priority they are protective, respiratory, and phonatory[87]. The arytenoid cartilages play an important role in all three basic functions. For example, the respiratory (normal mode of the larynx) function is mainly achieved by the movement of the arytenoids which open and close the vocal folds. One of the principle conditions that must be fulfilled in transforming the larynx from the respiratory mode to the phonatory mode is that the vocal ligaments must be apposed, which is attained by the adduction and apposition of the arytenoid cartilages in the median line thereby closing the vocal folds. How the motions of the arytenoids are controlled by the nervous system is still a major unsolved problem in neurolaryngology. Although the task of understanding neural control seems overwhelming, it could be made easier if a stronger theoretical platform were available to aid in its neurobiological investigation. Modeling the human larynx mathematically is the first step towards building such a theoretical

platform.

The first mathematical model of the larynx was suggested by Fink and Demarest in their 1978 book [16]. As described in Chapter 2, this model was mainly intended for speech/voice studies and assumed that the arytenoids are adducted and locked, thereby becoming a part of the cricoid cartilage. In other words, it assumed that the larynx was in the phonatory mode. The same model structure was applied to the model of voice fundamental frequency control by Farley [14]. Very few quantitative models have been developed to study the movements of the arytenoids[72,97], which, as pointed out above, is just as important in accomplishing the basic functions of the human larynx.

The goal of this chapter is to develop a dynamical model of the larynx concentrating on the aspect of the arytenoid movements. The model includes two parts: (1) the joint (skeletal) dynamics; and (2) the muscle dynamics. The cartilage and joint information obtained in Chapter 3; and the processed muscle EMG envelopes are applied to the model.

5.2 A Dynamical Model of the Larynx

To concentrate on the motion of the arytenoid, the movements of the cricoid and the thyroid cartilages are ignored in the model. The cartilages are considered as rigid bodies with mass and inertia. Based on the quantitative analysis of the joint geometry presented in Chapter 3, the cricoarytenoid joint is modeled as an ideal pin joint with the position of the pin chosen to be the axis determined by the optimization procedure described in Chapter 3. The right side and the left side of the cricoarytenoid joint are

modeled independently. Only the right side joint model is presented here. The left side joint is assumed to be similar.

The muscles are modeled as musculotendon actuators. A total of four muscles are included in the model, they are: (1) right Thyroarytenoid (TA), (2) right Posterior Cricoarytenoid (PCA), (3) right Lateral Cricoarytenoid (LCA), and (4) Interarytenoid (IA). The Cricothyroid (CT) muscles are left out of the model because their major function is to move the thyroid cartilage and they have little affect on the position of the arytenoids. See Figure 5.1 for the approximate locations of these muscles. Among the intrinsic laryngeal muscles the PCA is the only abductor (opener) of the vocal folds, all others act as adductors. The vocal ligament is considered as part of the thyroarytenoid muscle. Ligaments would be modeled as nonlinear springs. However, currently there is no quantitative information about any of the ligaments in the larynx; they are not included in the model. They can be inserted into the model easily once the data becomes available.

Each musculotendon actuator is modeled as a two-state, lumped-parameter entity, in series with tendon. Driving the musculotendon model is a first-order representation of the excitation-contraction (activation) dynamics.

5.2.1 Joint Dynamics

The dynamical equations governing the motion of the arytenoid were derived using Newton's laws. The analysis yields the following differential equation:

$$I\ddot{\theta} = T(\theta, \dot{\theta}) \tag{5.2.1}$$

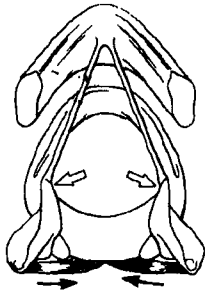

A. Posterior Cricoarytenoid

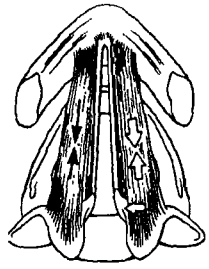

B. Thyroarytenoid

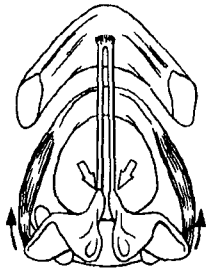

C. Lateral Cricoarytenoid

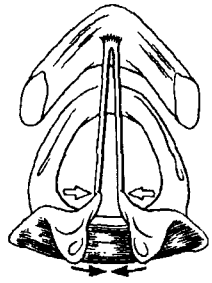

D. Interarytenoid

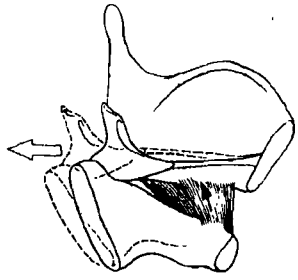

E. Cricothyroid

Figure 5.1: Laryngo-scopic view of the intrinsic laryngeal muscles (except for E. Adapted from Sasaki[87])

where θ, $\dot{\theta}$, $\ddot{\theta}$ are the angular displacement, velocity, and acceleration of the arytenoid; I is the inertia of the arytenoid cartilage about the joint axis; $T(\theta, \dot{\theta})$ is the total torque acted on the joint.

Three type of forces contribute to the torque T:

$$T(\theta, \dot{\theta}) = b(\theta, \dot{\theta}) + c(\theta)g + D(\theta)F_t(a, \theta, \dot{\theta}) \tag{5.2.2}$$

where $b(\theta)$ is a scalar describing both the centrifugal and Coriolis effects; $c(\theta)g$ is a scalar describing the gravitational effect; g is the gravity constant; $D(\theta)$ is a 1×4 moment-arm vector which transforms muscle forces into joint torques, and F_t is a 4×1 vector of muscle forces.

In the model simulation, the equation of motion (5.2.1) was generated using SD/FAST software in the form of C-language functions. The system description file for the joint model is given in Appendix B.

5.2.2 Musculotendon Dynamics

Figure 5.2 depicts the lumped parameter model for the muscle and tendon. This Hill-type model was developed by Zajac et al[122], and later modified by He and Levine by including muscle mass. The model contains a series elastic component (SEC) k_t through which the muscle force is exerted on the cartilages. The muscle is in series (off axis by the pennation angle α) with the SEC, and is assumed to consist of three components: an active force generator F_a representing the muscle contracile mechanism, a parallel elastic component k_p representing the passive muscle elasticity, and a parallel damping component B_m representing the viscosity of the muscle fiber

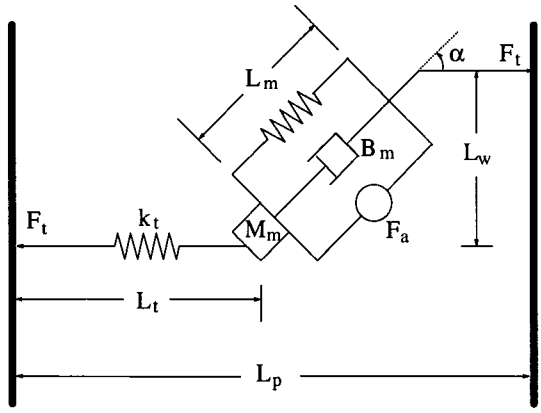

Figure 5.2: Mechanical representation of a muscle.

fluids. The path length L_p is the total length between the two end-points where the muscle is attached. It was assumed that all muscle fibers are equal in length, parallel to each other, and oriented at the same pennation angle α. The muscle volume was assumed to remain constant, or equivalently in 2D, muscle thickness L_w was assumed to remain constant during stretch or contraction.

The series elastic element, is modeled as a nonlinear spring which exhibits a quadratic force–length relation at small SEC lengths, and a linear relation for longer SEC lengths [91]:

$$F_t(\bar{L}_t) = \begin{cases} 0.0 & \bar{L}_t \leq 0 \\ 1480.3\bar{L}_t^2 & \bar{L}_t \leq 0.0127 \\ 37.5\bar{L}_t - 0.2375 & otherwise \end{cases} \tag{5.2.3}$$

where F_t is the SEC force, $\bar{L}_t = (L_t - L_{t_0})/L_{t_0}$ the normalized SEC length, L_{t_0} the SEC slack length (SEC length at rest).

The active muscle force is the product of three independent factors: (1) the force–length relation $f(\bar{L}_m)$, (2) the force–velocity relation $g(\bar{L}_m)$, and (3) the muscle

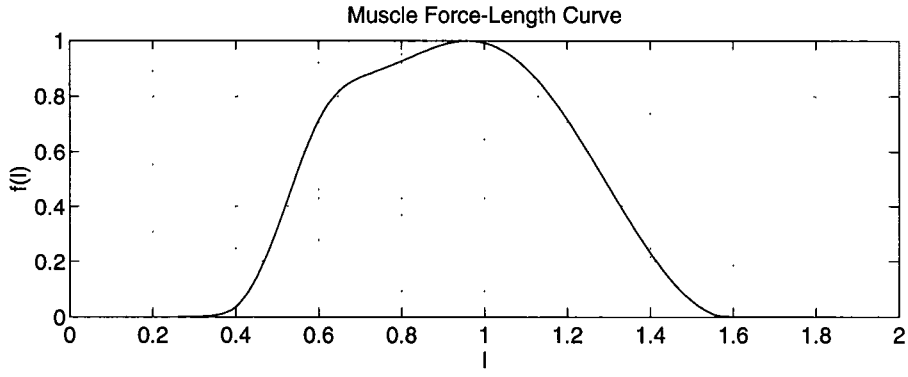

Figure 5.3: Force–length relation.

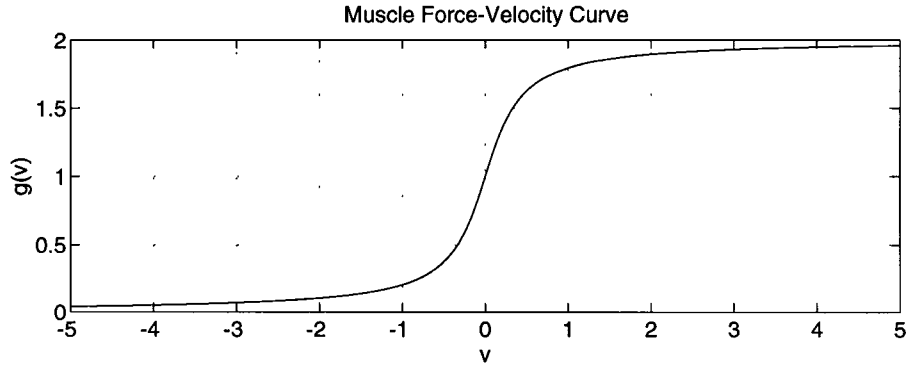

Figure 5.4: Force–velocity relation.

activation level a:

$$F_a = F_z f(\bar{L}_m) g(v) a \tag{5.2.4}$$

where $\bar{L}_m = L_m / L_{m_0}$, $v = \bar{L}_m / V_{max}$, F_a is the active muscle force, F_z the maximum isometric force, L_{m_0} the muscle length at which F_z is achieved, V_{max} the maximum shortening velocity, a the muscle activation level.

The force–length relation is shown in Figure 5.3. This can be approximated by many different curve fitting techniques[32,34,98,124]. Currently, the following curve-fitting formula is used[98]:

$$f(\bar{L}_m) = \begin{cases} 0.049117 e^{33.9594(\bar{L}_m - 0.41)} + 0.001 & \bar{L}_m \leq 0.41 \\ 0.5(1 - cos(5.28(\bar{L}_m + \frac{0.006859}{(\bar{L}_m - 0.62)^2 + 0.0361}))) & 0.41 \leq \bar{L}_m < 1.6 \\ 0.01147 e^{-50.2805(\bar{L}_m - 1.6)} + 0.001 & 1.6 \leq \bar{L}_m \end{cases} \tag{5.2.5}$$

The force–velocity relation is shown in Figure 5.4. This can also be approximated by many different curve fitting techniques[32,34,98]. Currently, the following curve-fitting formula is used[34]:

$$g(v) = 1 + 0.6369 \tan^{-1}(3.0v) \tag{5.2.6}$$

The passive muscle force is assumed to take effect at length $L_m > L_{m_0}$. It is generated by a stretch of the muscle fiber without electrical stimulation. The passive muscle force increases exponentially with respect to muscle fiber length L_m [75]:

$$F_p(\bar{L}_m) = A_p(e^{k_{p_e}(\bar{L}_m - 1)} - 1) \tag{5.2.7}$$

where F_p is the passive muscle force, $\bar{L}_m = L_m / L_{m_0}$ the normalized length of muscle, and A_p, k_{p_e} the stiffness coefficients.

The damping force satisfies that

$$F_d = b_m \dot{\tilde{L}}_m \tag{5.2.8}$$

where b_m is the damping coefficient.

The total force of a muscle is the sum of the passive force F_p, the active force F_a and the damping force F_d. According to Figure 5.2, the musculotendon dynamics is the following:

$$M_m \ddot{L}_m = F_t \cos\alpha - (F_p + F_a + B_m \dot{L}_m)\cos^2\alpha + \frac{M_m \dot{L}_m^2}{L_m}\tan^2\alpha \tag{5.2.9}$$

and

$$\alpha = \arcsin\frac{L_w}{L_m} \tag{5.2.10}$$

where L_w is the muscle thickness which is assumed to be a constant. A detailed derivation of the above equation can be found in [34].

The above musculotendon model includes two sets of parameters. One set uses non-specific muscle parameters. These parameters are assumed to be identical across all the muscles modeled. The other set includes the following four muscle-specific parameters: F_z the maximum isometric force, L_{m_0} the muscle length at which F_z is achieved, L_{t_0} the SEC length at rest, and α the muscle fiber pennation angle. Note that the muscle mass M_m is NOT a scaling factor of the muscle model. The details of the parameters of the four muscles studied can be found in the next section.

5.2.3 Activation Dynamics

The activation dynamics describes the relation between the neural stimulation to the muscle and its mechanical activation. The corresponding physiological process within

the muscle is the release, diffusion, and uptake of the Calcium ions that control the production of sliding forces between the intermuscular filaments. The most important characteristics of activation dynamics for this model are the different time constants for activation and deactivation, the low pass filter property, and the saturation of activation. It is assumed that the activation dynamics is independent of muscle contraction dynamics. The following first-order, nonlinear differential equation is used to describe the activation dynamics:

$$\dot{a}(t) = [u(t) - a(t)][k_1 u(t) + k_2] \tag{5.2.11}$$

with

$$0 \leq a(t) \leq 1 \tag{5.2.12}$$

$$0 \leq u(t) \leq 1 \tag{5.2.13}$$

where $u(t)$, $\forall t \in [t_0, t_f]$, taken as the rectified, filtered and smoothed electromyogram(EMG), is the neural excitation to the muscle, $a(t)$ the activation level of the muscle, $k_1 + k_2$ the rising time constant of the excitation, k_2 the falling time constant of the excitation.

The above activation dynamics has the following features: (1) the mechanical activation follows EMG envelope asymptotically, and is bounded between 0 and 1; (2) the rising of activation is faster than its decay; (3) different muscles can have different time constants k_1, k_2, i.e. faster muscles have faster responses. In the studies performed by Zajac et al[74,98,123]on the human high jump using this muscle model, it was discovered that the jump height is more sensitive to muscle strength than muscle speed and insensitive to musculotendon compliance (the ratio of tendon slack length

to muscle filber length). In our model simulation, we assumed that the degree of rotation of the arytenoid cartilage is not very sensitive to muscle speed. k_1 and k_2 are considered the same for all four muscles ($k_1 = 50$, $k_2 = 5$. See Sim[98]).

5.2.4 Complete Dynamics

The SEC force is the interface between the musculotendon dynamics and the skeletal dynamics; muscle activation couples the activation dynamics and the musculotendon dynamics. Figure 5.5 illustrates such relations. Figure 5.6 shows the locations of the joint axis and the four musculotendon actuators included in the model.

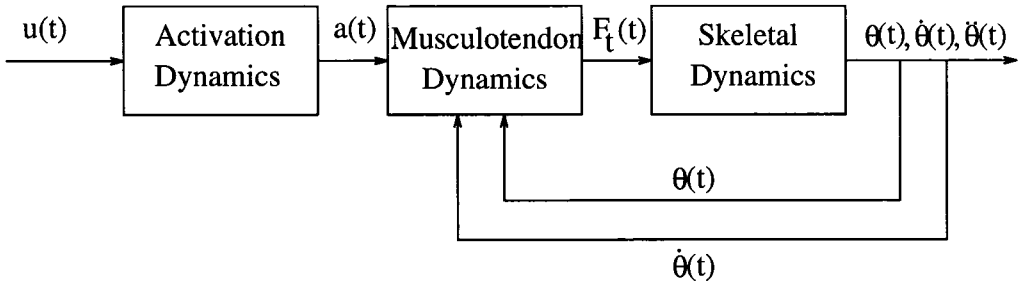

Figure 5.5: System diagram of the neuro-musculo-skeletal control system

By combining the equations of the skeletal, musculotendon and activation dynamics, we obtain the complete dynamics for the neuro-musculo-skeletal control system (NMSCS) of the human cricoarytenoid joint. It can be described by the following vector form equation:

$$\dot{x}(t) = f(x(t), u(t), t), \tag{5.2.14}$$

$$x(t_0) = x_0. \tag{5.2.15}$$

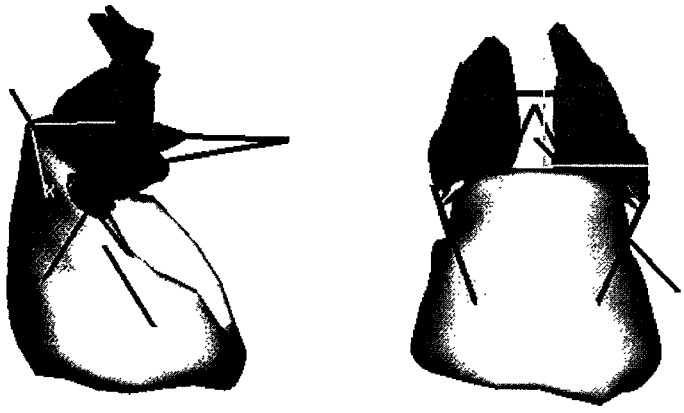

Figure 5.6: Muscles and joint axis (cartilage pictures by Selbie[94]).

In the above, $x=[x_1,\cdots,x_{14}]$ is the state vector of the system which consists of angles and angular velocities of the arytenoid, and the lengths, velocities and activations of the four muscles described above. $u=[u_1,\cdots,u_4]$ is the control vector of the system, where u_i is the neural excitation signal of the i-th muscle. The definition of the state variables and inputs is given below:

$$
\begin{array}{lll}
x_1=\theta & x_2=\dot{\theta} & \\
x_3=L_m^{TA} & x_4=\dot{L}_m^{TA} & x_5=a^{TA}(t) \\
x_6=L_m^{PCA} & x_7=\dot{L}_m^{PCA} & x_8=a^{PCA}(t) \\
x_9=L_m^{LCA} & x_{10}=\dot{L}_m^{LCA} & x_{11}=a^{LCA}(t) \\
x_{12}=L_m^{IA} & x_{13}=\dot{L}_m^{IA} & x_{14}=a^{IA}(t) \\
u_1=u^{TA}(t) & u_2=u^{PCA}(t) & \\
u_3=u^{LCA}(t) & u_4=u^{IA}(t) &
\end{array}
\tag{5.2.16}
$$

The 14 first order differential equations that describe the system are of the form:

$$
\begin{aligned}
\dot{x}_1 &= x_2 \\
\dot{x}_2 &= \tfrac{1}{I} T(x_1, x_2) \\
\dot{x}_3 &= x_4 \\
\dot{x}_4 &= \tfrac{1}{M_m^{TA}} (F_t^{TA} - F_p^{TA} - F_a^{TA} - B_m^{TA} x_4) \\
\dot{x}_5 &= (u_1 - x_5)(k_1 u_1 + k_2) \\
\dot{x}_6 &= x_7 \\
\dot{x}_7 &= \tfrac{1}{M_m^{PCA}} (F_t^{PCA} - F_p^{PCA} - F_a^{PCA} - B_m^{PCA} x_7) \\
\dot{x}_8 &= (u_2 - x_8)(k_1 u_2 + k_2) \\
\dot{x}_9 &= x_{10} \\
\dot{x}_{10} &= \tfrac{1}{M_m^{LCA}} (F_t^{LCA} - F_p^{LCA} - F_a^{LCA} - B_m^{LCA} x_{10}) \\
\dot{x}_{11} &= (u_3 - x_{11})(k_1 u_3 + k_2) \\
\dot{x}_{12} &= x_{13} \\
\dot{x}_{13} &= \tfrac{1}{M_m^{IA}} (F_t^{IA} - F_p^{IA} - F_a^{IA} - B_m^{IA} x_{13}) \\
\dot{x}_{14} &= (u_4 - x_{14})(k_1 u_4 + k_2)
\end{aligned}
\tag{5.2.17}
$$

5.3 Parameter Estimation

The above model depends on three sets of parameters: (1) muscle-specific parameters required by the muscle model; (2) linkage system parameters which describe the mechanical system consisting of the arytenoid cartilage and the cricoarytenoid joint, and (3) ligament parameters. Of the three, the least information we had was about laryngeal ligaments, for example, how many ligaments there are in the larynx which

affect the motion of the arytenoid, where they are attached and what their elastic properties are. Therefore, the ligaments were left out of the model.

5.3.1 Muscle Parameters

The current model uses muscle parameters derived from experimental data on the human laryngeal muscles. The following muscle-specific parameters were estimated for each of the four muscles included in the model:

- **Muscle Mass** M_m

  The data for laryngeal muscle mass was obtained from the literature. In 1960, Bowden and Scheuer [6] measured the wet and dry weights of all five intrinsic laryngeal muscle groups. The wet weights obtained are listed in Table 2.2. Since the muscle mass is not a scaling factor in the muscle model, its value was used to estimate the muscle maximum isometric force F_z (see below).

- **Optimal Fiber Length** L_{m_0}

  The optimal muscle fiber length is the length at which the maximum isometric force F_z is achieved. For the model, it was estimated from the MRI scans (Selbie[94]) and taken to be the distance between the two attachment points estimated for the corresponding muscle. The measurements were made by Dr. Selbie of NIH[94]. See Table 5.1 for results.

- **Maximum Isometric Force** F_z

  F_z was calculated using the following equation

$$F_z = S_m \times A_m \tag{5.3.1}$$

Table 5.1: Muscle Parameters

Muscle	Right TA	Right PCA	Right LCA	IA
M_m (g)	0.622	0.408	0.251	0.304
L_{m_0} (cm)	1.633	1.267	0.872	0.897
A_m (cm^2)	0.409	0.303	0.271	0.319
L_{t_0} (cm)	0.16	0.120	0.087	0.090
Attachments	(0.183, 1.418, -0.389)	(1.098, 0.567, -0.508)	(1.098, 0.567, -0.508)	(0.300, 0.958, 0.454)
	(-0.100, 2.820, -0.300)	(0.573, 0.103, -1.564)	(0.853, 1.032, -1.204)	(-0.597, 0.985, 0.454)

where A_m is the muscle physiological cross-sectional area, and S_m is the muscle stress. The value for muscle stress is controversial; it may vary among slow and fast muscles. A number between 20 to 35 N/cm^2 has been used by various researchers[103,122]. In our simulation, it was taken to be $28N/cm^2$.

The muscle cross-sectional area was estimated using the muscle mass M_m, fiber length L_{m_0} and the standard muscle density ($1.06g/cm^3$) as follows:

$$A_m = \frac{M_m}{1.06 L_{m_0}} \tag{5.3.2}$$

See Table 5.1 for the results of calculated muscle cross-sectional areas for the four muscles included in the model.

- **Tendon Slack Length L_{t_0}**

There is no evidence that there are substantial real tendons connecting the laryngeal muscle to the cartilages. However, there are always serial elasticities in the muscle which are lumped into the series elastic element in the muscle model. The compliance of the musculotendon actuator is determined by the ratio of the

tendon slack length to optimal muscle fiber length. In our model, this ratio was taken to be 0.1 for all four muscles, which correspond to very stiff actuators. The values for the "tendon" slack lengths are also listed in Table 5.1.

- **Fiber pennation Angle α**

  There is no information about the fiber pennation on any of the laryngeal muscles studied. Previous studies have shown that in order to affect the static and dynamic properties of the musculotendon actuators, the muscle fiber pennation must be very high[92,122]. Therefore in the model simulation it is reasonable to assume that α was equal to zero for all four muscles.

- **Attachments**

  One of the basic assumptions in the muscle model described in the previous section is that the muscle has point attachments. Although, in reality, the attachments of the laryngeal muscles are highly distributed, the action of each muscle can be approximated by one or more point-attached muscles that produce the equivalent pulling effects. The muscle attachment points were also estimated from the MRI scans [94] and the pictures in anatomy books.

Table 5.1 summarizes the muscle-specific parameters used in the model simulations. The optimal muscle fiber lengths and the attachment points were estimated using the MRI scans of Cartilage #1 (Selbie[94]). The numbers for the muscle attachments were measured with respect to the coordinate system we chose to represent the cartilages and joints. The reference frame used to define the cartilages is similar to the one used by Sellars[97]. The $x-y$ plane is the horizontal plane; the $y-z$ plane is

the sagittal plane and the $x-z$ plane is the frontal plane. The base of the cricoid is sitting on the horizontal plane. See Figure 3.8 for the chosen coordinate system.

5.3.2 Linkage System Parameters

The linkage system parameters were estimated based on a cadaver larynx (Cartilage #1). The masses of the arytenoids were obtained by weighing the cartilages on a balance (SARTORIUS, Model LC4800P with accuracy of 0.01 g) The center of mass and moments of inertia were estimated using the digitized cartilage surface data obtained from the MRI scans. The Monte Carlo Method[25]was applied in evaluating those integrals that define the center of mass and inertias assuming that the mass of the cartilage is uniformly distributed, i.e. the mass density is a constant. The center of mass and moments of inertia are defined as follows:

- Center of Mass:

$$\begin{aligned} x_c &= \frac{\int x dx dy dz}{\int dx dy dz} \\ y_c &= \frac{\int y dx dy dz}{\int dx dy dz} \\ z_c &= \frac{\int z dx dy dz}{\int dx dy dz} \end{aligned} \tag{5.3.3}$$

- Moments of Inertia:

$$\begin{aligned} I_{xx} &= m\int(y^2+z^2)dxdydz \\ I_{yy} &= m\int(x^2+z^2)dxdydz \\ I_{zz} &= m\int(x^2+y^2)dxdydz \\ I_{xy} &= m\int xydxdydz \\ I_{xz} &= m\int xzdxdydz \\ I_{yz} &= m\int yzdxdydz \end{aligned} \tag{5.3.4}$$

5.4 Computer Simulation Results

The dynamical model of the human cricoarytenoid joint was simulated using the parameters given in the above section. The model consists of a total of fourteen states $x = [x_1, \cdots, x_{14}]$. Among them, the first two states are the rotation angle and the angular velocity of the arytenoid cartilage; the rest of the state variables correspond to those defined in the muscle model (three state variables for each muscle: L_m, $\dot{L}_m$ and $a(t)$). The initial state in (5.2.15) is selected to represent the rest condition of the human larynx: the initial angular velocity of the arytenoid cartilage is zero; the initial muscle fiber lengths of all four muscles are equilibria of their corresponding musculotendon dynamics (5.2.9); the initial muscle velocities and initial levels of activations of all four muscles are zero.

The normalized muscle EMG envelopes obtained in Chapter 4 are applied to the activation dynamics as the input neural stimulus to the muscles. The vocal gesture for which the EMGs were recorded is the repetition of /*si*/. We expect to see the closing and opening movement of the arytenoid at each on-set and off-set of the gesture. The raw EMGs were filtered using the forward-backward Butterworth filter with cutoff frequency $f_c = 4\ Hz$ as presented in Chapter 4. The filtered EMG envelopes (Figure 4.7) were then downsampled at 100 Hz and normalized with respect to the maximum activation values for the corresponding muscles. Only the signals for RTA and PCA in Figure 4.7 were used in the simulation. For muscle LCA and IA, there were no EMGs available; they were simulated as passive muscles ($u(t) = 0$ for all t).

Figure 5.7 shows the results of the model simulation. The vocal gesture simulated was the repetition of /*si*/ in one breath. The top plot is the acoustic trace

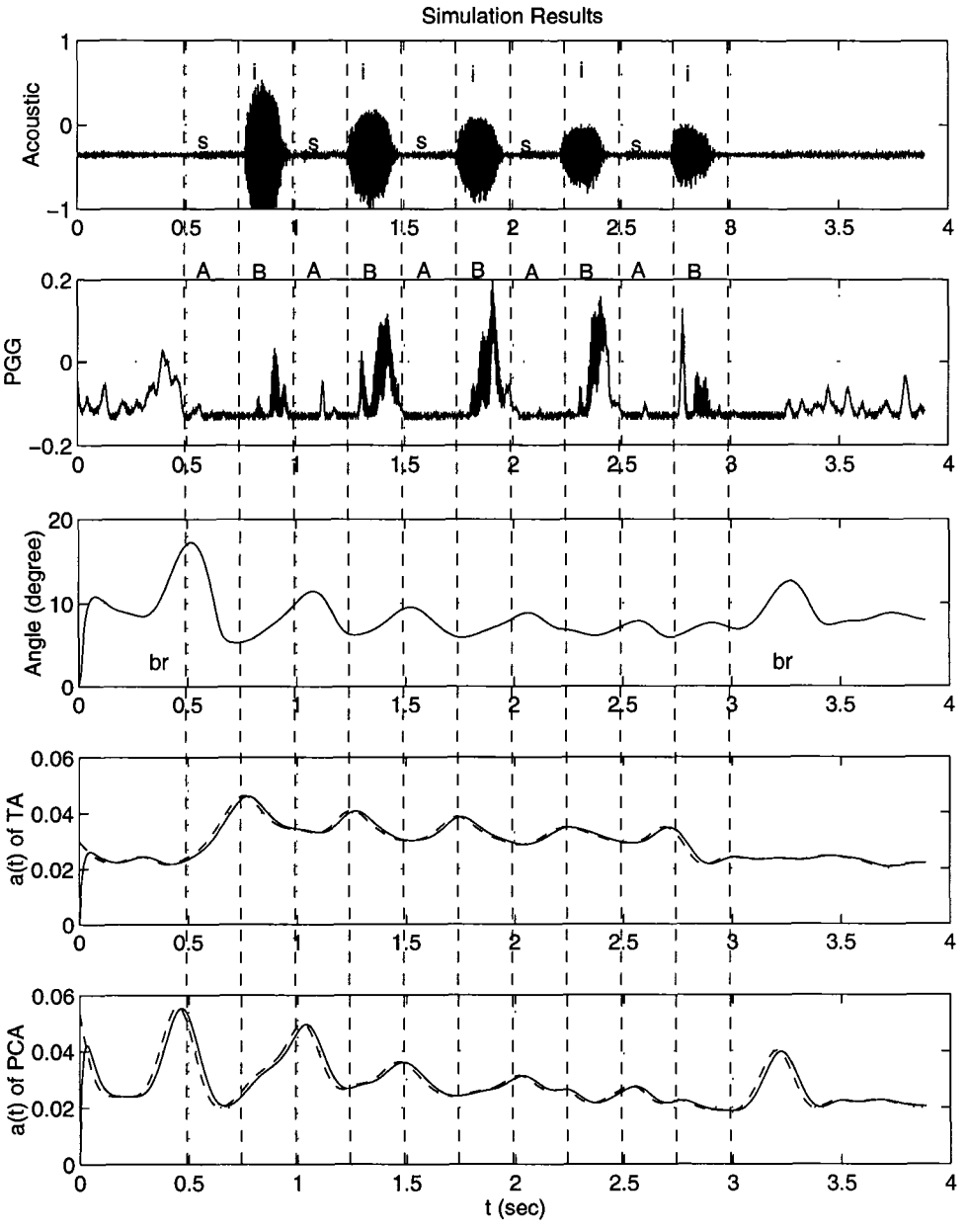

Figure 5.7: Plots of the model simulation results. The dashed lines in the bottom two plots indicate the input EMG envelopes. A - vocal fold abduction; B - vocal fold adduction; br - breath.

showing the timing of each /s/ and /i/ (as marked on the plot). The production of /s/ requires partial opening of the vocal folds while the production of /i/ corresponds to vocal fold adduction (closure). The second plot is the PGG signal (photoglottographic signal) recorded along with the EMGs by Ludlow et al. This signal indicates the changes in glottal opening during the gesture. The third plot is the rotation angle of the right arytenoid cartilage as the result of the simulated vocal gesture; the other two plots are the muscle activation levels of the TA and PCA muscle with the input normalized EMGs superimposed on them as dashed lines. The EMG envelope of the TA was normalized with respect to the the peak activation level of the TA muscle listed in Table 4.1. The PCA envelope was normalized with respect to its peak value in Table 4.1 and then scaled down by a factor of 0.1. From Table 4.1 we can see that the peak value of the PCA is almost 10 times smaller than that of the TA. We think this value is inaccurate because the PCA EMG was collected using a surface electrode while the others were using bipolar hooked wire electrodes. The normalized PCA indicated that the muscle was nearly 50% active while other muscles were less than 5% active, which is quite a mismatch. This is the reason for down scaling the PCA envelope.

Discussion

From Figure 5.7, the following observations are made:

- The peaks of the rotation angle of the arytenoid cartilage, which represent the largest openings of the vocal folds, occurred at each on-set of /s/ and each breath (the first and the last peak). The valleys of the angle occurred at each on-set of

/i/. This indicates that the vocal fold was abducted (opened) to produce /s/ and adducted (closed) to produce /i/, as observed from the experiment.

- There is a delay of about 0.1 second between the peaks of the rotation angle of the arytenoid and the peaks of the PGG signal. This may be explained by the fact that the glottal opening does not only depend on the position of the arytenoid cartilage but also on the air pressure that acted on the vocal folds. This delay may also indicate the inaccuracy of the model since only two muscles were actively involved.

- The peak activations of the PCA muscle occurred a little before the peaks of the rotation angle, indicating that the PCA was indeed acting as an abductor of the vocal folds.

- The peaks of the TA muscle activation level correspond to the valleys of the rotation angle θ, indicating that the TA muscle acted as an adductor of the vocal folds.

Because the location of the pin joint axis used in the model was the optimal "rocking" axis obtained by the optimization algorithm presented in Chapter 3, the movement trajectory of the vocal process of the arytenoid cartilage produced by the model agreed well with the motion data taken from the video recordings (Figure 3.24 and Figure 3.25). At the current stage, the best we can say is that the movement pattern of the arytenoid cartilage produced by the model is similar to that of the vocal gestures studied. The model cannot be fully tested for its accuracy until more motion data becomes available. The rotation angle of the arytenoid is sensitive to the

ratio of muscle strength (physiological cross-sectional area, mass) and the ratio of the muscle activation level of the two active muscles (TA and PCA). These two ratios have similar effect on the model, which is to change the force ratio between the two muscles. To see the effect of this, we chose to change the ratio of the muscle excitation level (by scaling the PCA EMG envelope up or down 50% from the value used to produce Figure 5.7. The results are given in Figure 5.8 (50% smaller) and Figure 5.9 (50% larger). From these two figures we can see that the basic features shown in Figure 5.7 still hold true except that the peak rotation angle of the arytenoid changed. The peak angle is proportional to the ratio of the PCA to the TA activation level.

5.5 Conclusion

The dynamical model of the human larynx presented in this chapter is a first attempt at developing a dynamical neural musculotendon skeletal model of the human larynx. Although the model is still at a preliminary stage of development, the simulations performed on it have shown some promising results. The movement pattern of the arytenoid cartilage produced by the model is similar to that of the vocal gestures studied. Both the thyroarytenoid and the posterior cricoarytenoid muscles functioned in the predicted ways.

The model can be improved a great deal as more data becomes available, such as more accurate muscle parameters, both anatomical measurements and physiological investigations of elasticities and viscosities of various laryngeal components (ligaments, elastic membranes, etc.), better EMG recordings and more motion data. As the model is expanded to incorporate more factors and better estimates of biological parameters,

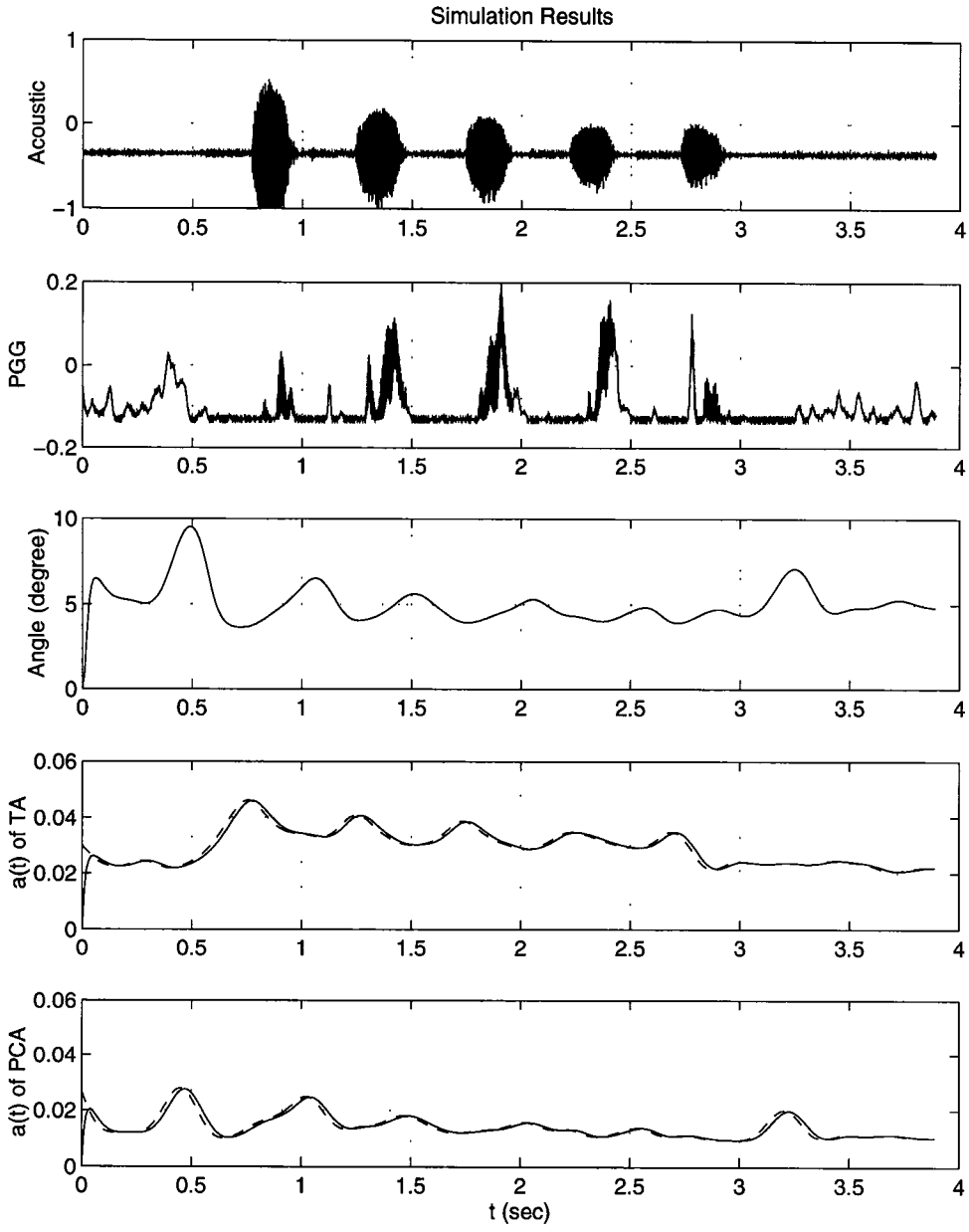

Figure 5.8: The model simulation results. The muscle activation level of the PCA is scaled down by 50%.

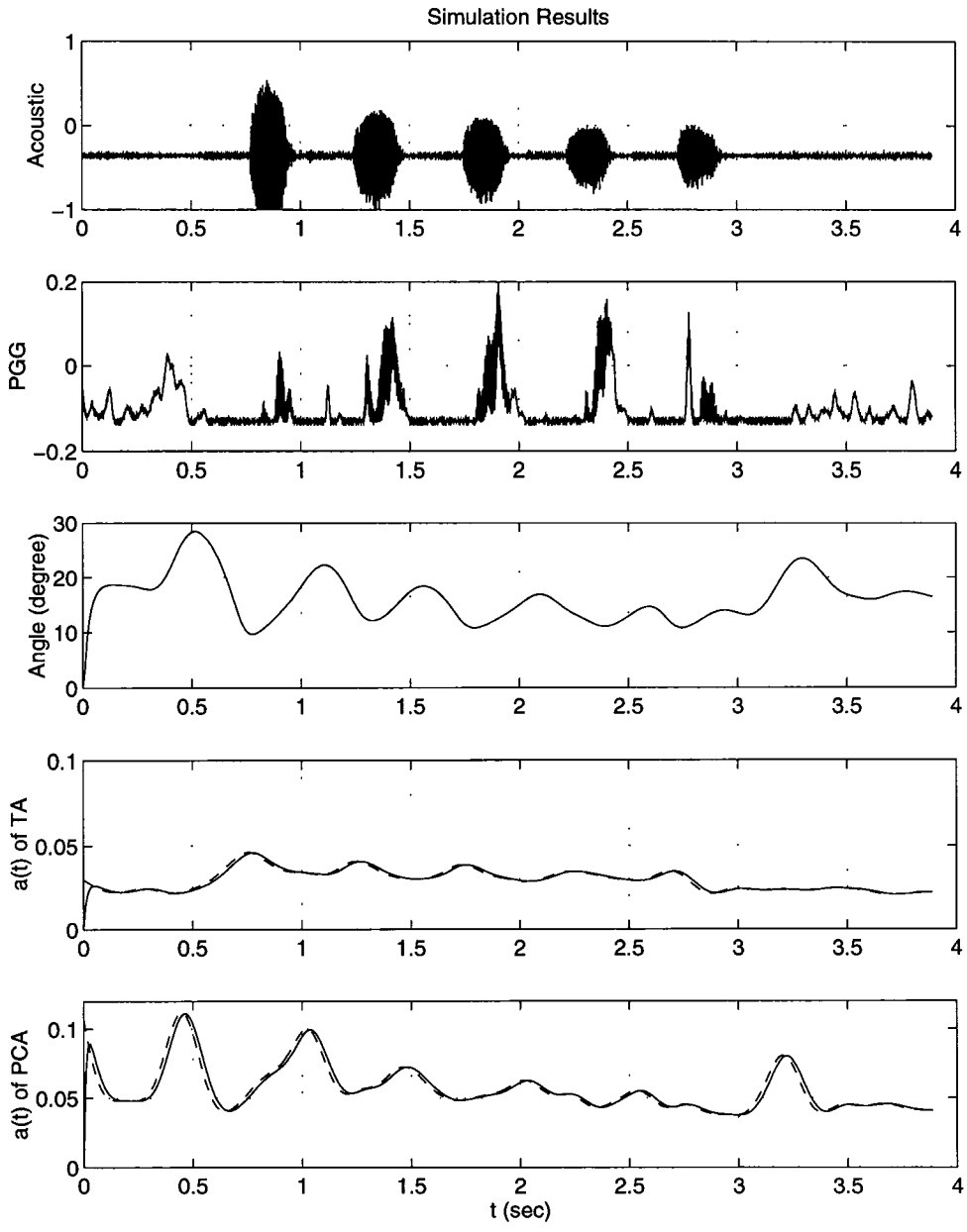

Figure 5.9: The model simulation results. The muscle activation level of the PCA is scaled up by 50%.

its usefulness may also increase.

Chapter 6

Conclusions and Future Research

6.1 Summary

In this dissertation, quantitative measurement and analysis was performed on the joint anatomy and motion at the cricoarytenoid joint of the human larynx. A dynamic neuro-musculo-skeletal model which describes such motion was developed. This research has been motivated by the search for treatment for various laryngeal motor control disorders as well as the lack of previous study of the biomechanical aspects of the biological functions (non-phonatory functions) of the human larynx. The model devised here is the first dynamical model of the human larynx which includes both muscles and the skeletal structures (cartilages).

The research focused on the motion of the arytenoid cartilages which controls the opening and closing of the vocal folds. To obtain quantitative information about the joint geometry, a 3D digitization method was proposed and implemented using a milling machine. Using this method, two sets of joint surfaces of the cricoarytenoid joint were digitized. A computer graphics software package was written to reconstruct

the joint surfaces as well as laryngeal cartilages on the Silicon Graphics' IRIS computer.

Using the joint surface data, an optimization problem was formulated to locate the best feasible rotation axis for the joint, assuming that the joint can be approximated by an ideal cylinder. The minimum variation in the joint gap was used as the objective function. The solution to the optimization problem gives an optimal rotation axis for the motion range of the arytenoid. Rotating around this axis results in a motion that has the most uniform joint gap, thus the smallest resistance produced by the fluid inside the joint gap. For the two cartilages studied, the optimal joint axis turned out to be the so called "rocking" axis of the arytenoid. Rotation about an axis that is vertical to the joint facet is also feasible but not optimal. The best such axis found by the optimization algorithm does not pass through the joint facet but rather is located outside the cricoid cartilage. The resulting rotation motion around this axis produces a "sliding" of the arytenoid. The movement trajectory produced by rotating around the optimal "rocking" axis matches the experimental data, while the one produced by the rotation about the vertical axis contradicts it.

Based on the study results obtained above, a neuro-musculo-skeletal model of the human larynx was developed. This model assumed that the larynx is not at the state of steady phonation so the arytenoids are not locked. The motion at the cricothyroid joint was ignored in the model and the cricoarytenoid joint was treated as an ideal cylinder/pin joint. The location of the joint axis used in the model was determined by the optimization procedure mentioned above. Four intrinsic laryngeal muscles were included in the model. A Hill's type model was used to model the dynamics of the muscle. The muscle and skeletal system parameters were estimated based on

experimental data found in the literature or on our own measurements. No animal data was used in our study. The rectified, smoothed EMGs were used as the neural input to the muscle model. A lowpass digital forward-backward Butterworth filter was designed to filter the rectified muscle EMG to obtain a smoothed envelope which is proportional to the muscle force. Computer simulation results have shown that the model indeed produces motions similar to those observed from live experiments for the laryngeal gesture tested.

6.2 What We Have Learned

Through the study presented in this dissertation, we have learned the following about the human laryngeal movements:

- The "rocking" motion is the optimal rotation of the cricoarytenoid joint under the most uniform joint gap criterion.
- The "sliding" motion is a feasible motion of the joint in terms of the joint surface geometry. If this motion is very limited, it must be restricted by other structures of the larynx (joint capsules, ligaments, etc.).
- The "vertical" rotation axis is not a solution under our criterion, i.e., this motion is restricted by the joint anatomy.
- The movement trajectories of the vocal process of the arytenoid rotating around the optimal "rocking" axis match the motion data while the ones for the "sliding" contradict it.

- For the "rocking" joint model, the muscle TA acts as an adductor and the PCA as an abductor of the vocal folds.

6.3 Future Research

The study presented in this dissertation is a first step towards the comprehensive understanding of the biomechanics of the human larynx. It is far from complete. There is still much work remaining to be done. Future research is needed in the following areas:

- The lack of data is the main obstacle preventing more detailed and accurate models to be developed and tested. More experiments need to be designed and performed to obtain quantitative information about the anatomy and the mechanical properties of the human laryngeal muscles, ligaments, the conus elasticus folds, etc. In order for the information to be useful for producing models, experiments have to be performed from a different perspective than in the past: less descriptive, more precise measurements.

- Currently, the laryngeal muscle EMGs are recorded without reference to the corresponding laryngeal motion. This information is much needed to validate any models developed. A method and a criterion are needed to measure and record the movement information during EMG recording.

- The current joint model is a very simple one. It only captures the major motion at the cricoarytenoid joint. More realistic joint models can be developed as more accurate data becomes available. A first step is to include the "sliding" motion

in the model when the ligament data becomes available to make it a two-degree-of-freedom model. The next step is to model the joint as a surface-to-surface contact joint. A starting point could be to apply the surface fitting method to the experimental data to obtain analytical joint surfaces to work with.

- The optimization algorithm presented in this dissertation can be extended to the more complicated joint models to determine the best movement direction based on the current position of the arytenoid.

- An optimal control model can be created to study those gestures with clear objectives. For example, a minimum time optimal control model can be used to study the protective functions of the human larynx (which require the vocal folds to be closed as fast as possible).

Appendix A

MATLAB Script Files for Filter Design and EMG Processing

A.1 Filter Design

```
%-----  Order Estimation  -----
% Linear Phase FIR
[n,fo,mo,w] = remezord( [4 6]/2500, [1 0], [0.1,0.29],2);
% Butterworth
[nb,wb]=buttord(4/2500,6/2500,0.5,20);
%-----  Lowpass Linear Phase FIR Filter Design  -----
b=remez(1500,fo,mo);
%-----  Lowpass Butterworth Filter Design  -----
fs=5000;                                %Sampling frequency
 N =3;                                   %Order of the filter
 fc=4;                                   %Cutoff frequency
```

```
 [b,a]=butter(N,fc/(fs/2));
%-----  Plotting Frequency Response  -----
[mag,phase,w]=dbode(b,a,1/5000);
clg
subplot(311)
semilogx(w(1:181)/(2*pi),20*log10(mag(1:181))),grid
xlabel('Frequency (Hz)')
ylabel('Gain (dB)')
subplot(312)
semilogx(w(1:181)/(2*pi),phase(1:181)),grid
xlabel('Frequency (Hz)')
ylabel('Phase (deg)')
subplot(313)
semilogx(w(1:181)/(2*pi),40*log10(mag(1:181))),grid
title ('Equivalent Forward-Backward Filter')
xlabel('Frequency (Hz)')
ylabel('Gain (dB)')
orient tall
print
```

A.2 Spectrum Analysis

```
%-----  Spectrum Analysis  -----
Nf=18000;
```

```
% Original EMG
fa2=abs(fft(a2,Nf))*2/Nf;
fa3=abs(fft(a3,Nf))*2/Nf;
fa4=abs(fft(a4,Nf))*2/Nf;
fa5=abs(fft(a5,Nf))*2/Nf;
fa6=abs(fft(a6,Nf))*2/Nf;
% Filtered RTA
fy2=abs(fft(y2,Nf))*2/Nf;
fl2=abs(fft(l2,Nf))*2/Nf;
f=fs*(0:Nf/2-1)/Nf;
%-----  Plotting Original Spectra -----
clg
subplot(511)
semilogx(f,20*log10(fa2(1:Nf/2)))
ylabel ('RTA (dB)')
xlabel ('Frequency (Hz)')
axis([0.1 10000 -100 10])
subplot(512)
semilogx(f,20*log10(fa3(1:Nf/2)))
ylabel ('RCT (dB)')
xlabel ('Frequency (Hz)')
subplot(513)
semilogx(f,20*log10(fa4(1:Nf/2)))
ylabel ('LTA (dB)')
```

```
xlabel ('Frequency (Hz)')

axis([0.1 10000 -100 10])

subplot(514)

semilogx(f,20*log10(fa5(1:Nf/2)))

ylabel ('LCT (dB)')

xlabel ('Frequency (Hz)')

axis([0.1 10000 -100 10])

subplot(515)

semilogx(f,20*log10(fa6(1:Nf/2)))

ylabel ('PCA (dB)')

xlabel ('Frequency (Hz)')

axis([0.1 10000 -100 10])

%-----  Plotting Spectrum of RTA -----

clg

semilogx(f,20*log10(fa2(1:Nf/2)),'--')

ylabel ('Amplitude (dB)')

xlabel ('Frequency (Hz)')

hold on

semilogx(f,20*log10(fy2(1:Nf/2)),'m')

hold off

gtext('Original')

gtext('Butterworth Filtered')

orient landscape

print
```

```
clg
semilogx(f,20*log10(fa2(1:Nf/2)),'--')
title ('Figure 7.  Spectrum Analysis of EMG Signal (RTA)')
ylabel ('Amplitude (dB)')
xlabel ('Frequency (Hz)')
hold on
semilogx(f,20*log10(fl2(1:Nf/2)),'m')
hold off
gtext('Original')
gtext('Lag Filtered')
orient landscape
print
```

A.3 EMG Processing

```
%----- Input Rectified EMG Data  -----
load emg.dat;
t=emg(:,1);
a1=emg(:,2);
a2=emg(:,3);
a3=emg(:,4);
a4=emg(:,5);
a5=emg(:,6);
a6=emg(:,7);
```

```
a7=emg(:,8);

a8=emg(:,9);

%-----  Plotting Rectified EMG  -----

clg

subplot(611)

plot(t,a1)

ylabel ('Acoustic')

xlabel ('t (sec)')

subplot(612)

plot(t,a2)

ylabel ('RTA')

xlabel ('t (sec)')

subplot(613)

plot(t,a3)

ylabel ('RCT')

xlabel ('t (sec)')

subplot(614)

plot(t,a4)

ylabel ('LTA')

xlabel ('t (sec)')

subplot(615)

plot(t,a5)

ylabel ('LCT')

xlabel ('t (sec)')
```

```
subplot(616)
plot(t,a6)
ylabel ('PCA')
xlabel ('t (sec)')
orient tall
print
%-----  Forward-Backward Filtering of EMG Data  -----
y2=filtfilt(b,a,a2);
y3=filtfilt(b,a,a3);
y4=filtfilt(b,a,a4);
y5=filtfilt(b,a,a5);
y6=filtfilt(b,a,a6);
%-----  Plotting EMG Envolopes  -----
clg
subplot(611)
plot(t,a1)
ylabel ('Acoustic')
xlabel ('t (sec)')
subplot(612)
plot(t,y2)
ylabel ('RTA')
xlabel ('t (sec)')
subplot(613)
plot(t,y3)
```

```
ylabel ('RCT')

xlabel ('t (sec)')

subplot(614)

plot(t,y4)

ylabel ('LTA')

xlabel ('t (sec)')

subplot(615)

plot(t,y5)

ylabel ('LCT')

xlabel ('t (sec)')

subplot(616)

plot(t,y6)

ylabel ('PCA')

xlabel ('t (sec)')

orient tall

print
```

Appendix B

SD/FAST System Description File for the Joint Model

The part of linkage dynamics of the model described in Chapter 5 was generated using SD/FAST, a software product of the Symbolic Dynamics, inc. which is used in the development of high- performance analysis and design studies of mechanical systems. Given the system description, SD/FAST will generate the equations of motion of the system and implement them in the form of C-language functions. Using these C functions, analysis and design studies can be performed on any mechanical system which can be modeled as a set of rigid bodies interconnected by joints, influenced by forces, driven by prescribed motions, and restricted by constraints.

The following is a system description file for the cricoarytenoid joint model supplied to SD/FAST for generating the linkage dynamics.

```
#
#  This is an SD/FAST Input File describing the motion of the
#  cricoarytenoid joint which is modeled as an 1D pin joint
```

```
#

gravity =  0.000? 0.000? -980.000?


body = arytenoid

inb  = $ground

joint = pin

  mass = 0.290?

  inertia = 0.008628?   0.000701?    0.001316?

                ?       0.009548?   -0.000616?

                ?           ?        0.003652?

  bodytojoint = 0.3661? -0.0955? -0.7283?

  pin = 0.4995? 0.4790? -0.7219?
```

Appendix C

IRIS 3D Reconstruction and Display Programs

The programs included here were developed to create 3D pictures of any object (e.g. cartilages and bones) and animate their motions on the IRIS computer. The codes were written in C language, and can be run on any IRIS machines of model 4D or higher.

C.1 DISPLAY_3D.C

- **Purpose:**

  To display a 3D object.

- **Description:**

  This program displays a 3D object in the form of either a wireframe or a solid picture. The image can be rotated around the three orthogonal axes of the coordinate system by using the three buttons on the mouse. The image can also be enlarged or reduced in size by pressing the b-key (big) or the s-key (small) on the keyboard. To choose the wireframe picture, simply press the w-

key (wireframe). Pressing the s-key (solid) will produce a solid picture. The x, y and z axis are also displayed along with the object.

- **Usage:**

  In order to run this program, the user should supply a data file called "data.tri" which contains the 3D surface points of the object to be displayed. The data file should be in the following format:

  (1) Total number of serial sections (integer)

  (2) Number of points in the current section (integer)

  (3) List of 3D coordinates of all points in the current section such that any three consecutive points form a triangle on the surface of the object.

  To compile and run this program on an IRIS machine, type:

  cc display_3d.c -o display -lgl_s -lc_s -lm

  display

  To exit from the display, press the ESC key.

C.2 LARYNX_3D.C

- **Purpose:**

  To reconstruct laryngeal cartilages and joint surfaces, display joint axis and muscle attachments.

- **Description:**

  This program reconstructs the laryngeal cartilages and joint surfaces, and displays them in the form of 3D shaded renderings. A given joint axis as well as intrinsic laryngeal muscles will also be displayed in the form of straight lines. The images can be rotated around three orthogonal axes of the coordinate system by pressing one of the three buttons on the mouse and drag the mouse in the horizontal direction. The images of the right arytenoid cartilage and its joint facet can be rotated around the given joint axis by pressing the left and the right buttons on the mouse simultaneously and drag the mouse in the horizontal direction, or by pressing the o-key or the p-key on the keyboard. The images can also be enlarged or reduced in size by pressing the b-key (big) or the s-key (small) on the keyboard. Three axes of the chosen coordinate system are also displayed.

- **Usage:**

  In order to run this program, the user should supply the following input data files:

  1. The surface data points and surface normal vectors at each data point for every 3D object to be displayed.

2. One index file for each 3D object to be displayed indicating the connection pattern of the surface triangles.
3. A file containing the location and orientation of the joint axis.
4. A file containing the muscle attachment points for every muscle to be displayed.

To compile and run this program on a IRIS machine, type:

cc larynx_3d.c useful_func.c -o larynx -lgl_s -lc_s -lm

larynx

To exit from the program, move the cursor to the graphics window, then press the ESC key.

C.3 JOINT_3D.C

- **Purpose:**

  To animate the motion at the cricoarytenoid joints using a cylinder joint model.

- **Description:**

  This program animates the motion at the cricoarytenoid joints using a cylinder joint model. Two pieces of cylinders are used to represent the cricoid and arytenoid joint facets. Four types of motion can be simulated using the sliding bars on the control panel. They are (1)Rocking (w/o slipping) (2)Sliding and (3)Rotation about a vertical axis. The radii of the two cylinders were estimated using 3D measurements of the joint facets. The gap between the two cylinder surfaces can be adjusted using a sliding bar. The image in the main graphics window consists of two cylindrical surfaces representing the cricoid joint facets, two solid 3D arytenoids sitting on top of the cricoid cylinders, and two straight lines representing the vocal ligaments. A closer view of the motion between the two cylinder surfaces is displayed in a secondary graphics window. The images in both windows move simultaneous under the panel control. The images can be rotated around three orthogonal axes of the coordinate system by using the three buttons on the mouse. The images can can also be enlarged or reduced in size by pressing the b-key (big) or the s-key (small) on the keyboard. Three axes are also displayed in both windows.

- **Usage:**

  In order to run this program, the user should supply a data file called "data.tri"

which contains the 3D surface points of the arytenoid to be displayed. The data file should be in the following format:

(1) Total number of serial sections (integer)

(2) Number of points in the current section (integer)

(3) List of 3D coordinates of all points in the current section such that any three consecutive points form a triangle on the surface of the object.

To compile and run this program on a IRIS machine, type:

```
cc joint_3d.c -o joint -lgl_s -lc_s -lm
joint
```

To exit from the program, move the cursor to the main graphics window, then press the ESC key.

References

[1] AJMANI, M. L., "A metrical study of the laryngeal skeleton in adult Nigerians," *Journal of Anatomy*, 171, pp. 187–191, 1990.

[2] ALIPOUR-HAGHIGHI, F., TITZE, I. R. AND DURHAM, P., "Twitch response in the canine vocal muscle," *Journal of Speech and Hearing Research*, 30, pp. 290–294, Sept.,1987.

[3] ALIPOUR-HAGHIGHI, F., TITZE, I. R. AND PERLMAN, A. L., "Tetanic contraction in vocal fold muscle," *Journal of Speech and Hearing Research*, 32, pp. 226–231, June, 1989.

[4] BALBONI, G., "First data on the proportions of the human larynx," *Monit. Zool. Ital.*, 62 (suppl.), pp. 220–221, 1953.

[5] BALBONI, G., "Biometric study of the dimensions of the human larynx," *Arch. Ital. Anat. Embriol.*, 60, pp. 161–183, 1955.

[6] BOWDEN, R. E. M. AND SCHEUER, J. L., "Weights of the abductor and adductor muscles of the human larynx ," *J. Lar. Otol.*, 74, pp. 971–980, 1960.

[7] BRAUND, K. G., STEISS, J. E., MARSHALL, A. E., MEHTA, J. R. AND AMLING, K. A., "Morphologic and morphometric studies of the intrinsic laryngeal muscles in clinically normal adult dogs," *Am. J. Vet. Res.* , 49, no. 12, pp. 2105–2110, Dec.,1988.

[8] BRAYTON, R. K. AND SPENCE, R., *Sensitivity and Optimization.* New York, Elsevier Scientific Publishing Company, 1980.

[9] BRØNDBO, K., DAHL, H. A., TEIG, E. AND GUJORD, K. M., "The human posterior cricoarytenoid (PCA) muscle and diaphragm. A histochemical comparsion as a basis for reinnervation attempts," *Acta Otolaryngol. (Stockh)*, 102, pp. 474–481, 1986.

[10] CHOW, C. K. AND JACOBSON, D. H., "Studies of human locomotion via optimal programming," *Math. Biosci.* , 10, pp. 239–306, 1971.

[11] CLAASSEN, H. AND WERNER, J. A., "Fiber differentiation of the human laryngeal muscles using the inhibition reactivation myofibrillar ATPase technique," *Anatomy and Embryology*, 186, pp. 341–346, 1992.

[12] DICKSON, D. R. AND MAUE, W. M., *Anatomical and Physiological Bases of Speech.* Boston, MA, Little, Brown and Company, 1982.

[13] FAABORG-ANDERSEN, K., "Electromyographic investigation of intrinsic laryngeal muscles in humans," *Acta Physiol. Scand.*, 41 (Suppl. 140), 1957.

[14] FARLEY, G. R., "A quantitative model of voice F_0 control," *Journal of Acoustical Society of America*, 95, no. 2, pp. 1017–1029, Feb., 1994.

[15] FINK, B. R., *The Human Larynx: A Functional Study.* New York, NY, Raven Press, 1975.

[16] FINK, B. R. AND DEMAREST, R. J., *Laryngeal Biomechanics.* Cambridge, MA, Harvard University Press, 1978.

[17] FLANAGAN, J. L. AND LANDGRAF, L., "Self-oscillating Source for vocal tract synthesizers ," M.I.T, Conference on Speech Communication and Professions, 1967.

[18] FRABLE, M. A., "Computation of motion at the cricoarytenoid joint," *Archives of Otolaryngology*, 73, pp. 73–78, May, 1961.

[19] FUJITA, M., LUDLOW, C. L., WOODSON, G. E. AND NAUNTON, R. F., "A new surface electrode for recording from the posterior cricoarytenoid muscle," *Laryngoscope*, 99, pp. 316–320, 1989.

[20] GIAT, Y., "Prediction of muscular synergism and antagonism of human upper extremity: A dynamic optimization approach," University of Maryland, College Park, Ph. D. dissertation, 1990 .

[21] GÖERTTLER, K., "Die Anordnung, Histologie und Histogenese der quergestreiften Muskulatur im menschlichen Stimmband," *Zschr. Anat. Entw.*, 115, pp. 352–401, 1950.

[22] GRABOWER, H., "Die Verteilung und Zahl der Nervenfasern in den Kehlkopfmuskeln und die Hinfälligheit des Erweiterers der Stimmritze," *Arch. f. Laryng. u. Rhin.*, 16, p. 189, 1904.

[23] GRAY, H., *Gray's Anatomy* (36th edition). New York, NY, Churchill Livingstone, 1980.

[24] HAJI, T., MORI, K., OMORI, K. AND ISSHIKI, N., "Mechanical properties of the vocal fold: stress-strain studies," *Acta Otolaryngol.*, 112, pp. 559–565, 1992.

[25] HAMMERSLEY, J. M. AND HANDSCOMB, D. C., *Monte Carlo Methods* . London, Methuen, 1964.

[26] HAPPAK, W., ZRUNEK, M., PECHMANN, U. AND STRÈINZER, W., "Comparative histochemistry of human and sheep laryngeal muscles," *Acta Otolaryngol. (Stockh)*, 107, pp. 283–288, 1989.

[27] HAST, M. H., "Mechanical properties of the cricothyroid muscle," *Laryngoscope*, 76, pp. 537–548, 1966.

[28] HAST, M. H., "Physiological mechanisms of phonation: tension of the vocal fold muscle," *Acta Oto-Laryng.*, 62, pp. 309–318, 1967.

[29] HAST, M. H., "Mechanical properties of the vocal fold muscle," *Pract. oto-rhino-laryg.*, 29, pp. 53–56, 1967.

[30] HAST, M. H., "The primate larynx. A comparative physiological study of intrinsic muscles," *Acta Oto-laryng.*, 67, pp. 84–92, 1969.

[31] HATZE, H., "The complete optimization of human motion," *Math. Biosci.*, 38, pp. 99–135, 1976.

[32] HATZE, H., "A myocybernetic control model of skeletal muscle," *Biological Cybernetics*, 25, pp. 103–119, 1977.

[33] HATZE, H., "Neuromusculoskeletal control systems modeling - a critical survey of recent developments," *IEEE Trans. on Automatic Control*, AC-25, pp. 375–385, 1980.

[34] HE, J., "A feedback control analysis of the neuro-musculo-skeletal system of a cat hindlimb," University of Maryland, College Park, Ph. D. dissertation, 1988 .

[35] HESTENES, M. R., *Conjugate-Direction Methods in Optimization.* Berlin, Spring-Verlag, 1980.

[36] HILL, A. V., "The maximum work and mechanical efficiency of human muscles and their most economical speed," *J. Physiol.*, 56, pp. 19–41, 1938.

[37] HIRANO, M., "Structure and vibratory behavior of the vocal fold," in *Dynamic Aspects of Speech Production*, M. Sawashima and F. S. Cooper, Eds. Tokyo, Japan: University of Tokyo Press, 1977.

[38] HIRANO, M. AND KURITA, Y., "Cover-body theory of vocal fold vibration," in *Speech Science*, R. G. Daniloff, Ed. San Diego, CA: College-Hill Press, 1985.

[39] HIROSE, H., USHIJIMA, T., KOBAYASHI, T. AND SAWASHIMA, M., "An experimental study of the contraction properties of the laryngeal muscles in the cat," *Ann. Otol.*, 78, pp. 297–307, 1969.

[40] HOF, A. L. AND VAN DEN BERG, J., "EMG to force processing IV: Eccentric-concentric contractions on a spring-flywheel set up," *Journal of Biomechanics*, 14, pp. 787–792, 1981.

[41] HOF, A. L. AND VAN DEN BERG, J., "EMG to force processing I: an electrical analogue of the Hill muscle model," *Journal of Biomechanics* , 14, pp. 747–758, 1981.

[42] HOF, A. L. AND VAN DEN BERG, J., "EMG to force processing III: Estimation of parameters for the for the human triceps surae muscle and assessment of the accuracy by means of a torque plate," *Journal of Biomechanics*, 14, pp. 771–785, 1981.

[43] HOF, A. L. AND VAN DEN BERG, J., "EMG to force processing II: Estimation of parameters of the Hill type muscle model for the human triceps surae by means of a calfergometer," *Journal of Biomechanics*, 14, pp. 759–770, 1981.

[44] ISHIZAKA, K. AND FLANAGAN, J. L., "Acoustic properties of a two-mass model of the vocal cords," *Journal of Acoustic Socety of America*, 51, p. 91, 1972.

[45] KAKITA, Y., HIRANO, M. AND OHMARU, K., "Physical properties of the vocal fold tissue: Measurements on excised larynges," in *Vocal Fold Physiology*, K. Stevens and M. Hirano, Eds. Tokyo, Japan: University of Tokyo Press, 1981.

[46] KANEKO, T., ASANO, H. AND MIURA, T., "Biomechanics of the vocal cord: stiffness ," *Practica. Otol. (kyoto)*, 64, pp. 1229–1235, 1971.

[47] KUCIŃSKI, P., OKRASZEWSKA, E. AND PISZCZ, W., "Variability of the course of cricothyroid muscle in humans," *Folia Morphol. (Warsz.)*, 38, no. 3, pp. 391–396, 1979.

[48] LACAU SAINT GUILY, J. AND FARDEAU, M., "Histoenzymology of human laryngeal intrinsic muscle fibers," *Ann. Oto-Laryng. (Paris)*, 100, pp. 1–12, 1983.

[49] LANG, J., FISCHER, K. AND NACHBAUR, S., "Über Maβe, Form und Formvarianten der Cartilagines thyreoidea et cricoidea," *Gegenbaurs morph. Jahrb. Leipzig*, 130, no. 5, pp. 639–657, 1984.

[50] LANG, J., FISCHER, K. AND NACHBAUR, S., "Über Längenmaβe und Querschnitte der Mm. cricoarytenoideus posterior et lateralis und Mm. arytenoidei," *Gegenbaurs morph. Jahrb. Leipzig*, 132, no. 2, pp. 231–243, 1986.

[51] LEE, T. Q. AND WOO, S. L-Y., "A new method for determining cross-sectional shape and area of soft tissues," *Journal of Biomechanical Engineering*, 110, pp. 110–114, May, 1988.

[52] LEVINE, W. S., CHRISTODOULOU, M. AND ZAJAC, F. E., "On propelling a rod to a maximum vertical or horizontal distance," *Automatica*, 19, 1983.

[53] LEVINE, W. S., ZAJAC, F. E., BELZER, M. R. AND ZOMLEFER, M. R., "Ankle controls that produce a maximal vertical jump when other joints are locked," *IEEE Trans. Automatic Control*, AC-28, pp. 1008–1016, 1983.

[54] LOEB, G. E. AND GANS, C., *Electromyography for Experimentalists.* Chicago, IL, The University of Chicago Press, 1986.

[55] LUDLOW, C. L., BAKER, M., NAUNTON, R. F. AND HALLETT, M., "Intrinsic laryngeal muscle activation in spasmodic dysphonia," in *Motor Disturbances I.* 1987.

[56] LUDLOW, C. L. AND FUJITA, M., "The coordination of intrinsic laryngeal muscle activation during phonatory and non-phonatory tasks," in *The Physiological Control of Mammalian Vocalization*, J. D. Newman, Ed. New York, NY: Plenum Publishing Corp., 1988.

[57] LUDLOW, C. L., SCHULZ, G. M. AND NAUNTON, R. F., "The effects of diazepam on intrinsic laryngeal muscle activtion during respiration and speech," *Journal of Voice*, 2, no. 1, pp. 70–77, 1988.

[58] LUDLOW, C. L., SEDORY, S. E. AND FUJITA, M., "Neurophysiological control of vocal fold adduction and abduction for phonation onset and offset during speech," in *Vocal Fold Physiology*, J. Gauffin and B. Hammarberg, Eds. San Diego, CA: Singular, 1991.

[59] LUENBERGER, D. G., *Optimization by Vector Space Methods.* New York, NY, John Wiley, 1969.

[60] LUENBERGER, D. G., *Linear and Nonlinear Programming* (2nd Edition). Reading, MA, Addison-Wesley Publishing Company, 1984.

[61] MA, B., "The dynamics and time optimal control for the skeletal system of humans pedaling a stationary bicycle," University of Maryland, College Park, M.S. Thesis, 1989.

[62] MÅRTENSSON, A. AND SKOGLUND, C. R., "Contraction properties of intrinsic laryngeal muscles," *Acta Physiological Scandinavia*, 60, pp. 318–336, 1964.

[63] MALINOWSKI, A., "The shape, dimensions, and process of calcification of the cartilagenous framework of the larynx in relation to age and sex in the Polish population," *Folia Morphologica*, 26, no. 2, pp. 121–132, 1967.

[64] MALMGREN, L. T. AND GACEK, R. R., "Histochemical characteristics of muscle fiber types in the posterior cricoarytenoid muscle," *Ann. Otol.*, 90, pp. 423–429, 1981.

[65] MAUE, W. M. AND DICKSON, D. R., "Cartilages and ligaments of the adult human larynx," *Archives of Otolaryngology*, 94, pp. 432–439, Nov., 1971.

[66] MAYET, A. AND MUNDNICH, K., "Beitrag zur Anatomie und zur Funktion des M. Cricothyreoideus und der Cricothyreoiodgelenke," *Acta Anat.*, 33, pp. 273–288, 1958.

[67] MCMAHON, T. A. AND GREENE, P. R., "The influence of track compliance on running," *Journal of Biomechanics*, 12, pp. 893–904, 1979.

[68] MCMILLAN, T., "3D digitizing," *Computer Graphics World*, pp. 45–50, Jan., 1989.

[69] MINNIGERODE, B., "Messungen über die Lage einiger auf den Schilknorpel projizierter Teile des Kehlkopfinneren," *HNO*, 5, pp. 51–56, 1955.

[70] MOSSALLAM, I., KOTBY, M. N., ABD-EL-RAHMAN, S. AND EL-SAMMA, M., "Attachment of the posterior cricoarytenoid muscle and ligament at the base of the arytenoid cartilage," in *Proceedings of International Conference on Voice, a satellite meeting of XX congress of IALP.* Kurume, Japan: Dept. of Otol., Head and Neck Surgey, Kurume University, 1986.

[71] MOSSALLAM, I., KOTBY, M. N., ABD-EL-RAHMAN, S. AND EL-SAMMA, M., "Attachment of some internal laryngeal muscles at the base of the arytenoid cartilage," *Acta Otolaryngol. (Stockh)*, 103, pp. 649–656, 1987.

[72] NEUMAN, T. R., HENGESTEG, A., LEPAGE, R. P., KAUFMAN, K. R. AND WOODSON, G. E., "Three-dimensional motion of the arytenoid adduction procedure in cadaver larynges," *Annals of Otology, Rhinology & Laryngology*, 103, no. 4, pp. 265–270, April, 1994.

[73] NUBAR, Y. AND CONTINI, R., "A minimal principle in biomechanics," *Bull. Math. Biophys.*, 23, pp. 337–391, 1961.

[74] PANDY, M. G. AND ZAJAC, F. E., "Dependence of jumping performance on muscle strength, muscle-fiber speed, and tendon compliance," in *Modeling and Control of Biomechanical Systems, 1989 ASME Winter Annual Meeting in San Francisco*, vol. DSC-17 , J. L. Stein, J. A. Ashton-Miller and M. G. Pandy, Eds. New York, NY: The American Society of Mechanical Engineers, pp. 59–63, 1989.

[75] PANDY, M. G., ZAJAC, F. E., SIM, E. AND LEVINE, W. S., "An optimal control model for maxmum-height human jumping," *Joural of Biomechanics*, 23, pp. 1185–1198, 1990.

[76] PERLMAN, A. L. AND DURHAM, P. L., "In vitro studies of vocal fold mucosa during isometric conditions," in *Laryngeal Function in Phonation and Respiration*, T. Baer, C. Sasaki and K. Harris, Eds. Boston, MA: College-Hill Press, 1987.

[77] PERLMAN, A. L. AND TITZE, I. R., "Measurement of viscoelastic properties in live tissue," in *Vocal Fold Physiology: Biomechanics, Acoustics and Phonatory Control*, I. R. Titze and R. C. Scherer, Eds. Denver, CO: Denver Center for the Performing Arts, 1985.

[78] PERLMAN, A. L. AND TITZE, I. R., "Tetanic response of the cricothyroid muscle," *Ann. Otol. Rhinol. Laryngol.*, 100, pp. 626–631, 1991.

[79] PERLMAN, A. L., TITZE, I. R. AND COOPER, D. S., "Elasticity of canine vocal fold tissue," *Journal of Speech and Hearing Research*, 27, pp. 212–219, June, 1984.

[80] POLAK, E., *Computational Methods in Optimization*. New York, NY, Academic Press, 1971.

[81] PRESS, W. H., FLANNERY, B. P., TEUKOLSKY, S. A. AND VETTERLING, W. T., *Numerical Recipes in C - The Art of Scientific Computing.* Cambridge, Cambridge University Press, 1988.

[82] RAASCH, C. C., "The use of musculoskeletal models and optimization to study coordination strategies and synergies in cycling," Stanford University, Ph. D. dissertation, 1994.

[83] ROSENFIELD, D. B., MILLER, R. H., SESSIONS, R. B. AND PATTEN, B. M., "Morphologic and histochemical characteristics of laryngeal muscle," *Archives of Otolaryngology*, 108, Oct., 1982.

[84] SADEH, M., KRONENBERG, J. AND GATON, E., "Histochemistry of human laryngeal muscles," *Cellular and Molecular Biology*, 27, no. 6, pp. 643–648, 1981.

[85] SAHGAL, V. AND HAST, M. H., "Histochemistry of primate laryngeal muscles," *Acta Otolaryngology*, 78, pp. 277–281, 1974.

[86] SAHGAL, V. AND HAST, M. H., "Effect of denervation on primate laryngeal muscles: a morphologic and morphometric study," *The Journal of Laryngology and Otology*, 100, pp. 553–560, May, 1986.

[87] SASAKI, C. T. AND ISAACSON, G., "Functional Anatomy of the Larynx," *Otolaryngologic Clinics of Noth America*, 21, no. 4, pp. 595–612, Nov., 1988.

[88] SATO, F. AND HISA, Y., "Mechanical properties of the intrinsic laryngeal muscles and biomechanics of the glottis in dogs," in *Neurolaryngology: Recent Advances*, M. N. Hirano, J. A. Kircher and D. M. Bless, Eds. Boston-Toronto-San diego: College-Hill Press, 1987.

[89] SATO, K., KURTA, S., HIRANO, M. AND KIYOKAWA, K., "Distribution of elastic cartilage in the arytenoids and its physiologic significance," *Annals of Otology, Rhinology & Laryngology*, 99, no. 5, pp. 363–368, May, 1990.

[90] SAWASHIMA, M., "Laryngeal research in experimental phonetics," *Current Trends in Linguistics*, 12, pp. 1303–1448, 1974.

[91] SCHUTTE, L. M., "Using musculoskeletal models to explore atrategies for improving performance in electrical stimulation-induced leg cycle ergometry," Stanford University, Ph. D. dissertation, 1992.

[92] SCOTT, S. H. AND WINTER, D. A., "A comparison of three muscle pennation assumptions and their effect on isometric and isotonic force," *J. Biomechanics*, 24, no. 2, pp. 163–167, 1991.

[93] SELBIE, W. S. AND LUDLOW, C. L., "Developing a mathematical model of the human larynx testing two proposed models of the cricoarytenoid joint using videolaryngoscopy," *Abstracts of the International Society of Biomechanics*, XIV, 1993.

[94] SELBIE, W. S., LUDLOW, C. L., GEWALT, S. AND JOHNSON, A., "Quantifying the size and shape of the human laryngeal cartilages using MRI ," Submitted to the Journal of Morphology, 1994.

[95] SELLARS, I. AND KEEN, E. N., "The anatomy and movements of the cricoarytenoid joint," *The Laryngoscope*, 88, pp. 667–674, 1978.

[96] SELLARS, I. AND SELLARS, S., "Cricoarytenoid joint structure and function," *The Journal of Laryngology and Otology*, 97, pp. 1027–1034, Nov.,1983.

[97] SELLARS, I. AND VAUGHAN, C. L., "A biomechanical investigation of cricoarytenoid joint kinematics," in *Biomechanics*, vol. VIII-A, H. Matsui and K. Kobayashi, Eds. Champaign, IL: Human Kinetics Publishers, 1983.

[98] SIM, E., "The application of optimal control theory for analysis of human jumping and pedaling," University of Maryland, College Park, Ph. D. dissertation, 1988.

[99] SNELL, C., "On the function of the crico-arytenoid joints in the movements of the vocal cords," *Proc. Kon. Nederl. Acad. Wet.*, 50, pp. 1370–1381, 1947.

[100] SOBOTTA, J. AND FIGGE, F. H. J., *Atlas of Human Anatomy* (8th English Edition), vol. II. New York, Hafner Publishing Company, Inc., 1965.

[101] SONESSON, B., "Die funktionelle Amatomie des Cricoarytenoidgelenkes," *Zschr. Anat. Entw.*, 121, pp. 292–303, 1958.

[102] SONESSON, B., "On the anatomy and vibratory pattern of the human vocal folds," *Acta Otolaryngology*, suppl. 156, 1960.

[103] SPECTOR, S. A., GARDINER, P. F., ZERNICKE, R. F., ROY, R. R. AND EDGERTON, V. R., "Muscle architecture and force-velocity characteristics of cat soleus and medial gastrocnemius: Implications for motor control," *J. Neurophysiol.*, 44, pp. 951–960, 1980.

[104] TAKASE, S., "Studies on the intrinsic laryngeal muscles of mammals: Comparative anatomy and physiology," *Otologia Fukuoka*, 10 , no. Suppl. 1 , 1964.

[105] TEIG, E., DAHL, H. A. AND THORKELSEN, H., "Actomyosin ATPase activity of human laryngeal muscles," *Acta Otolaryngol. (Stockh.)*, 85, pp. 272–281, 1978.

[106] TITZE, I. R., "The human vocal cords: a mathematical model, part I," *Phonetica*, 28, pp. 129–170, 1973.

[107] TITZE, I. R., "The human vocal cords: a mathematical model, part II," *Phonetica*, 29, pp. 1–21, 1974.

[108] TITZE, I. R. AND STRONG, W., "Normal modes in vocal cord tissues," *J. Acoust. Soc. Am.*, 57, pp. 736–744, 1975.

[109] VAN DEN BERG, J., "Myo-elastic-aerodynamic theory of voice production," *Journal of Speech and Hearing Research*, 1, pp. 227–244, 1958.

[110] VAN DEN BERG, J. AND TAN, T. S., "Results of experiments with human larynxes," *Pract. oto-rhino-laryng.*, 21, pp. 425–450, 1959.

[111] VAN LEEMPUTTE, M. AND WILLEMS, E. J., "EMG quantification and its application to the analysis of human movements," *Med. Sport Science*, 25, pp. 177–194, 1987.

[112] VON LEDEN, H. AND MOORE, P., "The mechanics of the cricoarytenoid joint," *Archives of Otolaryngology*, 73, pp. 63–72, May, 1961.

[113] WALL, F. J., *Statistical Data Analysis Handbook*. New York, McGraw-Hill, 1986.

[114] WILLIS, W., "On vowel sounds, and on reedorgan pipes," *Transactions of the Cambridge Philosophical Society*, 3, p. 231, 1830.

[115] WINTER, D. A., *Biomechanics and motor control of human movement* (2nd edition). New York, NY, Wiley, 1990.

[116] WINTER, J. AND STARK, L., "Muscle models: what is gained and what is lost by varying model complexity," *Biological Cybernetics*, 55, no. 5, pp. 403–420, 1987.

[117] WOO, S. L-Y., GOMEZ, M. A., SEGUCHI, Y., ENDO, C. AND AKESON, W. H., "Measurements of mechanical properties of ligament substance from a bone-ligament-bone preparation," *J. Orthop. Res.*, 1, pp. 22–29, 1983.

[118] WOO, S. L-Y., ORLANDO, C. A., CAMP, J. F. AND AKESON, W. H., "Effects of postmortem storage by freezing on ligament tensile behavior," *Journal of Biomechanics*, 19, no. 5, pp. 399–404, 1986.

[119] WOOD, J. E., "A ststistical-mechanical model of the molecular dynamics of striated muscle during mechanical transients," *Lec. in Appl. Math.*, 19, pp. 213–259, 1981.

[120] WUSTROW, F., "Bau und Funktion des menschlichen Musculus vocalis," *Zschr. Anat. Entw.*, 116, pp. 506–522, 1952.

[121] YOKOYAMA, T., FURUKAWA, M. AND HIRANO, M., "Structure and stiffness of the human and canine vocal cords," *Res. Rep. Faculty Technol. Nagasaki Univ.*, 10, pp. 75–82, 1977.

[122] ZAJAC, F. E., "Muscle and tendon: properties, models, scaling, and application to biomechanics and motor control," in *CRC Critical Reviews in Biomedical Engineering*, J. R. Bourne, Ed. Boca Raton, FL : CRC Press, Inc., 1988.

[123] ZAJAC, F. E., "Muscle coordination of movement: a perspective ," *Journal of Biomechanics* , 26 , no. Suppl. 1, pp. 109–124, 1993.

[124] ZAJAC, F. E., LEVINE, W. S., CHAPELIER, J. AND ZOMLEFER, M. R., "Neuromuscular and musculoskeletal control models for the human leg," in *Proceedings of American Control Conference.* pp. 229–234, June, 1983.

[125] ZEMLIN, H. R., DAVIS, P. AND GAZA, C., "Fine morphology of the posterior cricoarytenoid muscle," *Folia Phoniatrica*, 36, pp. 233–240, 1984.

[126] ZEMLIN, W. R., in *Speech and Hearing Science: Anatomy and Physiology* (3rd edition). Englewood Cliffs, NJ: Prentice-Hall, 1988.

[127] ZENKER, W., "Vocal muscle fibers and their motor endplates," in *Research potentials in voice physiology*, D. W. Brewer, Ed. New York: State Univ. New York, 1964.